

TECHNISCHE UNIVERSITÄT MÜNCHEN

Department Chemie

Lehrstuhl II für Organische Chemie

Development of Compounds Suitable for NMR Quantum Computing

Arnaud Djintchui Ngongang

Vollständiger Abdruck der von der Fakultät für Chemie der Technischen Universität
München zur Erlangung des akademischen Grades eines

Doktors der Naturwissenschaften

genehmigten Dissertation.

Vorsitzende: Univ-Prof. Dr. Sevil Weinkauf

Prüfer der Dissertation: 1. Univ-Prof. Dr. Steffen J. Glaser

2. Univ-Prof. Dr. Klaus Köhler

Die Dissertation wurde am 06.07.2011 bei der Technischen Universität München
eingereicht und durch die Fakultät für Chemie am 01.09.2011 angenommen.

To my parents and my beloved wife.

ACKNOWLEDGEMENTS

I am grateful to my supervisor Prof. Dr. S. J. Glaser for welcoming me and giving me the opportunity to carry out a Ph.D. in his group. I also wish to express my sincere thanks to him for choosing the interesting topic on which I worked during my stay in his research group.

I would like to sincerely thank the DAAD-Deutsch Akademischer Austausch Dienst for offering me a scholarship without which I certainly would not study in such good conditions.

I would like to thank Prof. Dr. Klaus Koehler for accepting to be one of my examiners.

I thankfully acknowledge Prof. Dr. Eike Brunner for his helpful discussions relating to the high pressure NMR device.

I am indebted to Dr. Raimund Marx whose encouragement, academic guidance, time and permanent advices made this work possible. I really learned a lot from you throughout my study.

I also wish to thank all the members of the Glaser group past and present that I met. I sincerely liked and enjoyed the social atmosphere among us all this time. I found in you a second family in Germany.

I wish to thank all the Kessler group members for their assistance with some chemicals.

My special gratitude goes to Albert Schroeder for teaching me many lab techniques and to Mrs. Martha Fill for her help with the administration needs and her motherly advices.

I would like to thank to Raimund Marx, Xiaodong Yang, Fatiha Kateb and Manoj Nimbalkar who introduced to me the basics of NMR and sometimes assisted me for the experiments setup. I wish also to thank Dr. Rainer Haessner for his technical intervention.

I am grateful to Esther Noelle, Divita Garg and Robert Fischer for agreeing to read and correct English mistakes of this thesis.

A sweeping thank you goes to all my teachers, colleagues and friends from my High School “Lycée du Manengouba-Nkongsamba” and Universities (Université de

Dschang and Université de Yaoundé I) who have supported me in various ways during all my study and my stay in Cameroon.

I acknowledge the moral assistance of my adoptive families in Germany. Thank you very much to families Erich and Denise Becker, Gaetan and Maimouna Meli Kouala, Francis and Aicha Nzeukeyo, Jean Louis and Josiane Ntakpe Ntakpe, Jean Aimé and Laure Djaleu Kepdem, Serge and Marie Thérèse Messing in Munich, Alain Charly and Armelle Tagne kuate in Dortmund, and Solange Marie Kwakam in Berlin.

I am indebted especially to my sisters: Christelle, Charlotte, Nadie, Adeline, Solange and Léontine, and my brothers: Billy, Ledoux, Jules and the late Jean-Baptiste. I extend the same thanks to my entire family, without whose permanent support so many achievements, including this degree would not have been completed. I would like to say thank you particularly to Mr. Mathieu Nankep and Mrs. Apoline Nankep in Yaoundé-Cameroon.

Last but not the least, my most heartfelt gratitude goes to my beloved wife Esther Noelle “Bébé Ngoh” for her understanding and trustworthy love and also to my parents Mr. Pierre Ngongang and Mrs. Rebecca Ngongang born Nguenang for their precious moral, financial and permanent support without which I would not have reached this point. To you I dedicate this thesis.

SUMMARY

Today the trend is to automate everything that can be computerized and to finish this task in shortest time possible. Computers thus play an important role in our everyday life which is no more to be demonstrated. The performance of computers is continuously enhanced, but this development has its limits. Therefore, computer scientists try to design a completely new generation of information processing machines. The quantum computer could be part of this new generation. Although the theory of quantum computing is clearly understood, it has proven extremely difficult to physically realize a quantum computer of which the information-processing capability is known to be much greater than that of a corresponding classical computer. The use of Nuclear Magnetic Resonance (NMR) as a technology for the implementation of quantum computers is well recognized. However, both the “software” (quantum algorithms) as well as the “hardware” (the molecule) are required to achieve this purpose. But, for NMR quantum computers, the design, the synthesis as well as the characterization of suitable molecules are very challenging.

In relation to the concept of the spin chain design, a 13-qubit molecule (^{13}C -labeled 12-fluorododecanal) has been developed in order to implement the quantum mirror experiments and the efficient transfer of encoded states along the spin chain. The complex spectral patterns (overlapped ^1H and ^{13}C NMR signals); the coincidence along with the strong coupling of carbon resonances of the molecule did not permit the direct use of the synthesized molecule for quantum computing experiments. Therefore, Lanthanide shift reagents (LSR) have been used in order to alter chemical shifts. The corresponding tests were performed with unlabeled 12-fluorododecanal and unlabeled 12-(triphenylmethoxy)dodecan-1-ol.

Besides the design and the synthesis of a molecule for spin chain quantum computing experiments, the spin-lattice (T_1) and the spin-spin (T_2) relaxation times of small organic molecules were measured in supercritical carbon dioxide (SC CO_2) and compared to those obtained in common low viscosity NMR samples. Quantum computing experiments using longer pulse sequence blocks would have been implemented on the samples presenting an increase in the relaxation time T_2 in supercritical carbon dioxide. But only a few cases fulfilling this requirement were observed.

Finally, a 3-qubit molecule which is very well suited for thermal state NMR quantum computing was developed and synthesized: 2- ^{13}C -labeled Diethyl 2-fluoromalonate. Using this compound, the complete quantum algorithm for the evaluation of the Jones Polynomial was experimentally implemented. The 3-qubit thermal state NMR quantum computer was capable of evaluating the Jones Polynomial of the link 6.2.3 for several nontrivial values within the domain of definition. An exponential speedup in comparison to classical computers was established. The obtained experimental results were in very good agreement with both the theoretical expectations and the simulations.

ZUSAMMENFASSUNG

In der heutigen Gesellschaft besteht der Trend, alles zu automatisieren, was von Computern gesteuert werden kann. Und diese Umstellung soll in der kürzest möglichen Zeit erfolgen. Dementsprechend sind Computer aus unserem Alltag nicht mehr wegzudenken. Computer werden ständig weiterentwickelt und in ihrer Leistung gesteigert. Dieser stetigen Entwicklung sind jedoch Grenzen gesetzt, weshalb Wissenschaftler nach einer komplett neuen Generation von Computern suchen. Der Quantencomputer könnte diese neue Art von Computergeneration darstellen. Das Konzept eines Quantencomputers ist klar formuliert, und die prinzipielle Funktionsweise ist weitestgehend erforscht; dennoch hat sich die physikalische Realisierung solch eines Quantencomputers als sehr schwierig und aufwändig herausgestellt. Da die Leistungsfähigkeit eines Quantencomputers – zumindest bei einigen Aufgabenstellungen – jegliche Form von klassischen Computern bei weitem übertrifft, ist die Erforschung von physikalischen Realisierungen des Quantencomputer-Konzeptes diesen immensen Aufwand wert. Die Kernmagnetresonanzspektroskopie („Nuclear Magnetic Resonance“, NMR) ist eine vielversprechende Methode, einen Quantencomputer zu realisieren. Dafür ist es notwendig, sowohl die „Software“ (Quantenalgorithmen), als auch die „Hardware“ (das Molekül) speziell für die Realisierung mittels NMR zu optimieren. Insbesondere das Design, die Synthese und die Charakterisierung eines für das NMR-Quantenrechnen sehr gut geeigneten Moleküls sind hierbei besonders anspruchsvolle Aufgaben.

Im Zusammenhang mit dem Spinketten-Konzept wurde ein 13-Quantenbit (13-Qubit) beinhaltendes Molekül entwickelt: ^{13}C -markiertes 12-Fluordodecanal. Unter Verwendung dieser „Hardware“ sollten sowohl Quantenzustand-Spiegelexperimente, als auch der effiziente Polarisationstransfer entlang von Spinketten demonstriert werden. Sowohl komplexe Signalüberlappungen in den entsprechenden NMR-Spektren, als auch die Anwesenheit von starker Kopplung zwischen einigen Spins der Kette verhinderten die direkte Verwendung des synthetisierten Moleküls für die geplanten Quantencomputer-Experimente. Deshalb wurden Lanthanid-Shiftreagenzien eingesetzt, um die chemischen Verschiebungen der einzelnen Spins zu verändern. Die entsprechenden Versuche wurden

mit unmarkierten Substanzen durchgeführt: 12-Fluordecanal und 12-(Triphenylmethoxy)-dodecan-1-ol.

Neben dem Design und der Synthese von Molekülen, die für Spinketten-Quantencomputer-Experimente eingesetzt werden können, wurden auch Relaxationszeiten von kleinen Molekülen in verschiedenen niedrigviskosen Lösemitteln untersucht: Es wurden sowohl longitudinale (T_1) als auch transversale (T_2) Relaxationszeiten für eine Vielzahl von Substanzen gemessen. Als extrem niedrigviskoses Lösemittel wurde superkritisches Kohlenstoffdioxid (SC CO_2) ausgewählt. Die Relaxationszeiten darin gelöster Substanzen wurden gemessen und mit den Relaxationszeiten verglichen, die sich ergeben, wenn dieselben Substanzen in häufig verwendeten niedrigviskosen NMR-Lösemitteln gelöst werden. Ziel dieses Vergleiches war es, Substanzen zu finden, die in superkritischem Kohlenstoffdioxid erheblich längere T_2 -Relaxationszeiten aufweisen, als in üblichen NMR-Lösemitteln. Quantencomputer-Experimente mit besonders langen Pulssequenzen, bei denen eine ausreichend lange T_2 -Relaxationszeit von entscheidender Bedeutung ist, sollten anschließend implementiert werden. Es wurden jedoch nur wenige Substanzen gefunden, bei denen das superkritische Kohlenstoffdioxid zu längeren T_2 -Relaxationszeiten geführt hat; und die Erhöhung von T_2 war in diesen Fällen auch nicht sehr markant.

Schlussendlich wurde noch ein besonders gut geeignetes 3-Qubit-Molekül designt und synthetisiert: 2- ^{13}C -markierter 2-Fluor-malonsäure-diethylester. Mit Hilfe dieser „Hardware“ wurde der komplette Quantenalgorithmus für die Evaluation des Jones Polynoms implementiert. Der resultierende 3-Qubit-Quantencomputer war in der Lage, das Jones Polynom des Links 6.2.3 an einer Vielzahl von Stellen des Definitionsbereiches auszuwerten. Dabei ergab sich ein exponentieller Geschwindigkeitsvorteil gegenüber klassischen Computern. Die entsprechenden experimentellen Ergebnisse stimmten sowohl mit den theoretischen Werten als auch mit den Simulationsergebnissen sehr gut überein.

TABLE OF CONTENTS

ACKNOWLEDGEMENTS

SUMMARY	i
ZUSAMMENFASSUNG	iii
TABLE OF CONTENTS	v
ABBREVIATIONS	x
LIST OF FIGURES	xii
LIST OF TABLES	xvi
PRELIMINARY	1
REFERENCES	3

CHAPTER 1: SYNTHESIS OF A 13 QUBIT MOLECULE FOR SPIN CHAIN QUANTUM COMPUTING EXPERIMENTS

1. INTRODUCTION	4
2. ORGANIC SYNTHESIS	5
2.1 Reduction of 1,12-dodecanedioic acid to 1,12-dodecanediol	6
2.2 Protection of one hydroxyl group: Monotritylation of 1,12-dodecanediol	6
2.3 Substitution of the hydroxyl group by a fluorine atom	6
2.4 Deprotection reaction	7
2.5 Oxidation of 12-fluorododecan-1-ol to 12-fluorododecan-1-al	7
3. RESULTS AND DISCUSSION	9
3.1 One Dimensional NMR Experiments	9
3.2 Two Dimensional NMR Experiments	12
CONCLUSION AND PERSPECTIVES	21
4. EXPERIMENTAL SECTION	22
4.1 Materials and Methods	22
4.2 Synthesis and description of the unlabeled compound	23
4.2.1 Reduction of 1,12-dodecanedioic acid to 1,12-dodecanediol using lithium aluminium hydride (LiAlH ₄)	23

4.2.2 Monotritylation of 1,12-dodecanediol using Triphenylmethyl Chloride (Trityl chloride or TrCl)	24
4.2.3 Fluorination of 12-triphenylmethanododecan-1-ol using DAST (DiethylAminoSulfur Trifluoride)	26
4.2.4 Deprotection using Triethyl-Silyl Triflate/Triethylsilane and Tetra-n-butylammonium fluoride (TBAF)	28
4.2.5 Oxidation of 12-fluoro-dodecan-1-ol using DMP (Dess-Martin Periodinane)	29
4.3 Synthesis and description of the ^{13}C -labeled compound	30
4.3.1 Reduction of ^{13}C dodecanedicarboxylic acid to ^{13}C -labeled dodecanediol using Lithium Aluminum hydride	30
4.3.2 Monotritylation of ^{13}C -labeled 1,12-dodecanediol using Triphenylmethane Chloride (Trityl chloride or TrCl)	31
4.3.3 Fluorination of the ^{13}C -labeled 12-triphenylmethanododecan-1-ol using DAST (DiethylAminoSulfur Trifluoride)	33
4.3.4 Deprotection using Triethyl-Silyl Triflate/Triethylsilane and Tetra-n-butylammonium fluoride (TBAF)	34
4.3.5 Oxidation of ^{13}C -labeled 12-fluoro-dodecan-1-ol using DMP (Dess-Martin Periodinane)	35
5. TWO DIMENSIONAL NMR EXPERIMENTS	35
5.1 Two Dimensional HSQC NMR experiment	35
5.2 Two Dimensional HMBC NMR experiment	36
5.3 Two Dimensional C-C TOCSY NMR experiment	37
REFERENCES	38

CHAPTER 2: USE OF LANTHANIDE SHIFT REAGENTS FOR THE ASSIGNMENT OF ^{13}C NMR SIGNALS OF ALKYL CHAINS	39
1. MOTIVATION AND MAIN OBJECTIVES	39
2. THEORY	40
3. EXPERIMENTAL RESULTS AND DISCUSSION	41
3.1 Experiments using a test molecule: 2-methylundecanal	41
3.2 Lanthanide shift reagents experiments with unlabeled 12- fluorododecanal	47
4. EXPERIMENTAL STUDY: COMPLEXATION OF THE ALCOHOL FUNCTION WITH LANTHANIDE SHIFT REAGENTS	53
4.1. Experiments of 1-octanol with lanthanide shift reagents	53
4.2 Study of the complexation of 12-(triphenylmethoxy)dodecan-1-ol with various lanthanide shift reagents	57
4.2.1 NMR spectroscopy of 12-(triphenylmethoxy)dodecan-1-ol	57
4.2.2 Experimental results: 12-(triphenylmethoxy)dodecan-1-ol) with added $\text{Eu}(\text{fod})_3$ LSR	59
5. COMPARATIVE STUDY: USE OF VARIOUS CONCENTRATIONS OF YB(FOD)$_3$ TO ALTER THE NMR SPECTRA OF 12- (TRIPHENYLMETHOXY)DODECAN-1-OL IN CDCl_3	60
CONCLUSION AND OUTLOOK	63
REFERENCES	66

CHAPTER 3: PROTON RELAXATION TIMES OF SMALL ORGANIC MOLECULES IN SUPERCRITICAL CARBON DIOXIDE (SC CO₂)	67
1. MOTIVATION AND MAIN OBJECTIVES	67
2. CONCEPTION OF THE EQUIPMENT	71
3. THEORY	72
3.1 Viscosity of fluids	72
3.2 Rotational Correlation Time τ_c and Relaxation Times T_1 and T_2	72
3.3 Relaxation Time Measurements	73
3.3.1 Longitudinal or spin-lattice relaxation time T_1	73
3.3.2 Transverse or spin-spin relaxation time T_2	74
4. EXPERIMENTAL RESULTS	75
EXPERIMENTAL SETUP	75
CONCLUSION AND PERSPECTIVES	79
REFERENCES	80
APPENDIX 1 MANUAL GUIDE OF THE HIGH PRESSURE DEVICE (English version)	81
APPENDIX 2 MANUAL GUIDE OF THE HIGH PRESSURE DEVICE (German version)	86

CHAPTER 4: DEVELOPMENT OF A 3-QUBIT THERMAL STATE NMR QUANTUM COMPUTER FOR THE EXPERIMENTAL IMPLEMENTATION OF AHARONOV/JONES/LANDAU (AJL) QUANTUM ALGORITHM	91
INTRODUCTION	91
1. KNOTS THEORY: KNOTS AND BRAIDS	92
1.1 Equivalent knots	92
1.2 Knot functions: Bracket Polynomial and Jones Polynomial	92
1.3 Determination of the Bracket Polynomial and the Jones Polynomial	92
1.4 Evaluation of the Bracket Polynomial using NMR quantum computing	94
2. PREVIOUS EXPERIMENTAL RESULTS	95
2.1 Using of a 2-qubit NMR quantum computer for the Jones Polynomial approximation of the Trefoil knot	95
2.2 Approximation of the Jones Polynomial of the non-trivial link 6.2.3 by NMR using a 3-qubit quantum computer	97
3. DESIGN AND SYNTHESIS OF A 3-QUBIT THERMAL STATE QUANTUM COMPUTER	99
4. EXPERIMENTAL SECTION	100
4.1 Synthesis of the desired product	100
4.2 NMR spectroscopy	101
4.2.1 One Dimensional (^1H and ^{13}C) NMR spectra of the product	101
4.2.2 Two Dimensional HSQC NMR spectra of the product	104
5. USE OF A 3-QUBIT THERMAL STATE QUANTUM COMPUTER FOR APPROXIMATING THE QUANTUM ALGORITHM OF THE NON-TRIVIAL LINK 6.2.3	106
CONCLUSION	107
EXPERIMENTAL SETUP	108
APPENDIX	109
Table 4.3: Some NMR data of the 2- ^{13}C -labeled Diethyl 2-fluoromalonate	
REFERENCES	110

ABBREVIATIONS

ACN	Acetonitrile
<i>t</i> Bu	<i>tert</i> -Butyl
cf.	Confer
δ	Chemical shift
1D	One dimensional
2D	Two dimensional
d	Doublet
dd	Doublet of Doublets
DAST	DiethylAminoSulfur Trifluoride
DMAP	4-Dimethylaminopyridine
DMP	Dess-Martin Periodinane
DMF	<i>N,N</i> -Dimethylformamide
DNA	Deoxyribonucleic Acid
Et	Ethyl
Fig.	Figure
h	Hour
HMBC	Heteronuclear Multiple Bond Correlation
HPLC	High Performance Liquid Chromatography
HSQC	Heteronuclear Single Quantum Coherence
Hz	Hertz
<i>J</i>	Scalar coupling constant
LiAlH ₄	Lithium aluminium hydride
LSR	Lanthanide Shift Reagents
m	Multiplett
M	Molar
MHz	Megahertz
min.	Minutes
mL	Milliliter
mmol	Millimol
NMR	Nuclear magnetic resonance

ppm	Parts per million
q	Quartett
s	Singulett
SI unit	International system unit
SC CO ₂	Supercritical carbon dioxide
t	Triplett
TBAF	Tributylammoniumfluorid
Et ₃ N	Triethylamine
TFA	Trifluoroacetic acid
THF	Tetrahydrofurane
TMS	Trimethylsilyl-
TOCSY	Total correlation spectroscopy
TrCl	Trityl chloride

LIST OF FIGURES

Figure 1.1: Synthesis route of both the unlabeled and the ^{13}C -labeled 12-fluorododecanal	8
Figure 1.2: ^1H NMR Spectrum of the unlabeled 12-fluorododecanal	9
Figure 1.3: ^{13}C NMR Spectrum of the unlabeled 12-fluorododecanal	10
Figure 1.4: ^1H NMR Spectrum of ^{13}C -labeled 12-fluorododecanal	10
Figure 1.5: ^1H decoupled ^{13}C NMR spectrum of the ^{13}C -labeled 12-fluorododecanal	11
Figure 1.6: 2D HSQC NMR spectrum of the unlabeled 12-fluorododecanal recorded at 750 MHz Bruker AV spectrometer in CDCl_3	14
Figure 1.7: High resolution (in carbon dimension) HSQC NMR spectrum of the unlabeled 12-fluorododecanal (expanded region 29-30 ppm) recorded at 750 MHz Bruker AV spectrometer in CDCl_3	14
Figure 1.8: One possible assignment of the unlabeled 12-fluorododecanal using single coherence ($^1J_{\text{C-H}}$)	15
Figure 1.9: 2D HMBC NMR Spectrum of 12-fluorododecanal in CDCl_3 (some expanded peaks) recorded at 750 MHz Bruker AV spectrometer in CDCl_3	18
Figure 1.10: One possible assignment of the unlabeled 12-fluorododecanal showing some 2D HMBC correlations	19
Figure 1.11: Tentative assignment of the ^{13}C -labeled 12-fluorododecanal molecule	20
Figure 1.12: 2D C-C TOCSY of the ^{13}C -labeled fluorododecanal with ^1H decoupled and mixing time $d_9 = 170$ ms	21
Figure 1.13: ^1H NMR Spectrum of the unlabeled 1,12-dodecandiol	23
Figure 1.14: ^{13}C NMR Spectrum of the unlabeled 1,12-dodecandiol	24
Figure 1.15: ^1H NMR Spectrum of the unlabeled 12-(triphenylmethoxy)dodecan-1-ol	25
Figure 1.16: ^{13}C NMR Spectrum of the unlabeled 12-(triphenylmethoxy)dodecan-1-ol	26
Figure 1.17: ^1H NMR Spectrum of the unlabeled 1-fluoro-12-(triphenylmethoxy)dodecane	27
Figure 1.18: ^{13}C NMR Spectrum of the unlabeled 1-fluoro-12-(triphenylmethoxy)dodecane	27
Figure 1.19: ^1H NMR Spectrum of the unlabeled 12-fluorododecan-1-ol	28
Figure 1.20: ^{13}C NMR Spectrum of the unlabeled 12-fluorododecan-1-ol	29
Figure 1.21: ^1H NMR Spectrum of ^{13}C -labeled 1,12-dodecandiol	30
Figure 1.22: ^{13}C NMR Spectrum of ^{13}C -labeled 1,12-dodecandiol	31
Figure 1.23: ^1H NMR Spectrum of ^{13}C -labeled 12-(triphenylmethoxy)dodecan-1-ol	32

Figure 1.24: ^{13}C NMR Spectrum of ^{13}C -labeled 12-(triphenylmethoxy)dodecan-1-ol	32
Figure 1.25: ^1H NMR Spectrum of ^{13}C -labeled 1-fluoro-12-(triphenylmethoxy)dodecane	33
Figure 1.26: ^{13}C NMR Spectrum of ^{13}C -labeled 1-fluoro-12-(triphenylmethoxy)dodecane	34
Figure 1.27: ^1H NMR Spectrum of ^{13}C -labeled 12-fluorododecan-1-ol	34
Figure 1.28: ^{13}C NMR Spectrum of ^{13}C -labeled 12-fluorododecan-1-ol	35
Figure 2.1: (a) Illustrative structure of the Europium complex. (b) Association of the Europium complex with the studied substrate	41
Figure 2.2: Tentative ^1H NMR assignment of 2-methylundecanal	42
Figure 2.3: ^1H NMR spectrum of 2-methylundecanal (0.4 mmol) in CDCl_3	42
Figure 2.4: Tentative ^{13}C NMR assignment of 2-methylundecanal	43
Figure 2.5: ^{13}C NMR spectrum of 2-methylundecanal (0.4 mmol) in CDCl_3	43
Figure 2.6: ^1H NMR spectra of 2-methylundecanal (0.4 mmol) with various LSR	44
Figure 2.7: ^{13}C NMR spectra of 2-methylundecanal (0.4 mmol) with different LSR	44
Figure 2.8: ^1H NMR spectrum of the unlabeled 12-fluorododecanal (0.07 mmol) in CDCl_3	47
Figure 2.9: ^{13}C NMR spectrum of 12-fluorododecanal (0.07 mmol) in CDCl_3	48
Figure 2.10: Possible assignment of the unlabeled 12-fluorododecanal molecule	48
Figure 2.11: ^1H NMR spectra of the unlabeled 12-fluorododecanal (0.07 mmol) with LSR at different concentrations in CDCl_3	49
Figure 2.12: ^{13}C NMR spectra of the unlabeled 12-fluorododecanal (0.07 mmol) with LSR at different concentrations in CDCl_3	50
Figure 2.13: Tentative ^1H NMR assignment 1-octanol	53
Figure 2.14: ^1H NMR spectrum of 1-octanol (0.2 mmol) in CDCl_3	53
Figure 2.15: Tentative ^{13}C NMR assignment 1-octanol	54
Figure 2.16: ^{13}C NMR spectrum (21-33 ppm) of 1-octanol (0.2 mmol) in CDCl_3	54
Figure 2.17: ^1H NMR spectra of 1-octanol (0.2 mmol) with different LSR in CDCl_3	54
Figure 2.18: ^{13}C NMR spectrum of 1-octanol (0.2 mmol) with different LSR (0.2eq) in CDCl_3	55
Figure 2.19: Tentative ^1H assignment of 12-(triphenylmethoxy)dodecan-1-ol based on NMR data and a simulation with Chemdraw	57
Figure 2.20: ^1H NMR spectrum of 12-(triphenylmethoxy)dodecan-1-ol in CDCl_3	57
Figure 2.21: Tentative ^{13}C assignment of 12-(triphenylmethoxy)dodecan-1-ol based on NMR data and a simulation with Chemdraw	58

Figure 2.22: ^{13}C NMR spectrum of 12-(triphenylmethoxy)dodecan-1-ol in CDCl_3	58
Figure 2.23: ^1H and ^{13}C NMR spectra of 12-(triphenylmethoxy)dodecan-1-ol (0.07 mmol) with (A) 0.005 mmol and (B) 0.01 mmol $\text{Eu}(\text{fod})_3$ in CDCl_3	59
Figure 2.24: ^1H NMR spectra of 12-(triphenylmethoxy)dodecan-1-ol (0.07 mmol) with $\text{Yb}(\text{fod})_3$ at different concentrations in CDCl_3	60
Figure 2.25: ^{13}C NMR spectra of 12-(triphenylmethoxy)dodecan-1-ol (0.07 mmol) with $\text{Yb}(\text{fod})_3$ at different concentrations in CDCl_3	61
Figure 2.26: HSQC spectrum of 12-(triphenylmethoxy)dodecan-1-ol (0.07 mmol) with 0.02 mmol $\text{Yb}(\text{fod})_3$ in CDCl_3 (expanded region 30-36 ppm)	63
Figure 3.1 Plot of the viscosity of carbon dioxide versus the pressure	69
Figure 3.2: High pressure setup for the supercritical CO_2 sample preparation	71
Figure 3.3: Inversion Recovery (IR) NMR Pulse Sequence	73
Figure 3.4: Plot of the longitudinal magnetization M_z versus the delay τ	73
Figure 3.5: Plot of the transverse magnetization $M_{x,y}$ versus the delay τ	74
Figure 3.6: Carr-Purcell-Meiboom-Gill (CP MG) NMR Pulse Sequence	75
Figure 4.1: The three Reidemeister moves	92
Figure 4.2: The Figure-Eight knot represented as a 3-strand braid	93
Figure 4.3: Isolated pulse sequence representation of different operators of the Figure-Eight knot	94
Figure 4.4: Pulse sequence blocks representation of different operators of the Figure-Eight knot	95
Figure 4.5: Coupling topology of chloroform (use as a 2-qubit NMR quantum computer)	96
Figure 4.6: Real (I_x) and Imaginary (I_y) parts for the implementation of the 2x2 block U (4x4 block cU) operator of the Figure-Eight knot	96
Figure 4.7: The link 6.2.3 like represented as a 4-strand braid	97
Figure 4.8: (a) 5-qubit molecule; (b) 3-qubit molecule; (c) Topology of the 5-qubit thermal state NMR quantum computer	98
Figure 4.9: Experimental results for the implementation of the 4x4 block of U (8x8 block of cU) obtained with the 5-qubit (H-C-N-F-P) molecule	98
Figure 4.10: Synthesis route of the 2- ^{13}C -labeled Diethyl 2-fluoromalonate molecule	101
Figure 4.11: ^1H NMR spectrum of 2- ^{13}C -labeled Diethyl 2-fluoromalonate	102

Figure 4.12: Non ^1H -decoupled ^{13}C NMR spectrum of 2- ^{13}C -labeled Diethyl 2-fluoromalonate.	102
Figure 4.13: Non-decoupled 1D NMR spectra of 2- ^{13}C -labeled Diethyl 2-fluoromalonate showing the different coupling constants. (A) ^1H NMR; (B) ^{13}C NMR; (C) ^{19}F NMR	103
Figure 4.14: Coupling topology of the 3-qubit thermal state NMR quantum computer (2- ^{13}C -labeled Diethyl 2-fluoromalonate molecule)	103
Figure 4.15: 2D HSQC NMR spectra of 2- ^{13}C -labeled Diethyl 2-fluoromalonate	104
Figure 4.16: Mapping of a four quadrant system representing E.COSY like HSQC patterns	105
Figure 4.17: Coupling topology of the 3-qubit thermal state NMR quantum computer (2- ^{13}C -labeled Diethyl 2-fluoromalonate molecule) with the sign of the couplings	106
Figure 4.18: Experimental results for the implementation of the 4x4 block of U (8x8 block of cU) operator of the link 6.2.3.	107

LIST OF TABLES

Table 1.1: Tentative assignment of the unlabeled 12-fluorododecanal based on the HSQC NMR experiment	12
Table 1.2: 2D HMBC NMR data of the unlabeled 12-fluorododecanal in CDCl ₃	16
Table 2.1: Comparative shift effects of various ¹ LSR used to alter the ¹³ C NMR spectrum of 2-methylundecanal (0.4 mmol) in CDCl ₃	45
Table 2.2: Relaxation time T ₂ of -C=O of 2-methylundecanal (0.4 mmol) with different LSR in CDCl ₃	46
Table 2.3: Observed ¹³ C NMR lanthanide induced shifts of substrate 12-fluorododecanal in CDCl ₃ and the effect of added Eu(fod) ₃ , Yb(fod) ₃ and Pr(fod) ₃	51
Table 2.4: Relaxation T ₂ time of 12-fluorododecanal with 0.015 mmol Pr(fod) ₃ in CDCl ₃	52
Table 2.5: Summary of lanthanide ¹³ C NMR induced shifts of 1-octanol in CDCl ₃ and the effect of added Eu(fod) ₃ , Yb(fod) ₃ and Pr(fod) ₃	56
Table 2.6: Comparisons of Lanthanide induced ¹³ C NMR chemical shifts values of the substrate 12-(triphenylmethoxy)dodecan-1-ol (0.07 mmol) in CDCl ₃ with various mole of Yb(fod) ₃	62
Table 2.7: HSQC cross peaks of 12-(triphenylmethoxy)dodecan-1-ol (0.07 mmol) with 0.02 mmol Yb(fod) ₃ in CDCl ₃	63
Table 3.1: Viscosity of some organic solvents (at 20°C unless otherwise indicated)	68
Table 3.2: Comparison of the proton spin-lattice (T ₁) and the spin-spin (T ₂) relaxation time values of small organic molecules measured in common NMR solvents and in supercritical CO ₂	76
Table 3.3: Samples with added Lanthanide Shift Reagent (LSR) Yb(fod) ₃	78
Table 3.4: Samples with added Lanthanide Shift Reagent (LSR) Yb(fod) ₃ and increase of relaxation time in SC CO ₂	78
Table 3.4: Viscosity of some organic solvents (at 20°C unless otherwise indicated)	91
Table 4.1 One Dimensional NMR experimental setup	108
Table 4.2 Two Dimensional HSQC experimental setup	108
Table 4.3: Some NMR data of the 2- ¹³ C-labeled Diethyl 2-fluoromalonate dissolved in CD ₃ CN and CDCl ₃	109

PRELIMINARY

The importance of computers in our everyday life which includes digital data transfer, quick calculations and other huge operations is no more to demonstrate. However, when it comes to heavy calculations, the classical computer has some limitations such as requirement of long waiting time to complete a task. Therefore, computer scientists all over the world aim to make computers faster and more versatile. Nevertheless, even the most powerful mainframe computer reaches its limits when the complexity of the calculation scales up exponentially with the problem size. Richard Feynman has found a potential solution to that dilemma: he invented the concept of a quantum computer [1].

In fact a classical computer has a memory made up of bits which can only exist in a state corresponding to the logical state 0 or 1. In contrast to this, the fundamental unit of information in a quantum computer (called a “quantum bit” or “*qubit*”) can additionally be in a superposition state, where both of the logical bit values 0 and 1 exist at the same time. A quantum computer with n *qubits* can be in an arbitrary superposition of up to 2^n different states simultaneously, whereas a classical computer can only be in *one* of these 2^n states at a given time. Provided with a sufficient amount of qubits, a quantum computer therefore has a parallel computing power which exceeds anything a classical computer could ever reach.

The theory of quantum computing is well developed, but the physical realization of a quantum computer (building a quantum computer) has proved to be extremely difficult. Several approaches have been proposed and realized for a small number of qubits. But when it comes to implementing complete quantum algorithms on a quantum computer, most of the experimental realizations are based on Nuclear Magnetic Resonance (NMR). In liquid state NMR spectroscopy, the sample contains an ensemble of many identical spin systems (i.e. molecules) which are particularly well suited to act as qubits due to their isolation from the environment. In this ensemble, it is not possible to manipulate or to detect individual quantum systems [2]. Therefore, one has to find a way to transfer the concept of quantum computing to an ensemble of quantum mechanical systems. Two different approaches have been published so far:

- One initializes the NMR ensemble in a pseudo-pure state [3, 4] instead of a pure state. For many (not all) aspects of quantum computing a pseudo-pure state behaves similar to a pure state.
- One directly uses the thermal equilibrium state of the NMR ensemble. For this approach new quantum algorithms have to be developed [5-11].

In order to enhance the performance of quantum computers, the number of *qubits* has to be increased. For NMR quantum computers, chemical design, synthesis and characterization of suitable molecules is a very demanding challenge. The most promising concepts for molecules which can be used for large scale NMR quantum computing are the following:

- i) $(A-B)_n$ polymer design [12]
- ii) $(A-B-C)_n$ polymer design [13]
- iii) $A-(B)_n-C$ spin chain design [14, 15]

In all of these designs, it is no longer possible to individually control all qubits; identical qubits can be considered as a set or ensemble and thus will be easily controllable simultaneously during the computation. Nevertheless, they can be used for quantum computing, albeit with a larger number of qubits than in designs where all qubits can individually be controlled.

For my work, I focused on the spin chain design. Quantum mirror experiments [14, 15] and the efficient transfer of encoded states along the spin chain [15] can be implemented on such designs, even though only three different controls are available: control of A; control of all B-s at the same time; control of C.

REFERENCES

- [1] R. P. Feynman, *Int. J. Theo. Phys.* **21**, 467 (1982).
- [2] S. J. Glaser, R. Marx, T. Reiss, T. Schulte-Herbrüggen, N. Khaneja, J. M. Myers, A. F. Fahmy. Increasing the Size of NMR Quantum Computers in: *Quantum Information Processing*. pp. 53-65, Eds.: G. Leuchs, T. Beth, (Wiley-VCH), 2003.
- [3] D. G. Cory, A. F. Fahmy, and T. F. Havel, in *Proceeding of the 4th Workshop on Physics and Computation* (New England Complex Institute, Boston, MA, 1996), pp. 87-91.
- [4] D. G. Cory, A. F. Fahmy, and T. F. Havel, *Proc. Natl. Acad. Sci. USA* **94**, 1634 (1997).
- [5] E. Knill and R. Laflamme, *Phys. Rev. Lett.* **81**:5672-5675, 1988.
- [6] S. Parker and M. B. Plenio, *Phys. Rev. Lett.* **85**, N° 14, 2 October 2000.
- [7] J. M. Myers, A. F. Fahmy, S. J. Glaser and R. Marx, *Phys Rev. A* **63**, 032302 (2001).
- [8] D. Poulin, R. Laflamme, G. J. Milburn, and J. P. Paz, *Phys Rev. A* **68**, 20302 (2003).
- [9] A. F. Fahmy, R. Marx, W. Bermel, and S. J. Glaser, *Phys Rev. A* **78**, 022317 (2008).
- [10] G. Passante, O. Moussa, C. A. Ryan, and R. Laflamme, *Phys. Rev. Lett.* **103**.250501 (2009)
- [11] R. Marx, A. F. Fahmy, L. Kauffman et al., *Phys. Rev. A.* **81**, 032319 (2010).
- [12] S. C. Benjamin, *Phys Rev. A* **61**, 020301 (R) (2000).
- [13] Seth Lloyd, *Science*, Vol. **261**, 17 September 1993.
- [14] J. Fitzsimons, and J. Twamley, *Phys. Rev. Lett.* **97**:090502, (2006)
- [15] J. Fitzsimons, L. Xiao, S. C. Benjamin, and J. A. Jones, *Phys. Rev. Lett.* **99**:030501, (2007).
- [16] N. Khaneja and S. J. Glaser, *Phys Rev. A* **66**, 060301 (R) (2002).

CHAPTER 1: SYNTHESIS OF A 13 QUBIT MOLECULE FOR SPIN CHAIN QUANTUM COMPUTING EXPERIMENTS

1. INTRODUCTION

To achieve the goals of designing and synthesizing a suitable molecule, and using it for quantum computing experiments, several steps have to be taken. Both the “software” (i.e. quantum computing algorithms) as well as the “hardware” (the molecule) are required. Recently, new quantum computing concepts have been developed based on the use of spin chain molecules as the “hardware” [1]. According to one of this concept one has to design and synthesize a molecule that includes the following topology of spin- $\frac{1}{2}$ -nuclei: $A-(B)_n-C$ where all the B’s should be similar in chemical shift but nevertheless should only be weakly coupled [2].

A long ^{13}C -labeled carbon chain with two different organic functions at both extremities appeared to be suitable. Given the availability of only few such labeled molecules, the ^{13}C -labeled 1,12-dodecanedioic acid has been chosen to undergo some chemical transformations. The aim is to use the obtained molecule for the implementation of the efficient transfer of encoded states along the spin chain [3] as well as the quantum mirror experiments [1, 2].

After preliminary investigations, we focused on $\text{F}-(\text{CH}_2)_{11}-\text{CHO}$ (with 13 spin- $\frac{1}{2}$ -nuclei: one fluorine atom, eleven middle carbons, and one carbonyl) as a candidate molecule.

The unlabeled starting material (1,12-dodecanedioic acid) was used for first trials due to the high cost of the ^{13}C -labeled one. Thus, the transformation of the diacid to a diol using LiAlH_4 as the reduction reagent was set as the first and the easiest step [4]. The next step was the direct substitution of only one of the hydroxyl groups ($-\text{OH}$) of the diol by a fluorine atom using one of the most common fluorination agent i.e. DAST (DiethylAminoSulfur Trifluoride) in “right” amount. After several unsuccessful trials, this way was abandoned as it turned out that it is very difficult to selectively convert one of the hydroxyl groups to fluoride and leave the other unchanged, especially in symmetric molecules. Moreover, the reactions with dialcohols longer than four carbons give

primarily difluoride products whereas shorter diols either lead to larger amounts of sulfide ester products or react to cyclic ether products [5-7].

Therefore the use of a protecting group is needed in order to let react just one of the hydroxyl groups without touching the other. An appropriate protecting group had to be found for the reaction; one of the most useful protecting groups for the monoprotection of diols in mild reaction conditions and relatively short times, is the triphenylmethyl (or trityl = Tr) group and its mono and dimethoxy derivatives. Most of the attempts using trityl chloride reagents were unsatisfactory and obtained yields were lower as compared to the results reported in the literature [8-12]. It turned out that the selective monotritylation of symmetrical diols is difficult and rarely reproducible. An attempt of selective monoacetylation of the diol as described in [13] was also unsuccessful, although all the reported reaction conditions were met. Finally a modified version of the conventional conditions of monotritylation of diols [14] using a mixture of dichloromethane and 2, 5-dimethylfuran as solvents was used in order to obtain a satisfactory average yield (42 %). After protecting one of the hydroxyl groups, it was easy to substitute the other by a fluorine atom using DAST (DiethylAminoSulfur Trifluoride) as the fluorination reagent [15, 16].

The next step of the synthesis was the removal of the protecting group; different methods were also tested looking for the best result. Thus, reagents like diluted (aqueous) trifluoroacetic acid (TFA) in dichloromethane [17] or formic acid (HCOOH) in ether [11] were used without satisfaction before the combination of triethylsilyl triflate with triethylsilane [18] and tetra-n-butylammonium fluoride (TBAF) [19] led to the deprotected molecule with a good yield.

Once the protecting group was removed, the regained hydroxyl group was then simply oxidized by the means of Dess-Martin Periodinane (DMP) with a good yield [20].

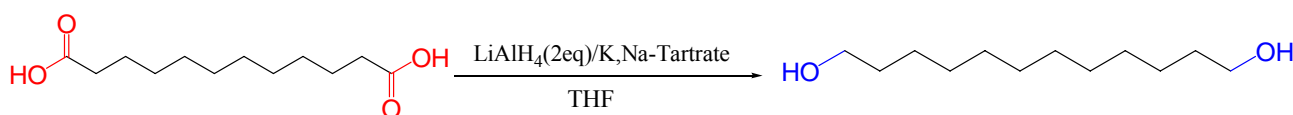
2. ORGANIC SYNTHESIS

As mentioned above the synthesis route (A) involving a direct fluorination of the diol was unsuccessful, another route (B) for our target molecule has then been defined in five steps. It should be noted that the procedure was firstly applied on the unlabeled starting

material (1,12-dodecanedioic acid) because the ^{13}C -labeled compound is commercially available only in small quantities and is very expensive.

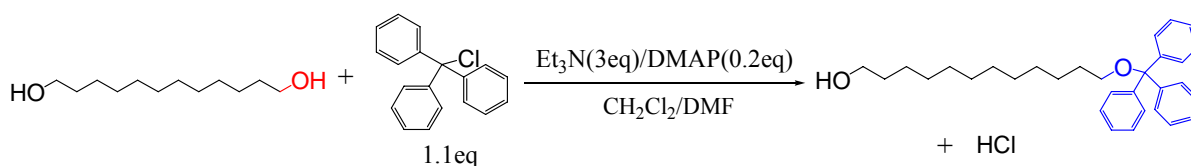
2.1 Reduction of 1,12-dodecanedioic acid to 1,12-dodecanediol

The first step of the synthesis was the reduction of the carboxylic groups to hydroxyl groups using lithium aluminium hydride (LiAlH_4) [4]. This step was one of the easiest; the product was obtained with over 95% yield and without any further purification needed.



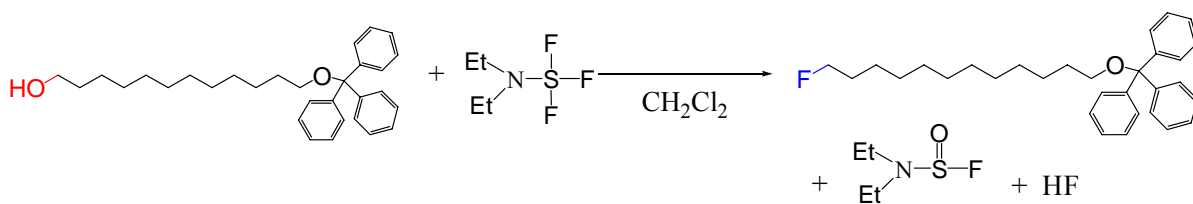
2.2 Protection of one hydroxyl group: Monotritylation of 1,12-dodecanediol

The second step was the protection of one of the hydroxyl groups of the diol using alcohol protecting groups. This step was particularly difficult and time consuming. Because the starting diol is perfectly symmetrical, it was not easy to protect one of the hydroxyl groups and let the other one react. Therefore many hydroxyl protective groups have been tested and the reaction using triphenylmethyl chloride (or Trityl chloride- TrCl) led to an acceptable yield [8-12]. Moreover, the purification (flash chromatography) also causes some loss of the product.



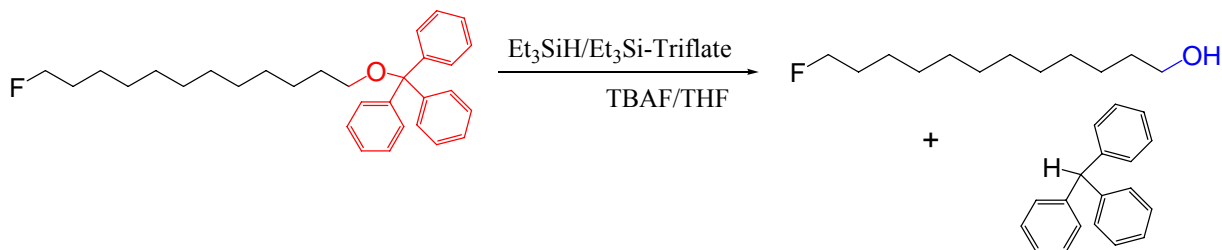
2.3 Substitution of the hydroxyl group by a fluorine atom

The third step i.e. the fluorination reaction was carried out using DAST (DiethylAminoSulfur Trifluoride) [15, 16] with an excess of this reagent. The fluorinated product was obtained after a flash chromatography with 60% average yield.



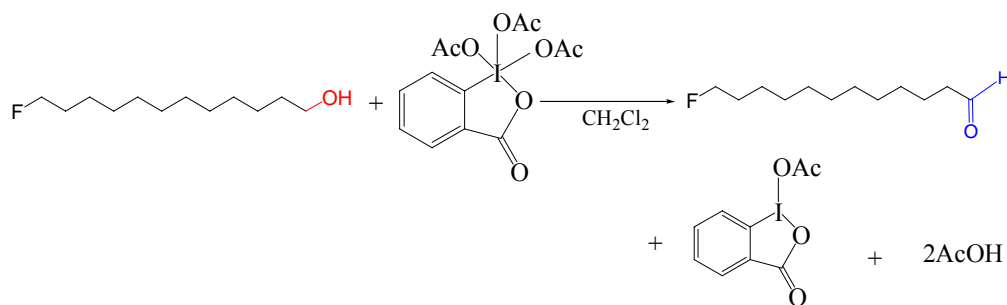
2.4 Deprotection reaction

The removal of the hydroxyl protective group, while the other alcohol function of the molecule had already been substituted by a fluorine atom, took place by adding Triethylsilyl Triflate/Triethylsilane and Tetra-*n*-butylammonium fluoride (TBAF) [18, 19]. The product was obtained with 70% yield after purification by flash chromatography.



2.5 Oxidation of 12-fluorododecan-1-ol to 12-fluorododecan-1-al

The last step of the synthesis route was the oxidation of the alcohol function to aldehyde using Dess-Martin Periodinane (DMP) [20]. This step was also very easy to perform and led to 95% average yield without any further purification of the product.



The figure below summarizes the synthesis route of both the unlabeled and the ^{13}C -labeled products.

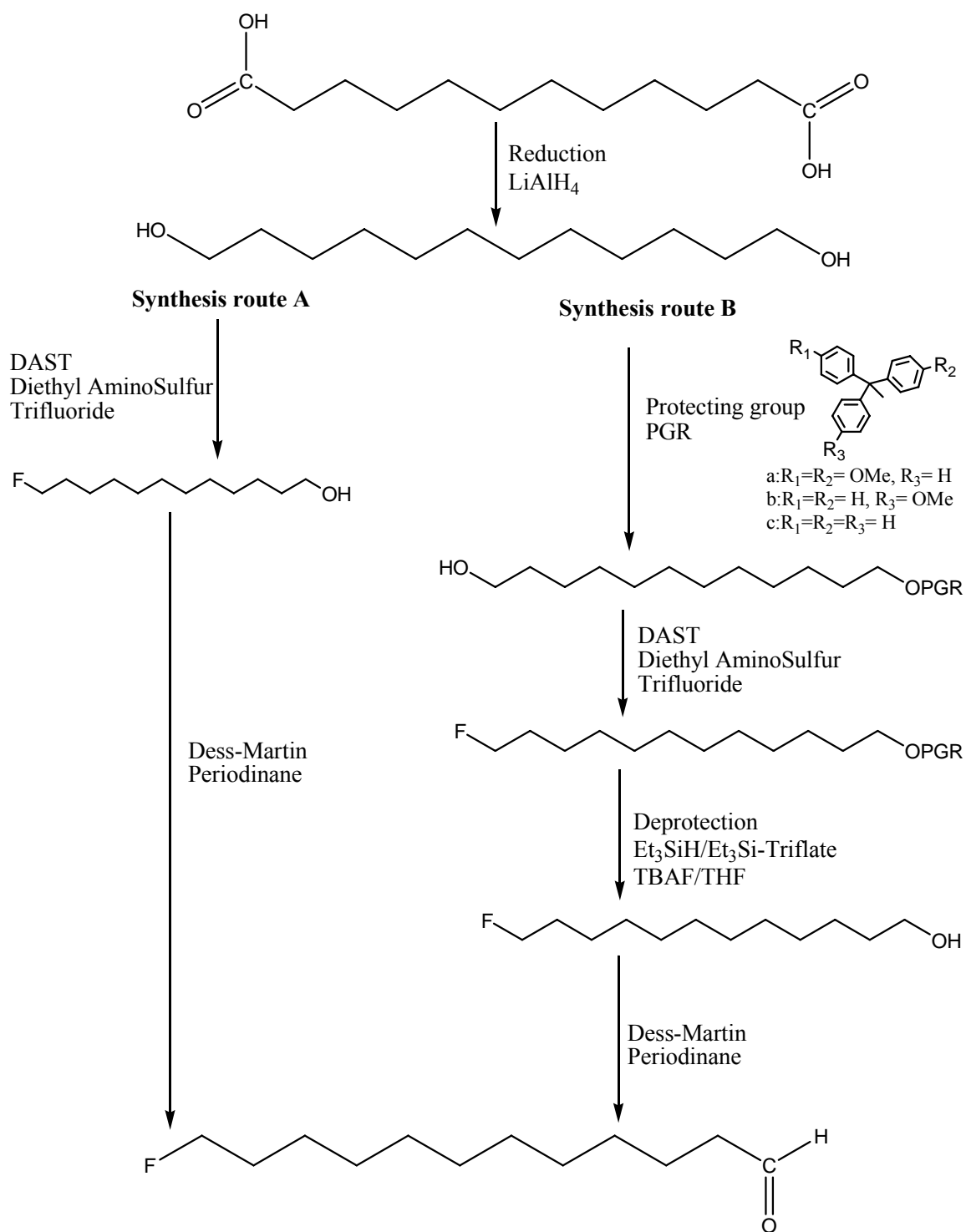


Figure 1.1: Synthesis route of the unlabeled and the ^{13}C -labeled 12-fluorododecanal compounds.

3. RESULTS AND DISCUSSION

The same procedure was used both for the synthesis of the unlabeled compound and for the ^{13}C -labeled compound. The ^{13}C -labeled compound reacted the same way as the unlabeled one, but some differences have been noticed on the obtained yields (for details see the experimental section).

Both products (unlabeled and ^{13}C -labeled 12-fluorododecanal) have been successfully synthesized and their structures were confirmed by recorded 1D and 2D NMR spectra.

3.1 One dimensional NMR analysis

^1H and ^{13}C NMR spectra of 12-fluorododecanal and the ^{13}C -labeled 12-fluorododecanal are described below.

a) NMR analysis of the unlabeled 12-fluorododecanal

^1H –NMR spectrum (600 MHz for ^1H , CDCl_3 , δ in ppm): 9.76 (t, 1H, $^3J_{\text{HH}} = 2$ Hz, H-C=O), 4.43 (dt, 2H, $^2J_{\text{HF}} = 47$ Hz, $^3J_{\text{HH}} = 6$ Hz, $\text{CH}_2\text{-F}$), 2.41 (td, 2H, $^3J_{\text{HH}} = 7$ Hz, $^3J_{\text{HH}} = 2$ Hz (H_{ald}), $\text{CH}_2\text{-C=O}$), 1.62 (m, 4H, 2CH_2), 1.30 (m, 16H, 8CH_2).

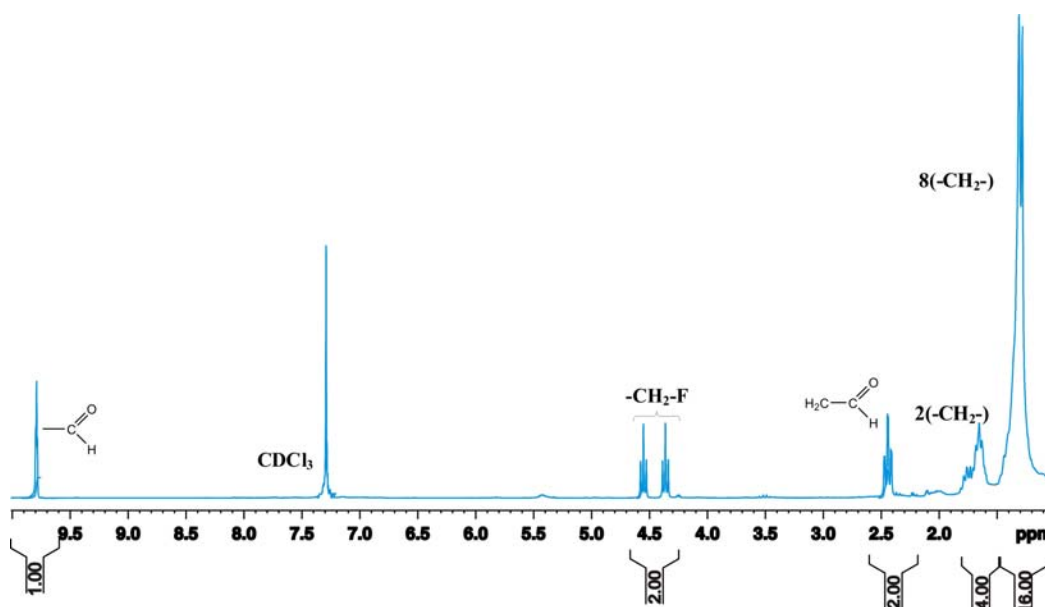


Figure 1.2: ^1H NMR spectrum of unlabeled 12-fluorododecanal.

^{13}C –NMR spectrum (150 MHz for ^{13}C , in CDCl_3 , δ in ppm): 202.76 (s, 1C, -C=O), 83.54 (d, 1C, $^1J_{\text{CF}} = 164$ Hz, $\text{CH}_2\text{-F}$), 43.89 (s, 1C, $\text{CH}_2\text{-C=O}$), 30.41 (d, 1C, $^2J_{\text{CF}} = 19$

Hz, $\text{CH}_2\text{-CH}_2\text{-F}$), 29.71 (s, 1C, CH_2), 29.53 (d, 1C, $^4J_{\text{CF}} = 3$ Hz, $\text{CH}_2\text{-CH}_2\text{-CH}_2\text{-CH}_2\text{-F}$), 29.37 (s, 1C, CH_2), 29.33 (s, 1C, CH_2), 29.21 (s, 1C, CH_2), 29.14 (s, 1C, CH_2), 25.15 (d, 1C, $^3J_{\text{CF}} = 5$ Hz, $\text{CH}_2\text{-CH}_2\text{-CH}_2\text{-F}$), 22.06 (s, 1C, CH_2).

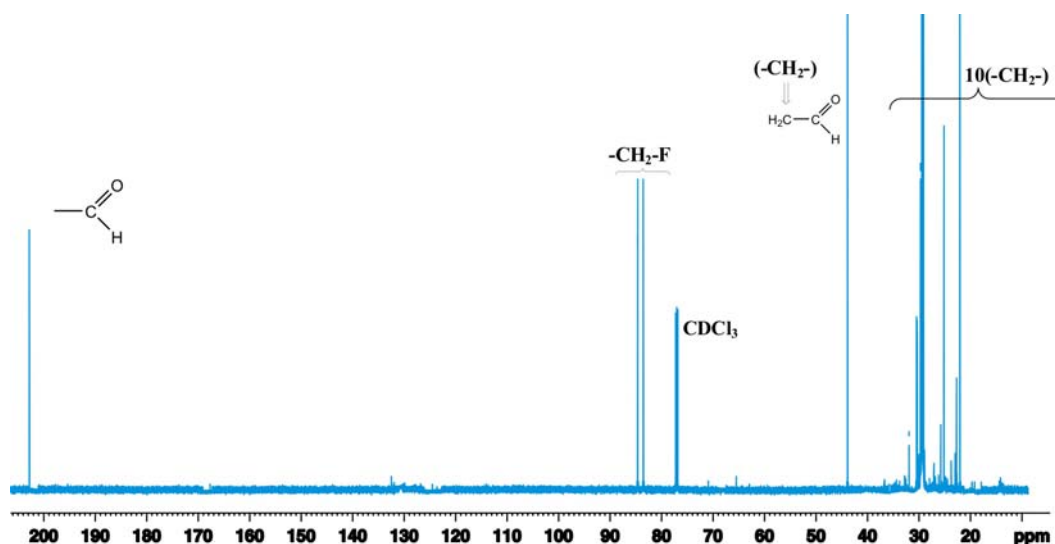


Figure 1.3: ^{13}C NMR spectrum of the unlabeled 12-fluorododecanal

b) NMR analysis of the ^{13}C -labeled 12-fluorododecanal

^1H –NMR spectrum (600 MHz for ^1H , in CDCl_3 , δ in ppm): 9.75 (dd, 1H, $^1J_{\text{CH}} = 169$ Hz, $^3J_{\text{HH}} = 26$ Hz, H-C=O), 4.44 (dtd, 2H, $^1J_{\text{CH}} = 151$ Hz, $^2J_{\text{HF}} = 47$ Hz, $^3J_{\text{HH}} = 7$ Hz, $\text{CH}_2\text{-F}$), 2.45 (ddt, 2H, $^1J_{\text{CH}} = 125$ Hz, $^2J_{\text{CH}} = 10$ Hz, $^3J_{\text{HH}} = 6$ Hz, $\text{CH}_2\text{-C=O}$), 1.55 (m, 20H, 10CH_2).

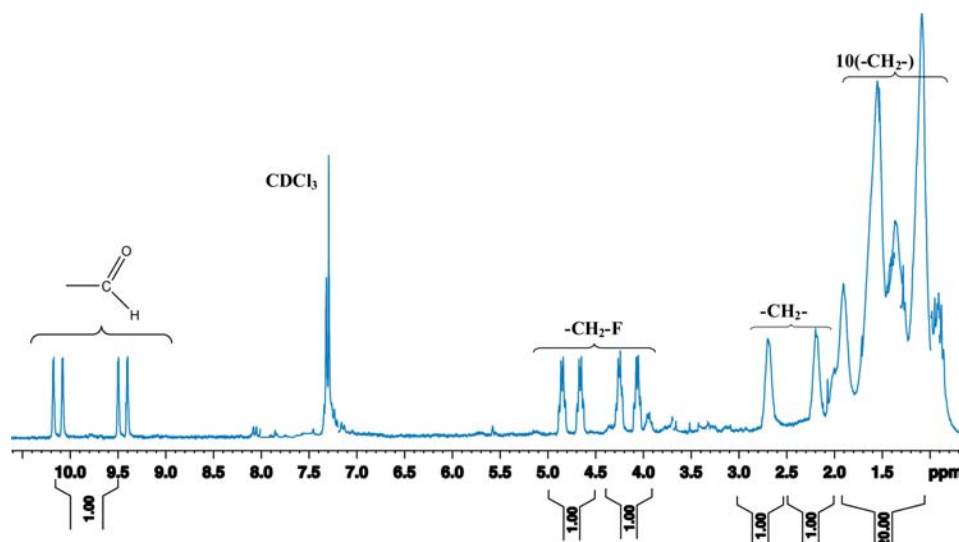


Figure 1.4: ^1H NMR spectrum of ^{13}C -labeled 12-fluorododecanal.

^{13}C -NMR spectrum (150 MHz for ^{13}C , CDCl_3 , δ in ppm): 202.84 (dd, $^1J_{\text{CC}} = 39$ Hz, $^2J_{\text{CC}} = 3$ Hz, 1C, $-\text{C}=\text{O}$), 84.56 (ddd, $^1J_{\text{CF}} = 166$ Hz, $^1J_{\text{CC}} = 38$ Hz, $^2J_{\text{CC}} = 3$ Hz, 1C, $\text{CH}_2\text{-F}$), 44.67 (ddd, $2\times^1J_{\text{CC}} = 39$ Hz, $^2J_{\text{CC}} = 4$ Hz, 1C, $\text{CH}_2\text{-C}=\text{O}$), 30.58 (ddd, $2\times^1J_{\text{CC}} = 39$ Hz, $^2J_{\text{CF}} = 20$ Hz, $^2J_{\text{CC}} = 16$ Hz, 1C, CH_2), 29.40 (m, 6C, 6 CH_2), 25.27 (t, 1C, $2\times^1J_{\text{CC}} = 33$ Hz, CH_2), 22.10 (t, 1C, $2\times^1J_{\text{CC}} = 33$ Hz, $\text{CH}_2\text{-CH}_2\text{-C}=\text{O}$).

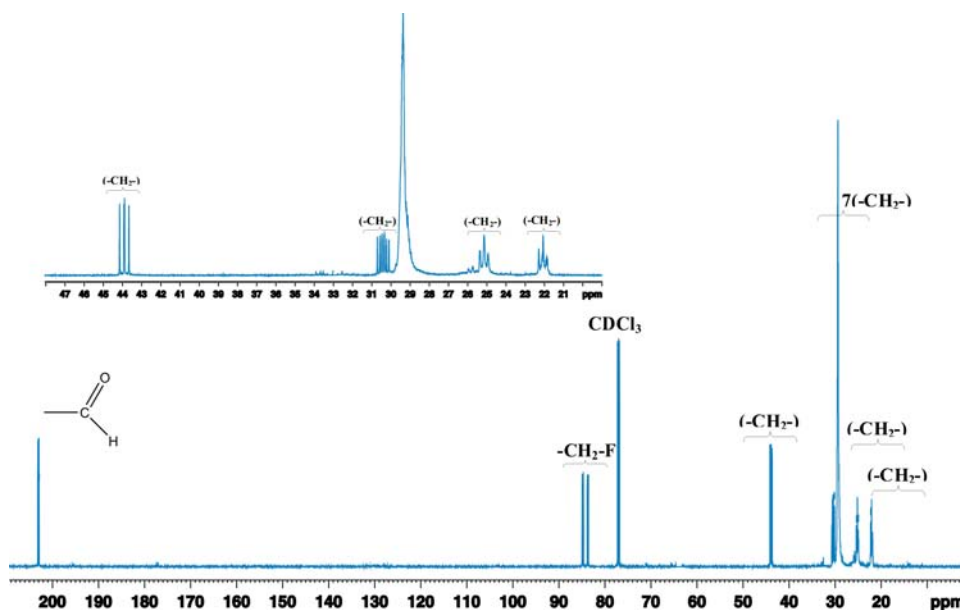


Figure 1.5: ^1H decoupled ^{13}C NMR spectrum of the ^{13}C -labeled 12-fluorododecanal.

The analysis of the 1D NMR spectra (^1H and ^{13}C) clearly showed the signals of the proton (9.75 ppm, s) and carbon (202.84 ppm, s) of the aldehyde function, the signal of the carbon atom bound to the fluorine atom $\text{CH}_2\text{-F}$ (84.56 ppm, for carbon, and 4.44 ppm for proton). However, proton and carbon signals (methylene groups CH_2 at the middle of the molecule) can not be distinguished. The NMR signals of these atoms are overlapped because of their similar chemical environment and multiple couplings which occur between them (multiplets: 1.29 ppm for protons and 29-30 ppm for carbons). Some carbons (22.10 and 25.27 ppm) and protons (~ 1.54 and ~ 1.65 ppm) signals can also be distinguished. The remaining non assigned atoms of the compounds have practically the same chemical environment and thus the chemical shift values are very close. It was therefore difficult to assign a chemical shift to each of them based only on these 1D NMR data. Two dimensional NMR experiments may be probably helpful for a complete assignment of these compounds.

3.2 Two dimensional NMR analysis

After the analysis of the 1D NMR spectra (^1H and ^{13}C) of both unlabeled and ^{13}C -labeled products, 2D NMR experiments were necessary to complete the assignment of these products. Since all the atoms of the ^{13}C -labeled product are magnetically sensitive (^{13}C -labeled atoms), these atoms will be coupled to each other and one would expect broad signals of the “similar” methylene groups of the labeled compounds. Therefore 2D experiments (HSQC and HMBC) were performed only on the unlabeled product.

a) 2D HSQC experiment [21, 22, 23, 24]

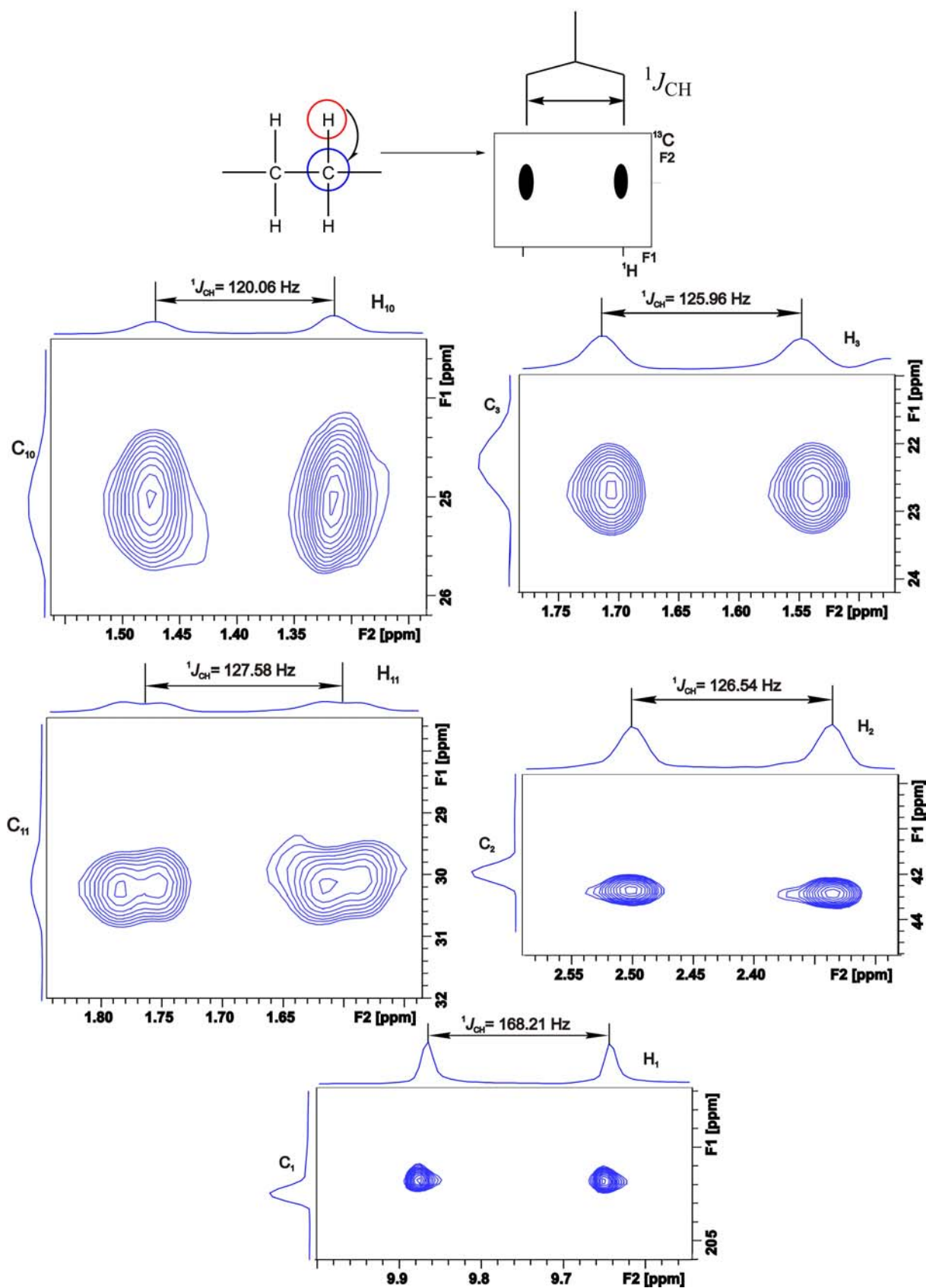
2D HSQC experiments were performed with the unlabeled 12-fluorododecanal in order to determine protons and carbons which are directly bound to each other.

The following cross peaks were observed on the 2D HSQC spectra.

Table 1.1: Tentative assignment of the unlabeled 12-fluorododecanal based on the HSQC NMR experiment.

Position	Group	δ_{C} [ppm]	δ_{H} [ppm]	$^1J_{\text{CH}}$ [Hz]
1	CHO	202.76	9.76	168.21
2	CH ₂	43.89	2.42	126.54
3	CH ₂	22.06	1.63	125.96
4	CH ₂	29.14	1.32 ^a	125.49
5	CH ₂	29.33	1.29 ^a	125.31
6	CH ₂	29.24	1.32 ^a	123.43
7	CH ₂	29.71	1.27 ^a	114.73
8	CH ₂	29.37	1.29 ^a	124.94
9	CH ₂	29.45	1.29 ^a	124.38
10	CH ₂	25.15	1.39	120.06
11	CH ₂	30.41	1.68	127.58
12	CH ₂ -F	83.54	4.42	151.15, 47.75 ($^2J_{\text{HF}}$)

^a These protons could not be explicitly assigned because the ^1H NMR signals around 1.3 ppm were overlapped.



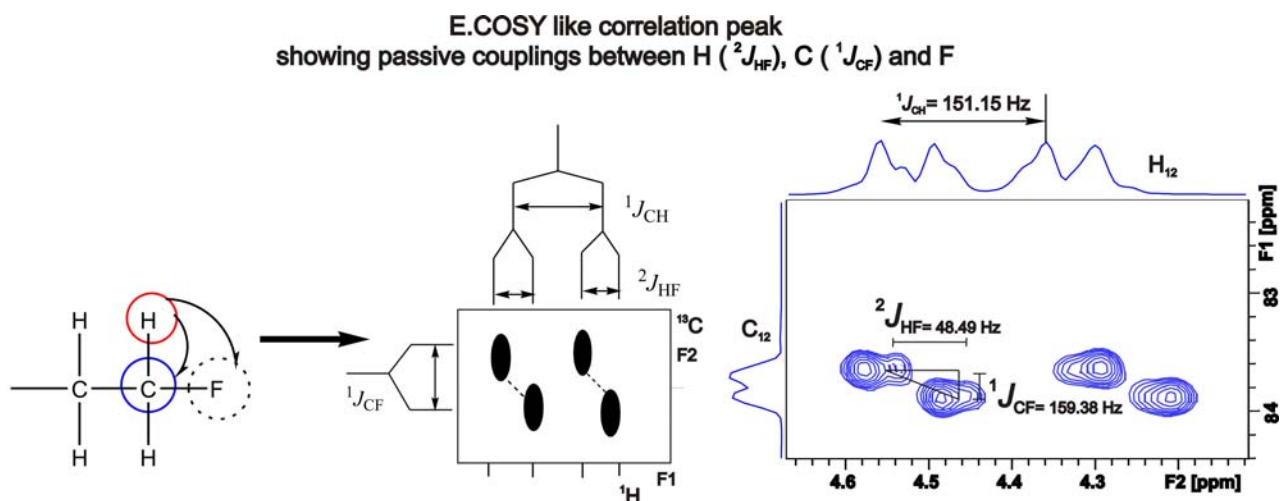


Figure 1.6: 2D HSQC NMR spectrum of the unlabeled 12-fluorododecanal recorded at 750 MHz Bruker AV spectrometer in CDCl_3 .

HQSC experiments were also performed with high resolution in the carbon dimension in order to distinguish the carbons whose chemical shifts are very close (region 29-30 ppm).

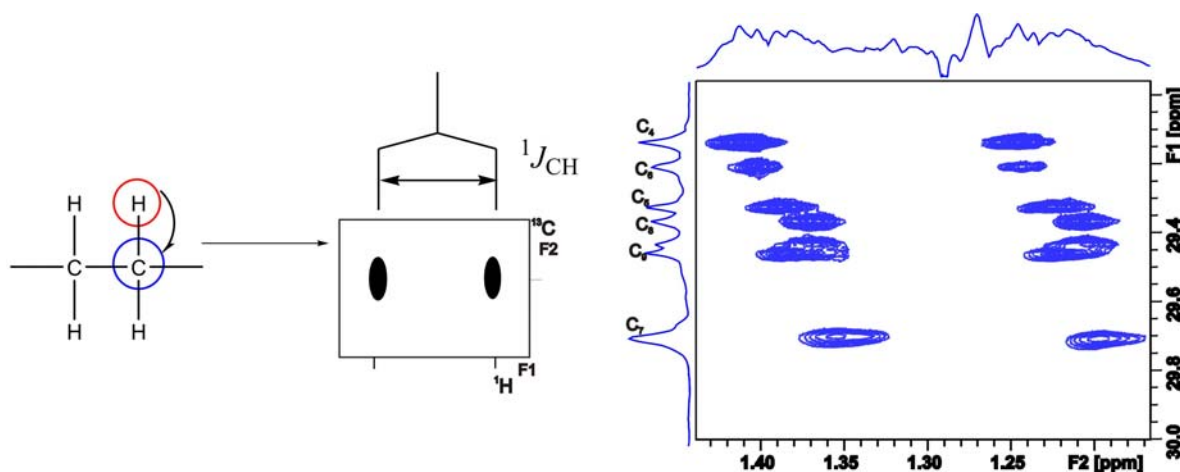


Figure 1.7: High resolution (in carbon dimension) HSQC NMR spectrum of the unlabeled 12-fluorododecanal (expanded region 29-30 ppm) recorded at 750 MHz Bruker AV spectrometer in CDCl_3 .

Based on 1D (^1H and ^{13}C) and 2D HSQC ($^1J_{C-H}$ single coherence) NMR data, the following assignment is proposed for the unlabeled 12-fluorododecanal.

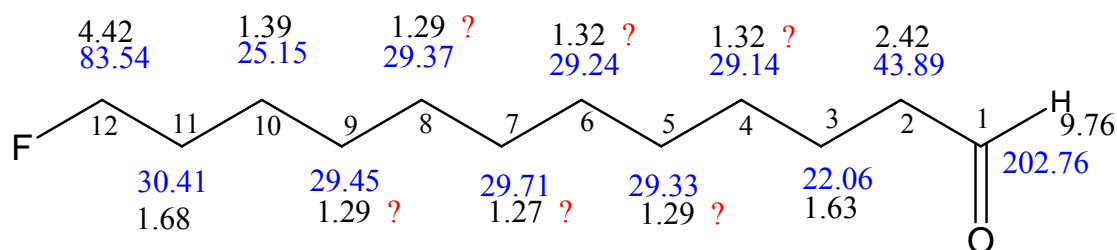


Figure 1.8: One possible assignment of the unlabeled 12-fluorododecanal using single coherence ($^1J_{C-H}$). Black: protons chemical shifts; blue: carbons chemical shifts. Values with a question mark (?) stand for NMR signals which could not be unambiguously assigned.

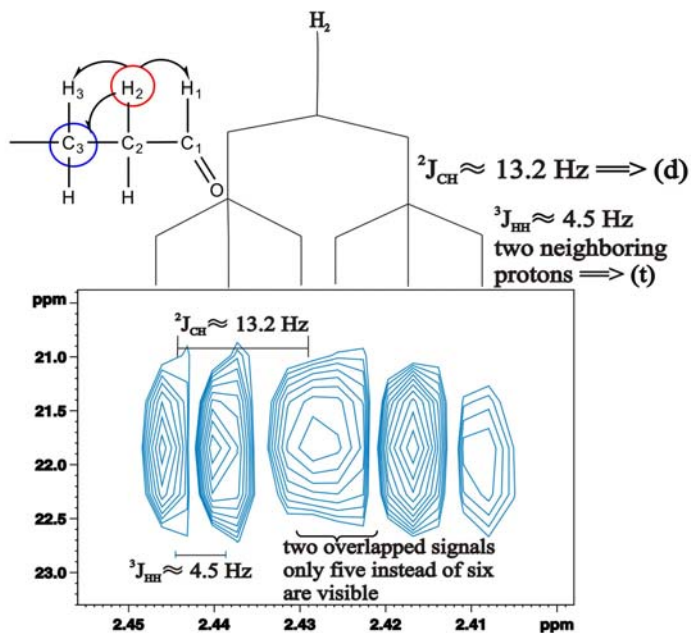
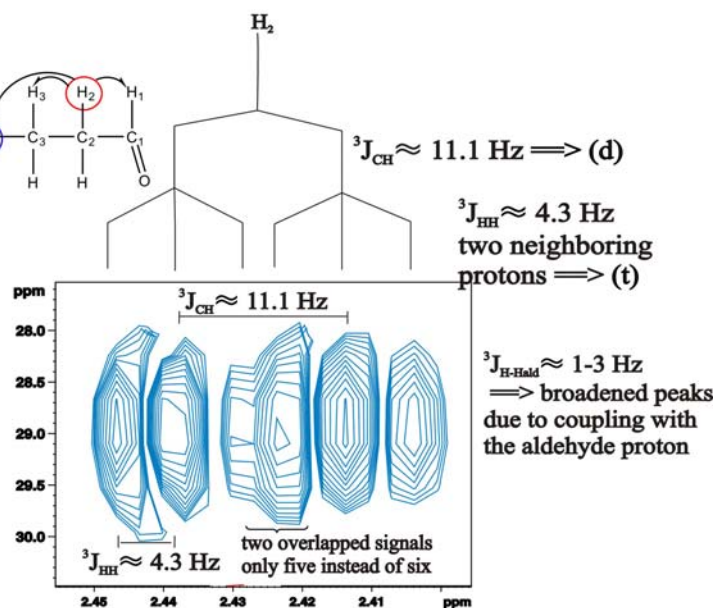
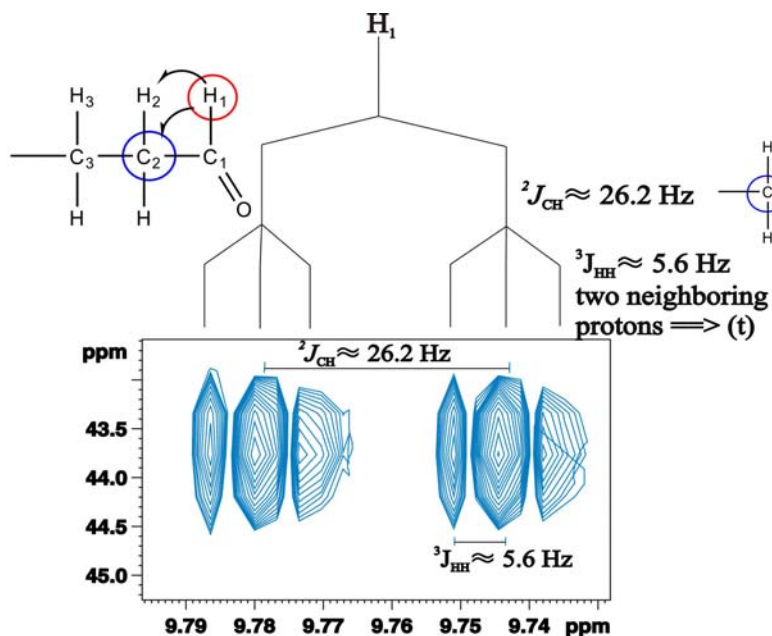
b) 2D HMBC experiment [25, 26]

The complete assignment of the molecule was not still accomplished after 1D and 2D HSQC experiments; therefore 2D HMBC experiment was acquired to detect more correlations between the atoms of the molecule.

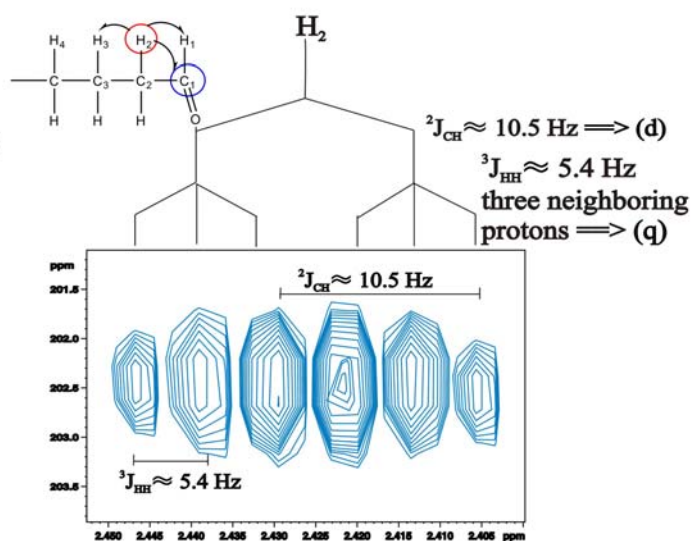
Table 1.2: 2D HMBC NMR data of the unlabeled 12-fluorododecanal in CDCl₃.

Position	Group	δ_C [ppm]	δ_H [ppm]	Multiplicity and J_{CH} [Hz]
1	CHO	202.76	2.42	$^3J_{CH}=10.5$ (d), $^3J_{HH}=5.4$ (q)
			1.62	$^3J_{CH}=13.1$ (d), $^3J_{HH}=6.6$ (p)
2	CH ₂	43.89	9.76	$^2J_{CH}=26.2$ (d), $^3J_{HH}=5.6$ (t)
			1.62	$^2J_{CH}=11.1$ (d), $^3J_{HH}=5.4$ (p)
3	CH ₂	22.06	2.42	$^2J_{CH}=13.2$ (d), $^3J_{HH}=4.5$ (q)
4	CH ₂	29.14	2.42	$^3J_{CH}=11.1$ (d), $^3J_{HH}=4.3$ (q)
5	CH ₂	29.33	-	-
6	CH ₂	29.24	-	-
7	CH ₂	29.71	-	-
8	CH ₂	29.37	-	-
9	CH ₂	29.45	-	-
10	CH ₂	25.15	4.43	$^3J_{CH}=4.6$ (d), $^3J_{HH}=8.3$ (t)
				$^2J_{HF}=47.7$ (d), $^2J_{CF}=19.9$ (d)
11	CH ₂	30.41	4.43	$^2J_{CH}=4.5$ (d), $^3J_{HH}=8.3$ (t)
				$^2J_{HF}=47.7$ (d), $^1J_{CF}=163.9$ (d)
12	CH ₂ -F	83.54	1.39	$^3J_{CH}=4.4$ (d), $^3J_{HH}=8.5$ (p)
			1.68	$^3J_{CH}=13.1$ (d), $^3J_{HH}=4.4$ (p)
				$^3J_{HF}=11.0$ (d), $^1J_{CF}=163.9$ (d)

Overlapped ¹H and ¹³C NMR signals could not permit a complete assignment of the molecule. The observed HMBC correlations are presented on the figures below.



$^3J_{H-Hald} \approx 1-3 \text{ Hz}$ too small \Rightarrow peaks are broader due to the coupling with the aldehyde proton



$^3J_{H-Hald} \approx 1-3 \text{ Hz}$ too small \Rightarrow peaks are broader due to the coupling with the aldehyde proton

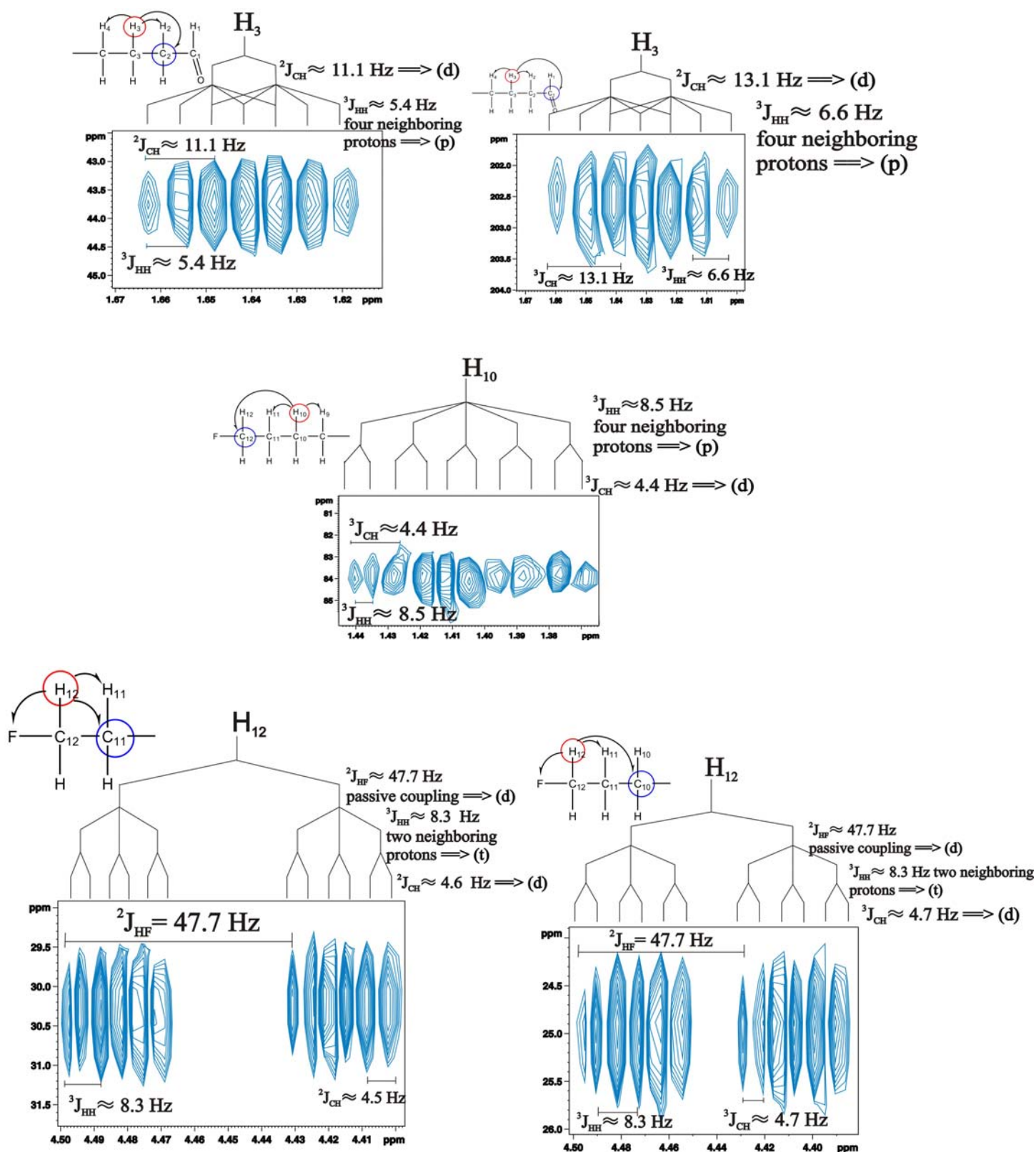


Figure 1.9: 2D HMBC NMR Spectrum of 12-fluorododecanal in CDCl_3 (some expanded peaks) recorded at 750 MHz Bruker AV spectrometer in CDCl_3 .

Based on the 2D HMBC, the previous 1D and 2D HSQC NMR data, the following assignment is proposed for the unlabeled 12-fluorododecanal. Although these spectra were recorded at high resolution, all correlations could not be clearly elucidated due to overlapped ^1H NMR signals.

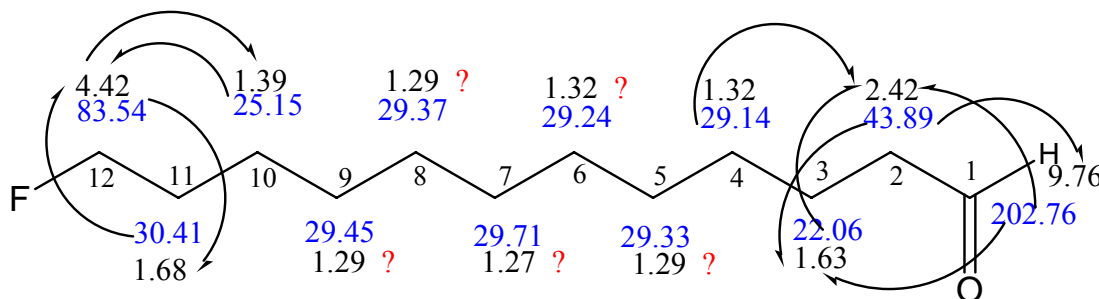


Figure 1.10: One possible assignment of the unlabeled 12-fluorododecanal showing some 2D HMBC correlations. Assignment was made based on 1D (^1H and ^{13}C) and 2D (HSQC, HMBC) NMR experiments. The middle carbon atoms could not be explicitly assigned because of their closely chemical shifts. The correlation between the carbon at 29.14 ppm and its neighboring protons (2.42 ppm) was also observed.

Besides the 1D NMR experiments (^1H and ^{13}C) performed with the ^{13}C -labeled compound, some C-C TOCSY experiments [27, 28] were also recorded with mixing times from $d_0=15$ and 170 ms (from $\sim 1/(2J)$ to $12 \times 1/(2J)$, for $^1J_{\text{CH}} = 35$ Hz) intent to cover the length of the molecule. The C-C TOCSY experiment with long mixing time ($d_0 = 170$ ms) showed a cross peak between the carbons C_{12} (84.56 ppm) and C_2 (44.67 ppm) i.e. between the $-\text{CH}_2\text{-F}$ and the $-\text{CH}_2$ adjacent to the carbonyl. There was no perceptible cross peak between the carbonyl and the carbon bound to the fluorine atom (two ends of the chain). An explanation could be the fact that the carbonyl carbon, which has a weak signal compared to other carbons, also relaxes very slowly ($T_1 \geq 20$ s). Therefore, the carbonyl signal was not perceptible during the acquisition time (total delay shorter than the relaxation time of the carbonyl, in this case the acquisition time was about 2.5 s and $d_1 = 2$ s). For practical reasons, TOCSY experiments with longer delay ($d_1 \sim 5T_1$ i.e. ≥ 60 s) which should have covered the whole bandwidth were not performed.

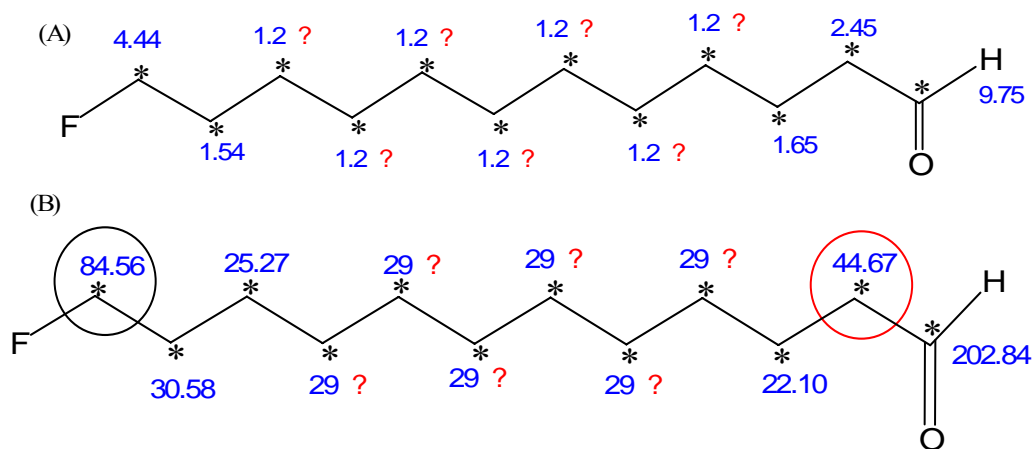


Figure 1.11: Tentative assignment of the ¹³C-labeled 12-fluorododecanal molecule. (A) ¹H assignment. (B) ¹³C assignment. The star (*) stands for the ¹³C-labeled carbon atom. Due to the overlap of ¹H and ¹³C NMR signals the assignment was only partially accomplished. The question mark (?) stands for the unresolved chemical shifts.

The C-C TOCSY cross peak observed on the experiment with long mixing time representing the correlation between the two carbons at the extrmities of the ¹³C-labeled molecule (surrounded atoms at 44.67 and 84.56 ppm on the Figure 1.11) as well as the full TOCSY spectrum are presented below.

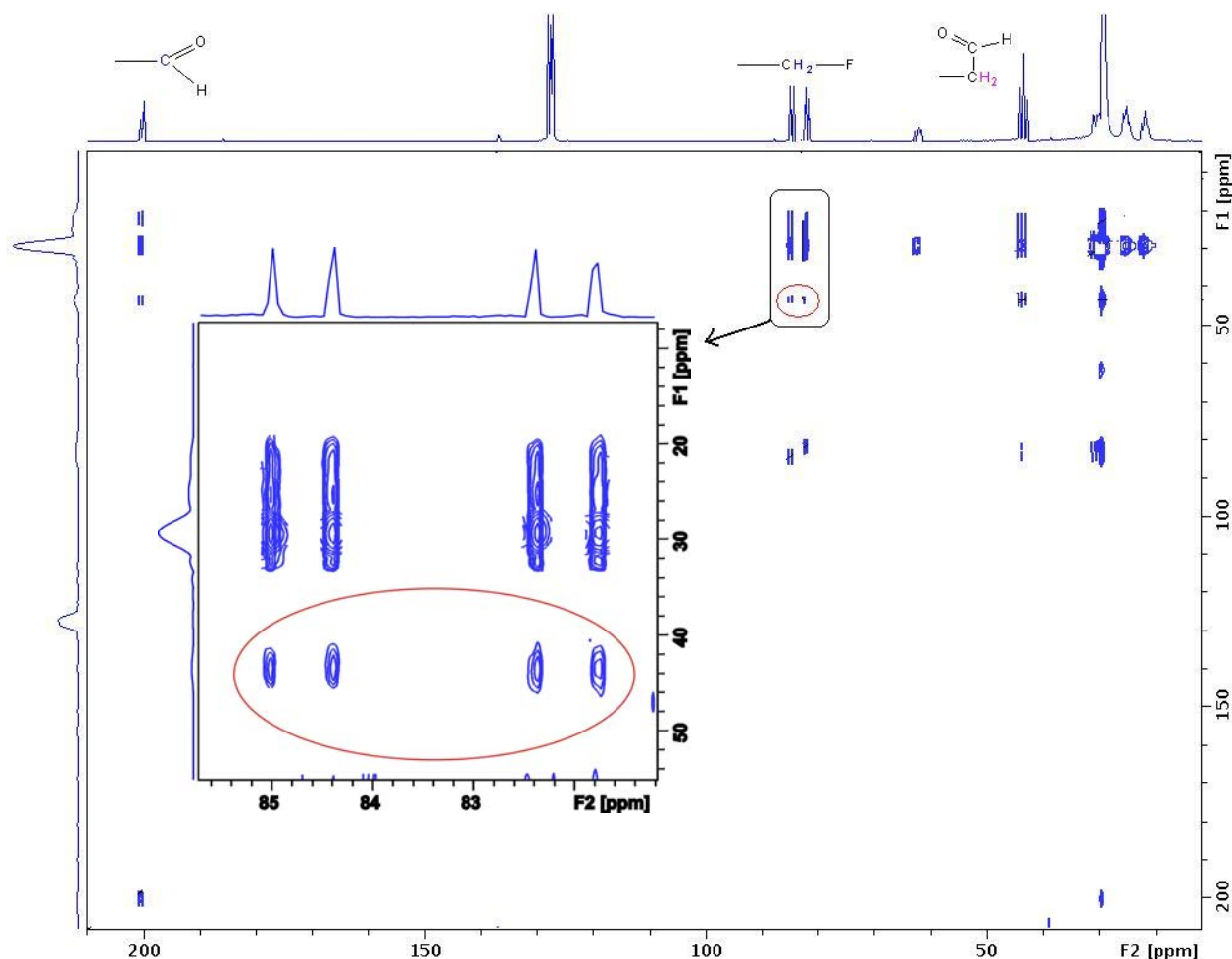


Figure 1.12: 2D C-C TOCSY of the ^{13}C -labeled fluorododecanal with ^1H decoupled and mixing time $d_9 = 170$ ms. Spectrum recorded at 250 MHz Bruker AV spectrometer in C_6D_6 .

CONCLUSION AND PERSPECTIVES

Our aim of designing and synthesizing the desired (spin chain) compound has been fully achieved. In fact, both products, unlabeled and ^{13}C -labeled 12-fluorododecanal, were obtained with a satisfactory purity as proved by the recorded NMR spectra. However, the next step i.e. the sample preparation and the implementation of quantum computing experiments using the ^{13}C -labeled compound could not be realized due to the strong coupling between the carbon atoms because of the poor resolution of the different NMR spectra. Consequently, the qubit system (i.e the nuclei: twelve ^{13}C and one ^{19}F) required for quantum computing experiments could not be clearly identified and moreover, most of these nuclei (carbons) are strongly coupled. An alternative had to be found in order to alter the chemical shifts of the middle carbon atoms, first of the unlabeled (which easier

to manipulate) and later of the ^{13}C -labeled 12-fluorododecanal products which the expectation of changing the strong couplings to weak couplings. Quantum computing experiments will be implemented if the coupling problem is solved.

4. EXPERIMENTAL SECTION

4.1 Materials and Methods

TLC-monitoring was performed on Merck DC silica gel plates (60 F-254 on aluminum foil). Spots were detected by UV-absorption at 254 nm and/or 366 nm and with Mo-stain (6.25 g phosphomolybdic acid, 2.5 g cerium-(IV)-sulfate and 15 mL sulfuric acid in 235 mL water) or potassium permanganate (5% in 1N aq. NaOH).

All technical solvents were distilled prior to use or purchased as anhydrous solvents. Reagents were purchased from *Merck*, *Fluka*, *Sigma Aldrich*, *VWR*, *Molekula* or *Acros* and were used without purifications.

^{13}C -labeled starting material was purchased from *Campro Scientific*, and *Isotec*.

Flash column chromatography was performed using silica gel 60 (63-200 μm) from *Merck* at 1-1.5 atm pressure using a Büchi Pump Manager C-615 apparatus.

^1H -NMR and ^{13}C -NMR spectra were recorded at 298K on a 600 MHz Bruker Avance, 500 MHz Bruker AV, or a 250 MHz Bruker AC spectrometer. Chemical shifts (δ) are given in *parts per million* (ppm) relative to Trimethylsilane (TMS).

The following solvent peaks were used as internal standards:

Benzene- d_6 : 7.16ppm (^1H -NMR) and 128.4ppm (^{13}C -NMR); CHCl_3 : 7.26ppm (^1H -NMR) and 77.0ppm (^{13}C NMR).

Acquisition and processing were performed and analyzed using Bruker software TOPSPIN 2.0, 2.1 or 3.03. Sequential assignment was accomplished by through-bond connectivities from Heteronuclear Multiple Bond Correlation (HMBC) and Heteronuclear Single Quantum Coherence (HSQC) spectra. Total Correlation Spectroscopy (TOCSY) spectra were recorded with mixing times between 15 ms and 170 ms.

4.2 Synthesis and description of the unlabeled compound

4.2.1 Reduction of 1,12-dodecanedioic acid to 1,12-dodecanediol using Lithium Aluminum hydride (LiAlH₄) [4].

1,12-dodecanedioic acid (10 g, 0.043 mol), white powder, was introduced into a 250 mL round-bottom flask with a magnetic stirrer and dried; LiAlH₄ (3.3 g, 0.086 mol, 2eq), a violet powder, in a 1 L round-bottom was also treated by the same method. After 1.5 h, 160 mL and 215 mL of Tetrahydrofuran were added to the dried powders (dodecanedioic acid and LiAlH₄ respectively) and stirred for about 30 min at room temperature. The solution of dodecanedioic acid was then slowly added to the LiAlH₄ suspension at 0°C. After stirring for 3 h at room temperature, the mixture was poured into a solution of Sodium Potassium tartrate (100 g in 200 mL H₂O) at 0°C, stirring for 2 h at room temperature. The dark violet solution became colorless, and was poured into a separatory funnel and extracted with ether. The organic layer was washed with brine, dried with Na₂SO₄ and evaporated in vacuum to give the 1,12-dodecandiol as a white solid (8.5 g, 97 %).

NMR analysis of the unlabeled 1,12-dodecandiol

¹H-NMR spectrum (250 MHz for ¹H, in CDCl₃, δ in ppm): 3.67 (t, ³J_{HH} = 6.6 Hz, 4H, 2CH₂), 1.58 (p, ³J_{HH} = 6.6 Hz, 4H, 2CH₂), 1.30 (m, 16H, 8CH₂).

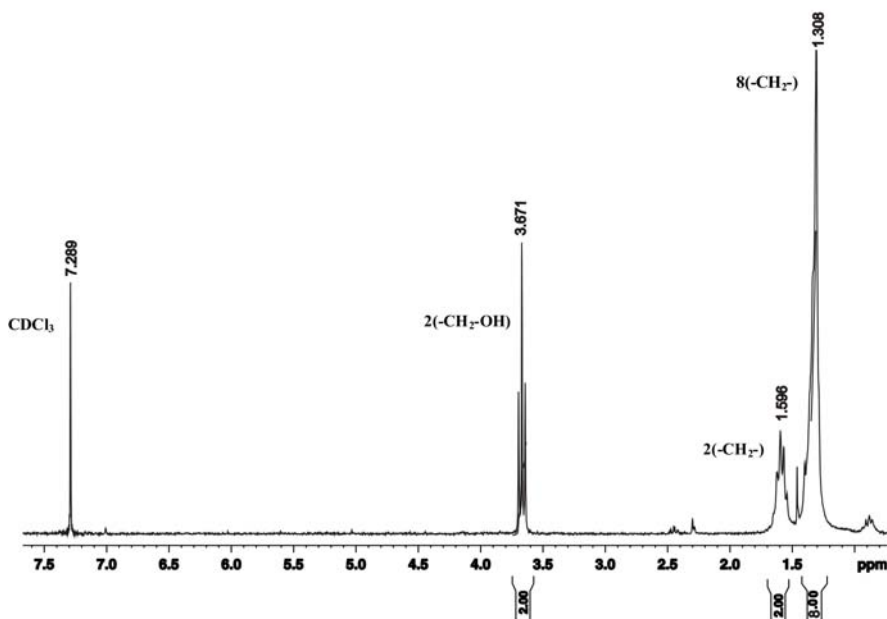


Figure 1.13: ¹H NMR spectrum of the unlabeled 1,12-dodecandiol.

^{13}C -NMR spectrum (62.5MHz for ^{13}C , in CDCl_3 , δ in ppm): 25.74 (s, 2C, 2CH₂), 29.42 (s, 2C, 2CH₂), 29.55 (s, 2C, 2CH₂), 29.59 (s, 2C, 2CH₂), 32.82 (s, 2C, 2CH₂), 63.12 (s, 2C, 2CH₂).

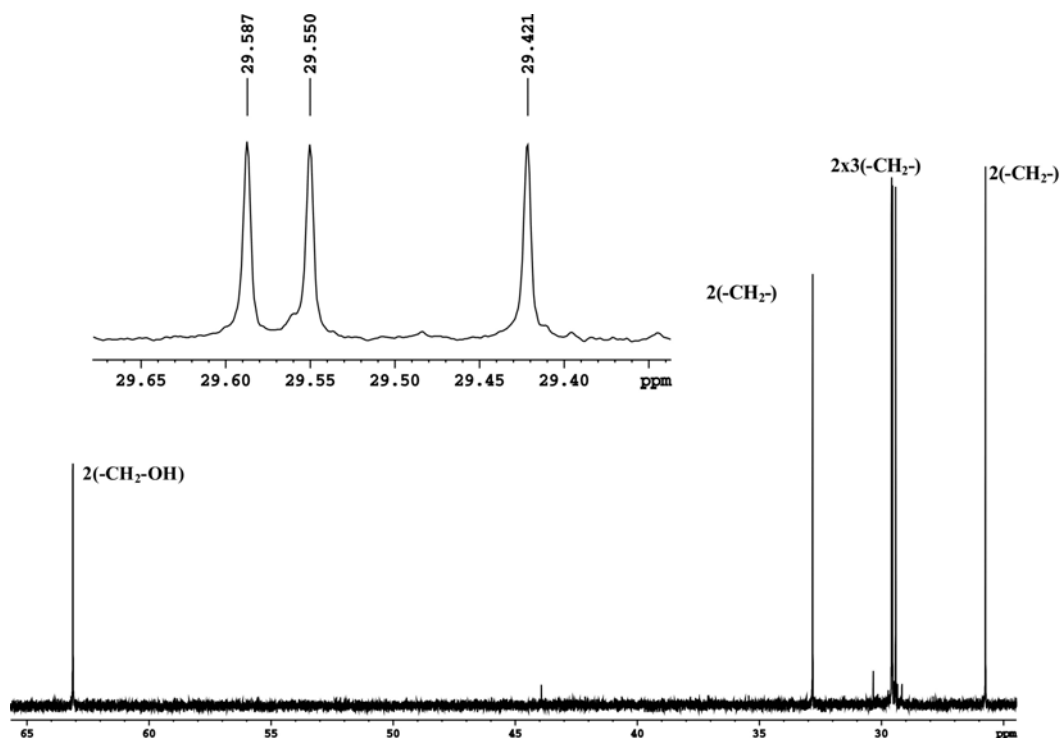


Figure 1.14: ^{13}C NMR spectrum of the unlabeled 1,12-dodecanediol.

4.2.2 Monotritylation of 1,12-dodecanediol using Triphenylmethyl Chloride (Trityl chloride or TrCl) [12]

1,12-dodecanediol (1 g, 4.94 mmol), white powder, in a 50 mL round-bottom flask and Triphenylmethyl chloride (Trityl chloride) (1.51g, 5.43 mmol, 1.1eq) in a 10 mL flask were dried. After 90 min, 5 mL CH_2Cl_2 were added to Trityl chloride and 10 mL DMF/ CH_2Cl_2 (1:1) were added to 1,12-dodecanediol and stirred for about 30 min at room temperature. Triethylamine (Et_3N) (2 mL, 14.83 mmol, 3eq) and 4-dimethylaminopyridine (DMAP) (127 mg, 0.98 mmol, 0.2eq) was added to the solution of 1,12-dodecanediol before the addition of trityl chloride solution and stirred for 3 hours at room temperature. The mixture was then concentrated under reduced pressure. The crude product (2.9 g) was dissolved in Chloroform/Methanol and purified by flash chromatography on silica gel ($\text{MeOH}/\text{CHCl}_3$ 0:100) to yield 1,12-

di(triphenylmethoxy)dodecane (678.5 mg, 0.98 mmol, 20 %) and (MeOH/CHCl₃ 1:100) to obtain 12-(triphenylmethoxy)dodecan-1-ol (855 mg, 1.99 mmol, 40 %) as a slight yellow oil. With a more polar system of MeOH/CHCl₃, gradient 3:100 to 5:100, the 1,12-dodecanediol was also recovered (300 mg, 1.48 mmol, 30 %).

NMR analysis of the unlabeled 12-(triphenylmethoxy)dodecan-1-ol

¹H –NMR spectrum (250 MHz for ¹H, in CDCl₃, δ in ppm): 7.48 (d, ²J_{HH} (ortho)= 8.1 Hz, 6H, H_{arom}), 7.33 (m, 9H, H_{arom}), 3.67 (t, ³J_{HH}= 6.6 Hz, 2H, CH₂), 3.09 (t, ³J_{HH}= 6.6 Hz, 2H, CH₂), 1.64 (m, 4H, 2CH₂), 1.35 (m, 16H, 8CH₂).

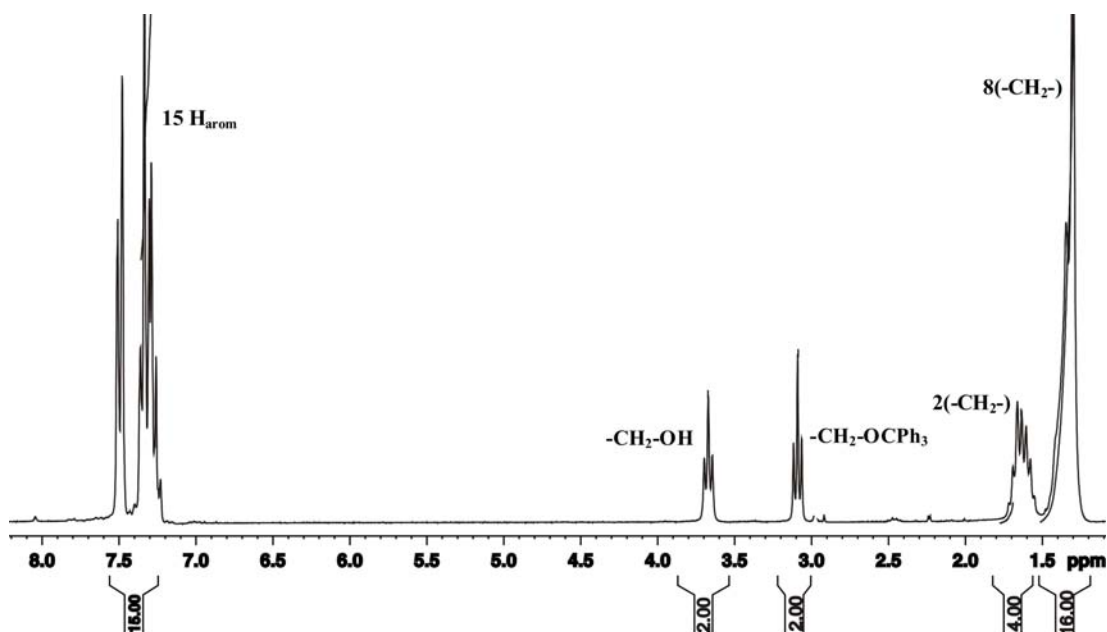


Figure 1.15: ¹H NMR spectrum of the unlabeled 12-(triphenylmethoxy)dodecan-1-ol.

¹³C–NMR spectrum (62.5MHz for ¹³C, in CDCl₃, δ in ppm): 144.67 (s, 3C, C_{quaternary}, C_{arom}), 127.20 (d, 12C, C_{arom}), 126.21 (s, 3C, C_{arom}), 86.33 (s, 1C, -O-CPh₃, C_{quaternary}), 63.75 (s, 1C, CH₂-OCPh₃), 63.06 (s, 1C, CH₂-OH), 32.83 (s, 1C, CH₂), 30.09 (s, 1C, CH₂), 29.67 (s, 5C, CH₂), 29.46 (s, 1C, CH₂), 26.31 (s, 1C, CH₂), 25.79 (s, 1C, CH₂).

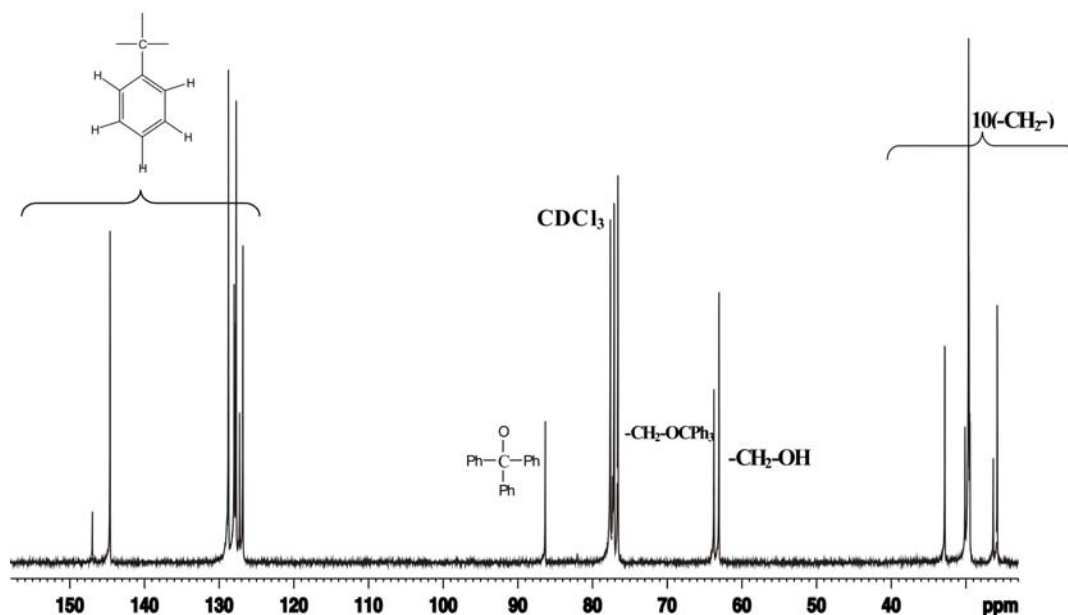


Figure 1.16: ^{13}C NMR spectrum of the unlabeled 12-(triphenylmethoxy)dodecan-1-ol.

4.2.3 Fluorination of 12-triphenylmethanododecan-1-ol using DAST (DiethylAminoSulfur Trifluoride) [15, 16].

500 mg of 12-(triphenylmethoxy)dodecan-1-ol (1.12 mmol) in a 25 mL round-bottom flask was dried. After 1 h it was dissolved in 10 mL CH_2Cl_2 and Diethylaminosulfur trifluoride (448 μL , 3.37 mmol, 3eq) was added under Argon. The mixture was stirred at room temperature for 24 hours and the solvent was removed under reduced pressure. The crude product was dissolved in CHCl_3 and purified by flash chromatography on silica gel (CHCl_3 100 %) to yield 1-fluoro-12-(triphenylmethoxy)dodecane (305 mg, 0.68 mmol, 61 %) as a light brown oil. Elution with $\text{MeOH}/\text{CHCl}_3$ 1:100 allowed to recover the 12-(triphenylmethoxy)dodecan-1-ol (166 mg, 0.37 mmol, 33 %).

NMR analysis of the unlabeled 1-fluoro-12-(triphenylmethoxy)dodecane

^1H -NMR spectrum (250 MHz, in CDCl_3 , δ in ppm): 7.48 (d, $^2J_{\text{HH}}$ (ortho)= 8.1 Hz, 6H, H_{arom}), 7.33 (m, 9H, H_{arom}), 4.48 (dt, 2H, $^2J_{\text{HF}}$ = 47.7 Hz, $^3J_{\text{HH}}$ = 5.6 Hz, $\text{CH}_2\text{-F}$), 3.09 (t, $^3J_{\text{HH}}$ = 6.6 Hz, 2H, $\text{CH}_2\text{-O-CPh}_3$), 1.66 (m, 4H, 2CH_2), 1.31 (m, 16H, 8CH_2).

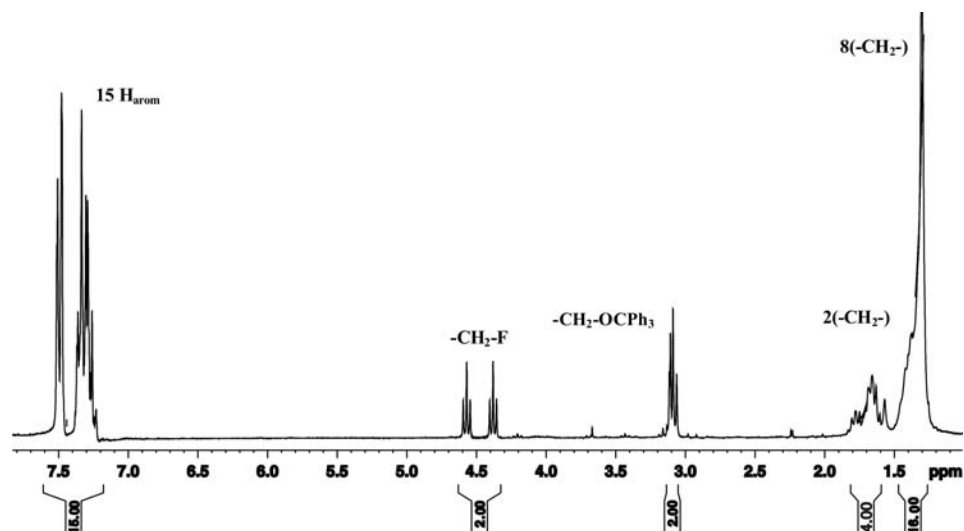


Figure 1.17: ^1H NMR spectrum of the unlabeled 1-fluoro-12-(triphenylmethoxy)dodecane.

^{13}C -NMR spectrum (62.5MHz for ^{13}C , in CDCl_3 , δ in ppm): 144.59 (s, 3C, $\text{C}_{\text{quaternary}}$, C_{arom}), 127.20 (d, 12C, C_{arom}), 126.21 (s, 3C, C_{arom}), 86.30 (s, 1C, -O-CPh₃, $\text{C}_{\text{quaternary}}$), 84.24 (d, 1C, $^1J_{\text{CF}} = 162$ Hz, $\text{CH}_2\text{-F}$), 63.72 (s, 1C, $\text{CH}_2\text{-OH}$), 30.59 (s, 1C, CH_2), 30.18 (d, 1C, CH_2), 29.58 (s, 5C, CH_2), 29.53 (s, 1C, CH_2), 26.29 (s, 1C, CH_2), 25.16 (d, 1C, CH_2).

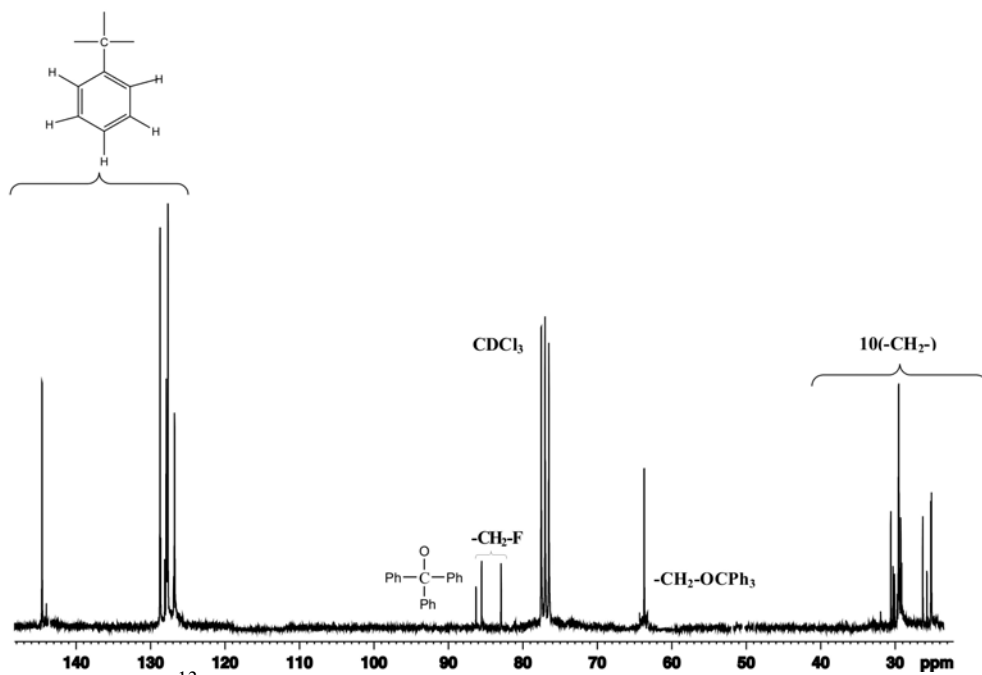


Figure 1.18: ^{13}C NMR spectrum of the unlabeled 1-fluoro-12-(triphenylmethoxy)dodecane.

4.2.4 Deprotection using Triethyl-Silyl Triflate/Triethylsilane and Tetra-*n*-butylammonium fluoride (TBAF) [18, 19].

Triethylsilane (107 μ L, 0.67 mmol, 1.2eq) and triethylsilyl triflate (65 μ L, 0.28 mmol, 0.5eq) were added to 250 mg of 1-fluoro-12-triphenylmethoxydodecane (0.56 mmol) in CH_2Cl_2 at room temperature. The resulting orange solution was stirred until the color disappeared after 5 min. The mixture was concentrated to dryness. The residue was then treated with 500 μ L, (0.84 mmol, 1.5eq) of 1.0 mmol/L TBAF in THF for 3 h at room temperature and the solvent was removed under reduced pressure. The crude product was dissolved in MeOH/ CHCl_3 and purified by flash chromatography on silica gel with CHCl_3 100 % to yield the recovery of 1-fluoro-12-(triphenylmethoxy)dodecane (50 mg, 0.11 mmol, 20 %) and MeOH/ CHCl_3 1:100, to obtain 12-fluoro-dodecan-1-ol (80.47 mg, 0.39 mmol, 70 %) as light yellow oil.

NMR analysis of the unlabeled 12-fluorododecan-1-ol

^1H –NMR spectrum (250 MHz for ^1H , in CDCl_3 , δ in ppm): 4.48 (dt, 2H, $^2J_{\text{HF}} = 47.7$ Hz, $^3J_{\text{HH}} = 5.6$ Hz, $\text{CH}_2\text{-F}$), 3.67 (t, $^3J_{\text{HH}} = 6.6$ Hz, 2H, $\text{CH}_2\text{-OH}$), 1.60 (m, 4H, 2CH_2), 1.30 (m, 16H, 8CH_2).

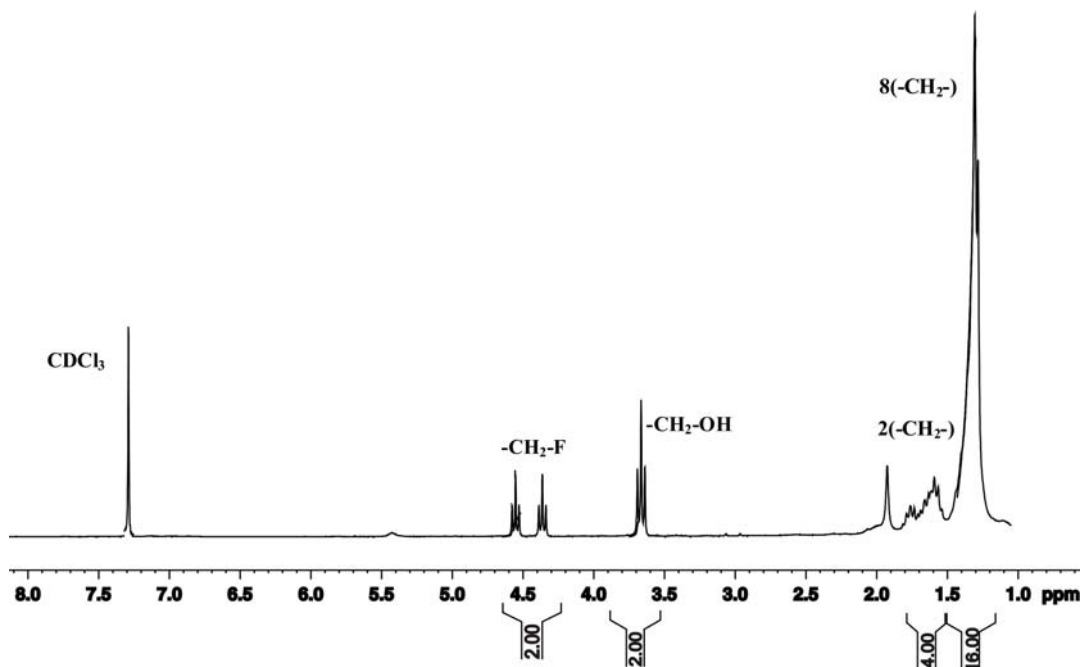


Figure 1.19: ^1H NMR spectrum of the unlabeled 12-fluorododecan-1-ol.

^{13}C -NMR spectrum (62.5MHz for ^{13}C , in CDCl_3 , δ in ppm): 84.24 (d, 1C, $^1J_{\text{CF}} = 163.8$ Hz, $\text{CH}_2\text{-F}$), 63.14 (s, 1C, $\text{CH}_2\text{-OH}$), 32.75 (s, 1C, CH_2), 30.42 (d, 1C, CH_2), 29.71 (s, 1C, CH_2), 29.58 (s, 1C, CH_2), 29.54 (s, 1C, CH_2), 29.50 (d, 1C, CH_2), 29.42 (s, 1C, CH_2), 29.24 (s, 1C, CH_2), 25.73 (s, 1C, CH_2), 25.15 (d, 1C, CH_2).

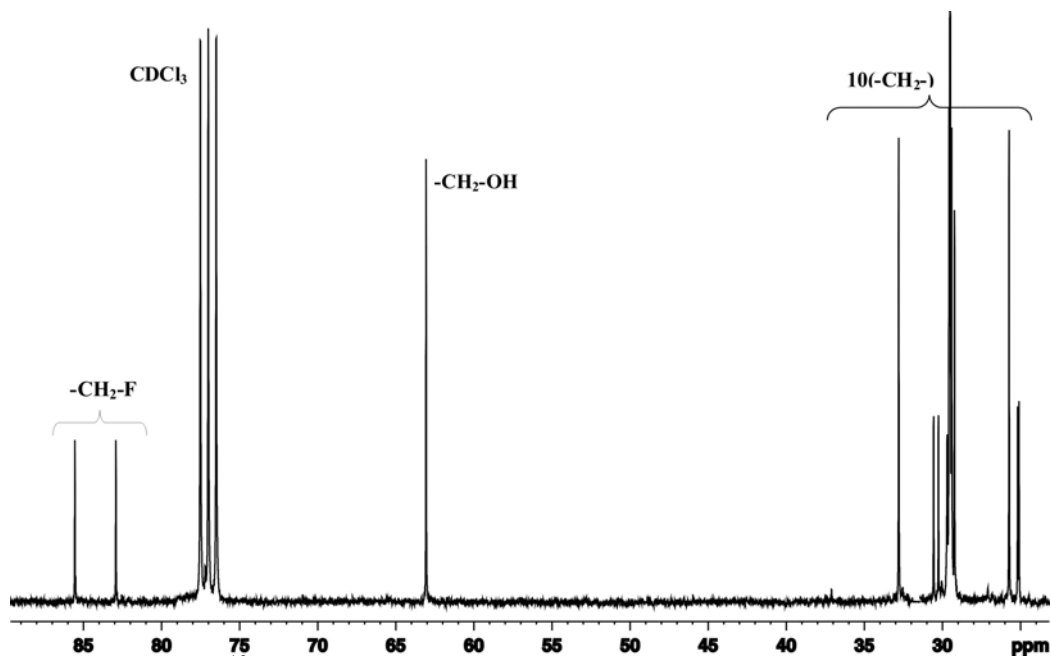


Figure 1.20: ^{13}C NMR spectrum of the unlabeled 12-fluorododecan-1-ol.

4.2.5 Oxidation of 12-fluoro-dodecan-1-ol using DMP (Dess-Martin Periodinane) [20]

80 mg (0.39 mmol) of dried 12-fluoro-dodecan-1-ol in 5 mL CH_2Cl_2 was added to Dess-Martin Periodinane (199 mg, 0.47 mmol, 1.2eq) in 10 mL CH_2Cl_2 . The mixture was stirred at room temperature. After 20min the mixture was diluted with 10 mL of diethylether and quenched with aqueous 1N NaOH. The aqueous layer was extracted three times with diethylether. The combined organic layers were subsequently washed with H_2O and dried over anhydrous sodium sulfate. Removal of the solvent and evaporation under reduced pressure gave pure 12-fluoro-dodecan-1-al (70 mg, 0.35 mmol, 88 %) as light yellow oil.

4.3 Synthesis and description of the ^{13}C -labeled compound

The same procedure used for the synthesis of the non labeled compound was also applied here to synthesize our ^{13}C -labeled compound. The ^{13}C -labeled material has reacted in almost the same way as the unlabeled one apart from some differences observed in the yields of the reactions.

4.3.1 Reduction of ^{13}C dodecanedicarboxylic acid to ^{13}C -labeled dodecanediol using lithium aluminum hydride (LiAlH_4) [4]

LiAlH_4 (330 mg, 8.684 mmol, 4eq) was added to 500 mg (2.17 mmol) of ^{13}C -labeled dodecanedioic acid and the desired ^{13}C -labeled 1,12-dodecanediol was obtained with 97 % yield (425 mg, 2.1 mmol).

For NMR spectra and analysis details of the ^{13}C -labeled compound see Section 3.1 a).

NMR analysis of ^{13}C -labeled 1,12-dodecandiol

^1H -NMR spectrum (250 MHz, in CDCl_3 , δ in ppm): 3.68 (d, $^1J_{\text{CH}} = 140.5$ Hz, 4H, $2\text{CH}_2\text{-OH}$), 1.35 (m, 20H, 10CH_2).

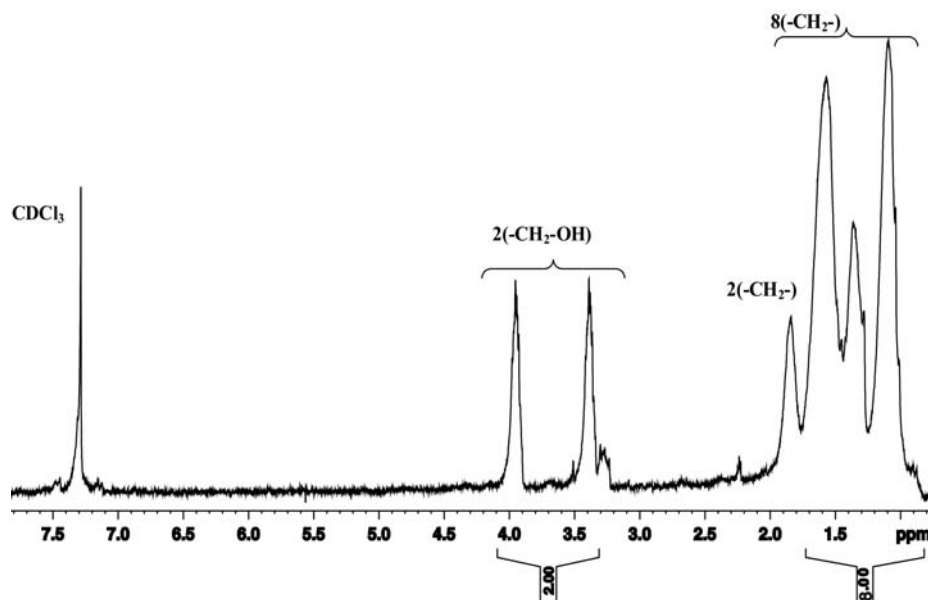


Figure 1.21: ^1H NMR spectrum of the ^{13}C -labeled 1,12-dodecandiol.

^{13}C -NMR spectrum (62.5 MHz for ^{13}C , in CDCl_3 , δ in ppm): 63.17 (d, $^1J_{\text{CC}} = 37.1$ Hz, 2C, 2 $\text{CH}_2\text{-OH}$), 32.82 (t, $^1J_{\text{CC}} = 35.5$ Hz, 2C, 2 CH_2), 29.60 (m, 6C, 2 CH_2), 25.74 (m, 2C, 2 CH_2).

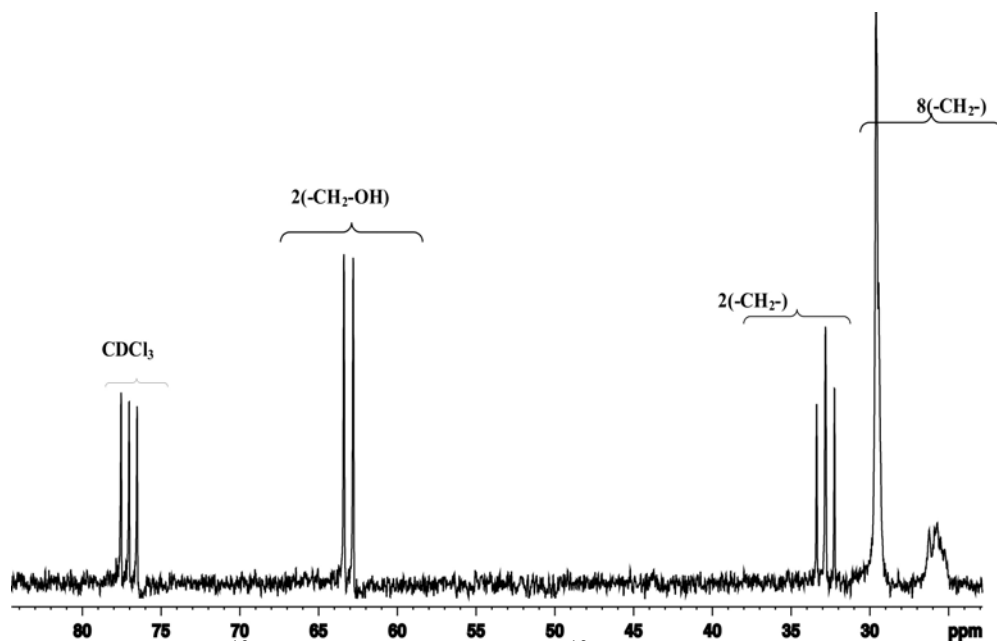


Figure 1.22: ^{13}C NMR spectrum of the ^{13}C -labeled 1,12-dodecanediol.

4.3.2 Monotritylation of ^{13}C -labeled 1,12-dodecanediol using Triphenylmethane Chloride (Trityl chloride or TrCl) [12].

300 mg (1.48 mmol) of ^{13}C -labeled 1,12-dodecanediol was used together with TrCl (456 mg, 1.63 mmol, 1.1eq), Et_3N (620 μL , 4.45 mmol, 3eq) and DMAP (38 mg, 0.3 mmol, 0.2eq) to yield the desired product i.e. 12-(triphenylmethoxy)dodecan-1-ol (210 mg, 0.47 mmol, 32 %), the side product 1,12-di(triphenylmethoxy)dodecane (445 mg, 0.65 mmol, 44 %) and the recovery of 1,12-dodecanediol (55 mg, 0.27 mmol, 18 %).

NMR analysis of ^{13}C -labeled 12-(triphenylmethoxy)dodecan-1-ol

^1H -NMR spectrum (250 MHz for ^1H , in CDCl_3 , δ in ppm): 7.48 (d, $^2J_{\text{HH}}$ (ortho) = 8.1 Hz, 6H, H_{arom}), 7.33 (m, 9H, H_{arom}), 3.46 (t, $^1J_{\text{CH}} = 140$ Hz, 4H, CH_2), 1.60 (m, 4H, 2 CH_2), 1.40 (m, 16H, 8 CH_2).

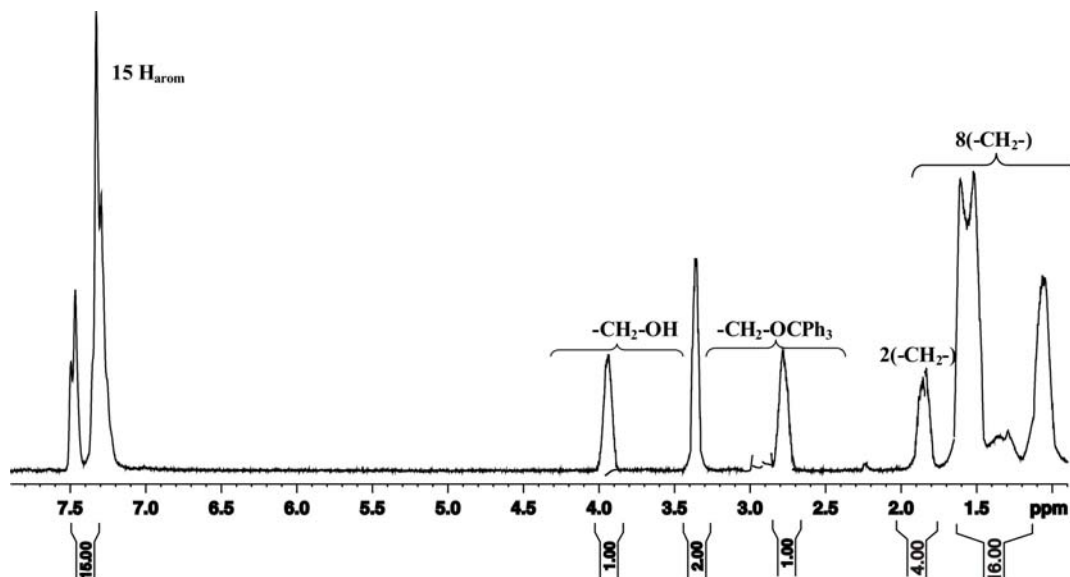


Figure 1.23: ^1H NMR spectrum of the ^{13}C -labeled 12-(triphenylmethoxy)dodecan-1-ol.

^{13}C -NMR spectrum (62.5 MHz for ^{13}C , in CDCl_3 , δ in ppm): 63.39 (t, $^1J_{\text{CC}} = 38.33$ Hz, 2C, 2 CH_2), 32.83 (t, $^1J_{\text{CC}} = 35.08$ Hz, 1C, CH_2), 29.65 (m, 8C, 8 CH_2), 26.25 (m, 1C, 1 CH_2).

It should be noted that for some ^{13}C -labeled compounds, the ^{13}C NMR spectra were recorded with only a few scans because only the ^{13}C -labeled NMR signals were of great interest. The presence of the trityl group on the molecule was previously confirmed by the ^1H NMR spectrum.

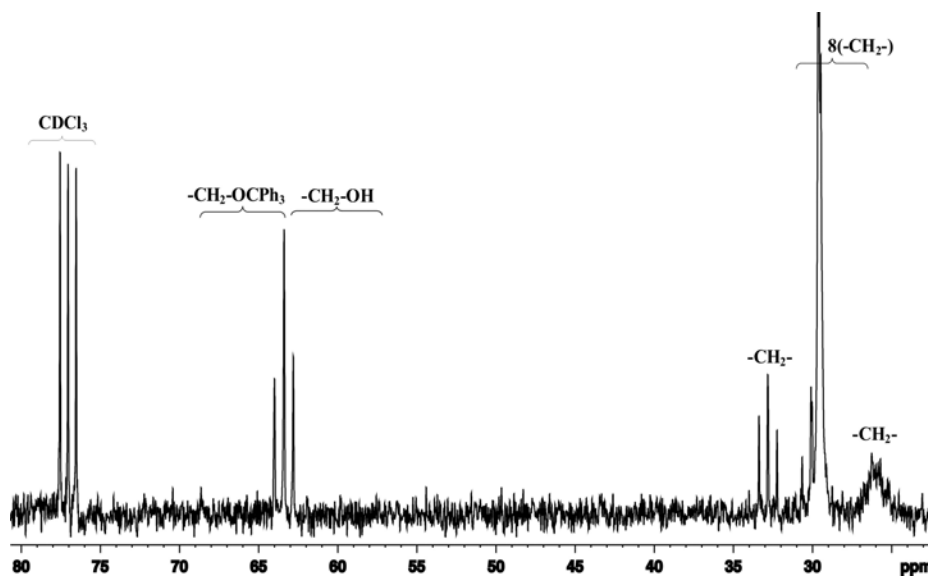


Figure 1.24: ^{13}C NMR spectrum of the ^{13}C -labeled 12-(triphenylmethoxy)dodecan-1-ol.

4.3.3 Fluorination of the ^{13}C -labeled 12-triphenylmethandodecan-1-ol using DAST (DiethylAminoSulfur Trifluoride) [15, 16].

DAST (125 μL , 1.35 mmol, 3eq) was added to 200 mg (0.45 mmol) of the ^{13}C 12-(triphenylmethoxy)dodecan-1-ol and the desired 1-fluoro-12-(triphenylmethoxy)dodecane was obtained with 84% yield (168 mg, 0.38 mmol) together with 10 % of the recovered 12-triphenylmethandodecan-1-ol (20 mg, 0.045 mmol).

NMR analysis of ^{13}C -labeled 1-fluoro-12-(triphenylmethoxy)dodecane

^1H -NMR spectrum (250 MHz for ^1H , in CDCl_3 , δ in ppm): 7.48 (d, $^2J_{\text{HH}}$ (ortho) = 8.1 Hz, 6H, H_{arom}), 7.33 (m, 9H, H_{arom}), 4.48 (dd, $^1J_{\text{CH}}$ = 150.5 Hz, $^2J_{\text{HF}}$ = 48.4 Hz, 2H, $\text{CH}_2\text{-F}$), 3.0 (d, $^1J_{\text{CH}}$ = 140 Hz, 2H, CH_2), 1.40 (m, 20H, 10CH_2).

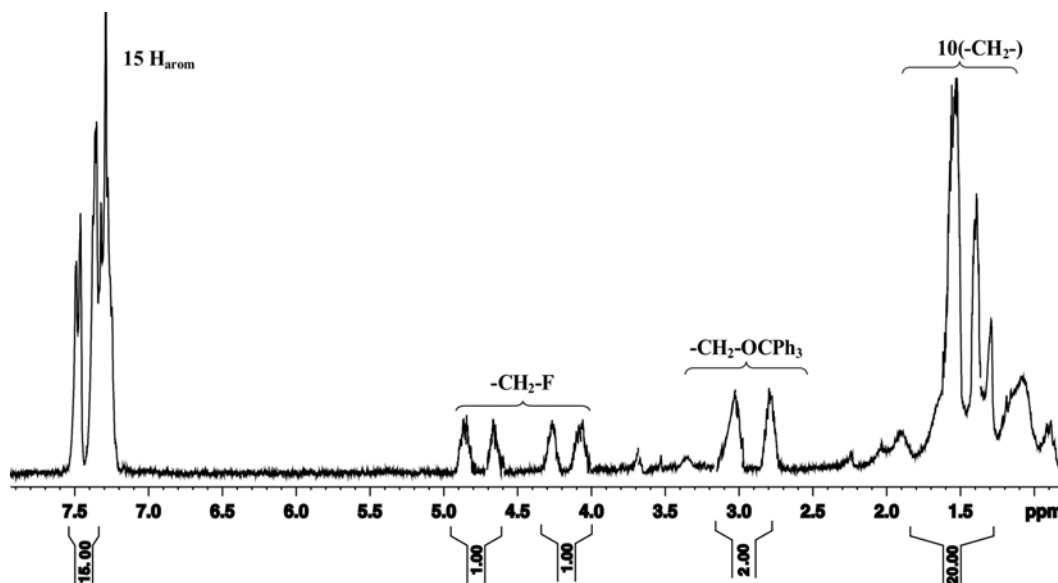


Figure 1.25: ^1H NMR spectrum of the ^{13}C -labeled 1-fluoro-12-(triphenylmethoxy)dodecane.

^{13}C -NMR spectrum (62.5 MHz for ^{13}C , in CDCl_3 , δ in ppm): 84.88 (dd, $^1J_{\text{CF}}$ = 163.8 Hz, $^1J_{\text{CC}}$ = 37.6 Hz, 1C, $\text{CH}_2\text{-F}$), 64.73 (d, $^1J_{\text{CC}}$ = 39.1 Hz, 1C, 1CH_2), 30.59 (m, 2C, CH_2), 29.54 (m, 7C, CH_2), 25.66 (m, 1C, CH_2).

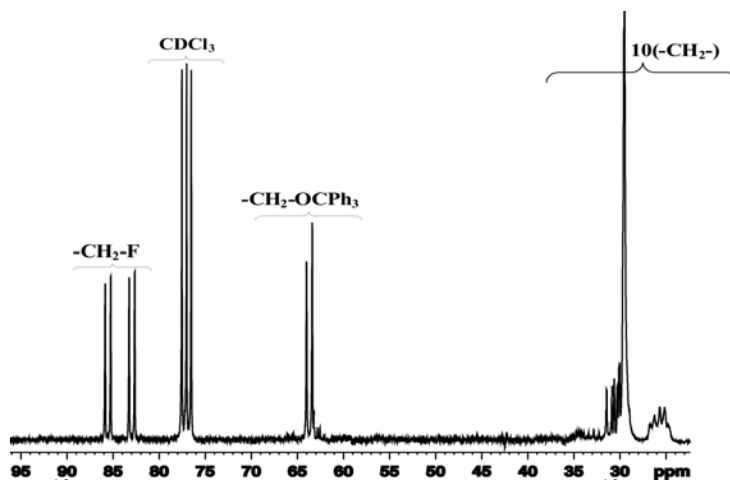


Figure 1.26: ^{13}C NMR spectrum of the ^{13}C -labeled 1-fluoro-12-(triphenylmethoxy)dodecane.

4.3.4 Deprotection using Triethyl-Silyl Triflate/Triethylsilane and Tetra-*n*-butylammonium fluoride (TBAF) [18, 19].

Et_3SiH (86 μL , 0.54 mmol, 1.2eq), Triethylsilyl triflate (52 μL , 0.22 mmol, 0.5eq) and TBAF (400 μL , 0.67 mmol, 1.5eq) were added to 200 mg (0.45 mmol) of 1-fluoro-12-(triphenylmethoxy)dodecane and 12-fluoro-dodecan-1-ol was obtained (70 mg, 0.34 mmol, 80 %) as well as 1-fluoro-12-(triphenylmethoxy)dodecane was recovered (40 mg, 0.09 mmol, 20 %).

NMR analysis of ^{13}C -labeled 12-fluoro-dodecan-1-ol

^1H –NMR spectrum (250 MHz for ^1H , in CDCl_3 , δ in ppm): 4.48 (dd, $^1J_{\text{CH}} = 150.5$ Hz, $^2J_{\text{HF}} = 48.4$ Hz, 2H, $\text{CH}_2\text{-F}$), 3.50 (d, $^1J_{\text{CH}} = 140$ Hz, 2H, CH_2), 1.40 (m, 20H, 10CH_2).

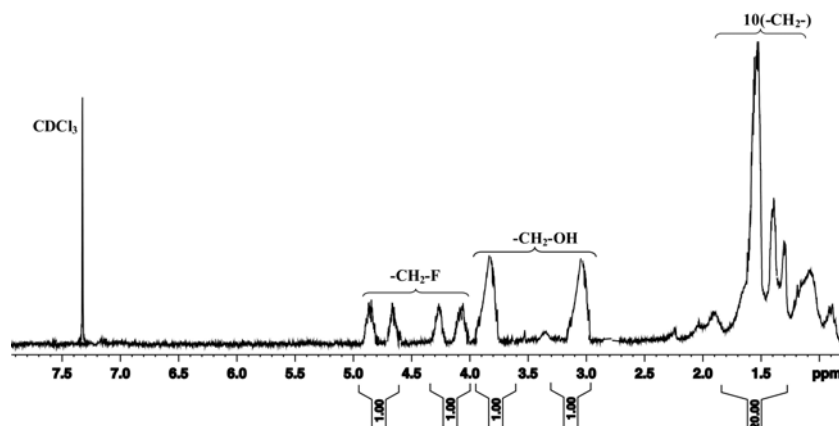


Figure 1.27: ^1H NMR spectrum of the ^{13}C -labeled 12-fluorododecan-1-ol.

^{13}C -NMR spectrum (62.5 MHz for ^{13}C , in CDCl_3 , δ in ppm): 84.88 (dd, $^1J_{\text{CF}} = 163.8$ Hz, $^1J_{\text{CC}} = 37.6$ Hz, 1C, $\text{CH}_2\text{-F}$), 63.14 (d, $^1J_{\text{CC}} = 36.6$ Hz, 1C, 1CH_2), 32.76 (t, $^1J_{\text{CC}} = 34.3$ Hz, 1C, CH_2), 29.54 (m, 8C, CH_2), 25.66 (m, 1C, CH_2).

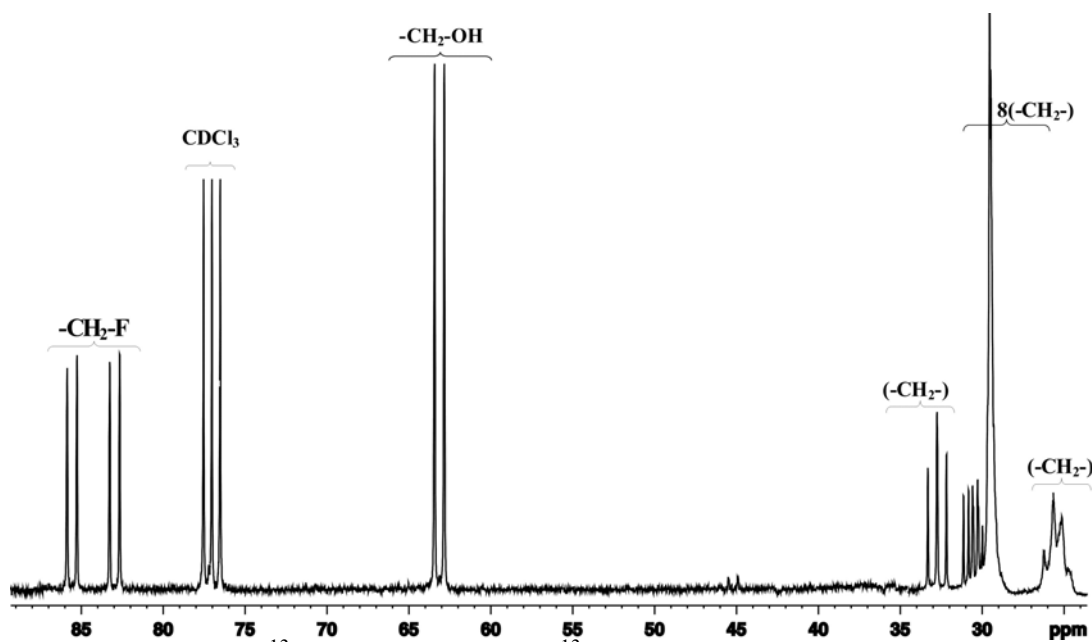


Figure 1.28: ^{13}C NMR spectrum of ^{13}C -labeled 12-fluorododecan-1-ol

4.3.5 Oxidation of ^{13}C -labeled 12-fluoro-dodecan-1-ol using DMP (Dess-Martin Periodinane) [20].

75 mg (0.37 mmol) 12-fluoro-dodecan-1-ol was added to Dess-Martin Periodinane (187 mg, 0.44 mmol, 1.2eq) led to 12-fluoro-dodecan-1-al (71 mg, 0.35 mmol, 96 %). For NMR spectrum and analysis details of the ^{13}C -labeled end product compound see Section 3.1 b of this chapter).

5. TWO DIMENSIONAL NMR EXPERIMENTS

5.1 Two Dimensional HSQC NMR experiment (750 MHz for ^1H , 187.5 MHz for ^{13}C)

2D H-1/X correlation via double inept transfer using sensitivity improvement; phase sensitive using Echo/Antiecho-TPPI gradient selection; with decoupling during acquisition; using trim pulses in inept transfer; using shaped pulses for all 180 degree pulses on f2 - channel; with gradients in back-inept.

Experimental Setup

	F2 (^1H)	F1 (^{13}C)
Pulse program	hsqcetgpsisp2.2 (available in the Bruker library)	
Time Dimension	2048	256 (1054 for high resolved experiment)
Acquisition Time[s]	0.114	0.003
FIDRES [Hz]	4.40	162.10 (FID resolution)
SW [ppm]	12	220
CNST2 [Hz]	145	equal to the default $J(\text{CH})$
D ₁ [s]	2	(delay $\sim 5T_1$)
O1P [ppm, Hz]	5 (3750.65)	(middle of ^1H NMR spectrum)
O2P [ppm, Hz]	105 (19805.14)	(middle of ^{13}C NMR spectrum)
Number of scans 40, Dummy Scans 4		
^1H hard pulse: 8.99 μs @-10.0dB		
PCPD2: 100 μs @10.9dB 90 degree pulse for decoupling sequence.		
^{13}C hard pulse: 15.22 μs @-22.0dB.		

5.2 Two Dimensional HMBC NMR experiment (750 MHz for ^1H , 187.5 MHz for ^{13}C)

2D $^1\text{H}/\text{X}$ correlation via heteronuclear zero and double quantum coherence, phase sensitive using Echo/Antiecho gradient selection with two-fold low-pass J-filter to suppress one bond correlations, no decoupling during acquisition).

Experimental Setup

	F2 (^1H)	F1 (^{13}C)
Pulse program	hmbcetgpl2nd (Available in the Bruker library)	
Time Dimension	4096	256
Acquisition Time[s]	0.227	0.003
FIDRES [Hz]	2.20	162.10 (FID resolution)
SW [ppm]	12	220
SW [Hz]	9014.42	41500.62

CNST2 [Hz]	145	default $J(\text{CH})$
CNST13 [Hz]	3 or 7	$J(\text{CH})$ long range (variable)
D_1 [s]	2	(delay $\sim 5 \times T_1$)
O1P [ppm, Hz]	5 (3750.65)	(middle of ^1H NMR spectrum)
O2P [ppm, Hz]	105 (19805.14)	(middle of ^{13}C NMR spectrum)

Number of scans 80, Dummy Scans 16

^1H 90 degree hard pulse: p1 8.99 μs @-10.0dB, p2 17.98 μs @-10.0dB

PCPD2: 100 μs @10.9dB 90 degree pulse for decoupling sequence.

^{13}C 90 degree hard pulse: 15.22 μs @-22.0dB.

5.3 Two dimensional C-C TOCSY NMR experiment (62.5 MHz for ^{13}C)

Pulse program: dipsi2ph (homonuclear Hartman-Hahn transfer using DIPSI2 sequence for mixing time, phase sensitive with ^1H decoupling during acquisition).

Experimental Setup

	F2 (^{13}C)	F1 (^{13}C)
Time Dimension	65k	256
Acquisition time[s]	2.45	0.128
FIDRES [Hz]	0.203	3.906 (fid resolution)

Number of scans= 16

D_1 = 2 s

Acquisition time 2.5 s

O1= 106 ppm (6666.90 Hz) middle of ^{13}C NMR spectrum

O2= 5.25 ppm (1313.18 Hz) middle of ^{13}C NMR spectrum

^{13}C : 90 degree hard pulse 12.5 μs @2.0dB; 90 degree TOCSY hard pulse 25 μs @8.0dB; Decoupling pulse pcdp: 68 μs @16.80dB, PL16= 11dB

REFERENCES

- [1] J. Fitzsimons, and J. Twamley, *Phys. Rev. Lett.*, **97**:090502, (2006).
- [2] J. Fitzsimons, L. Xiao, S. C. Benjamin, and J. A. Jones, *Phys. Rev. Lett.*, **99**:030501, (2007).
- [3] N. Khaneja and S. J. Glaser, *Phys. Rev. A* **66**, 060301 (2002).
- [4] Céline Girlanda-Junges et al, *Tetrahedron* 1998, **54**, 27, 7735-7748.
- [5] Atsushi Yoneda et al, *Chem. Commun.*, 2005, 3589-3590.
- [6] Dale F. Shellhamer et al, *J. Chem. Soc. Perkin Trans. 2*, 1995, 861-866.
- [7] Lila Somekh and Abraham Shanzer, *J. Am. Chem. Soc.*, 1982, **104**, 5836-5837.
- [8] T. W. Greene and P. G. M. Wuts, in *Protective Groups in Organic synthesis*, Wiley-Interscience, New York, 2nd Ed. (1991), pp.10-72.
- [9] Michael A. Pilkington-Miksa et al, *Eur. J. Org. Chem.*, 2008, 2900-2914.
- [10] Graham B. Jones et al., *Tetrahedron Asymmetry*, 1997, **8**, 11, 1797-1809.
- [11] Kang Ji-Hye et al., *J. Med. Chem.*, 2004, **47**, 16, 4000-4007.
- [12] T. J. Matray et al., *Bioconjugate Chemistry*, 2003, **8**, 2, 14642-16652.
- [13] Haruo Ogawa et al, *Chem. Commun.*, 1998, 495-496.
- [14] Masako Oikawa et al., *Synlett Letters*, July 1998, 757-760.
- [15] M. Ginisty, C. Gravier-Pelletier and Y. Le Merrer, *Tetrahedron Asymmetry*, 2006, **17**, 1, 142-150.
- [16] M. Hudlicky, *Journal of Fluorine Chemistry*, 1993, **60**, N° 2-3, 193-210.
- [17] B. Olofsson, R. Wijtmans, and P. Somfai, *Tetrahedron*, **58**, 30, 2002, 5979.
- [18] Hiroshi Imagawa et al., *Organic Letters* 2003, **5**, 2, 153-155.
- [19] M. J. Plunkett and J. A. Ellman, *J. Org. Chem.* 1997, **62**, 9, 2885-2893.
- [20] L. Lévêque, M. Le Blanc and R. Pastor, *Tetrahedron Lett.*, 1998, **39**, 48, 8857-8860.
- [21] G. Bodenhausen, and D. J. Ruben, *Chem. Phys. Lett.* 1980, **69**, 185-188.
- [22] A.G. Palmer III, J. Cavanagh, P.E. Wright & M. Rance, *J. Magn. Reson.*, **93**, 151-170 (1991).
- [23] L.E. Kay, P. Keifer & T. Saarinen, *J. Am. Chem. Soc.*, **114**, 10663-5 (1992).
- [24] J. Schleucher, M. Schwendinger, M. Sattler, P. Schmidt, O. Schedletzky, S.J. Glaser, O.W. Sorensen & C. Griesinger, *J. Biomol. NMR.*, **4**, 301-306 (1994).
- [25] A. Bax, and M. F. Summers, *J. Am. Chem. Soc.* 1986, **108**, 2093-2094.
- [26] D.O. Cicero, G. Barbato & R. Bazzo, *J. Magn. Reson.*, **148**, 209-213 (2001).
- [27] L. Braunschweiler, and R. R. Ernst, *J. Magn. Reson.* 1983, **53**, 521-528.
- [28] A. Bax, and D. G. Davis, *J. Magn. Reson.* 1985, **65**, 355-360.

CHAPTER 2: USE OF LANTHANIDE SHIFT REAGENTS FOR THE ASSIGNMENT OF ^{13}C NMR SIGNALS OF ALKYL CHAINS

1. MOTIVATION AND MAIN OBJECTIVES

After completing the synthesis of the target 13-qubit molecule (i.e. ^{13}C -labeled 12-fluorododecanal), the next step should be the experimental implementation of the recent theories including the efficient transfer of encoded states along spin chains [1] and quantum mirrors experiments [2, 3]. These approaches present a way for the efficient control of dynamics in spin chains of arbitrary length. For suitable quantum computing experiments, all qubits of the molecule should be identified and neighbouring qubits should be weakly coupled. Although high-resolution 2D experiments (HSQC, HMBC or TOCSY) have been performed on both unlabeled and ^{13}C -labeled compounds, ^1H and ^{13}C NMR signals were still overlapped. Moreover proton and carbon nuclei of those compounds were strongly coupled. Thus, the use of lanthanide shift reagents in order to differentiate the nuclei (carbons) of the molecule and turn strong couplings into weak couplings has emerged as a potential solution. For several decades now, it is known that lanthanide shift reagents are a convenient and economical means to solve the problem of overlapping lines and complex spectral patterns with resonances not only coincident but also strongly coupled [4]. Therefore some of the most efficient shift reagents i.e. complexes of paramagnetic lanthanide ions such as Europium(III) and Ytterbium(III) for downfield shifts and Praseodymium(III) for upfield shifts associated to one of the most commonly used ligands i.e. 1,1,1,2,2,3,3-heptafluoro-7,7-dimethyl-4,6-octanedione (FOD) were chosen. These NMR lanthanide shift reagents (LSR) have the ability to induce chemical shifts and thus simplify complex NMR spectra. Complexes of Europium [$\text{Eu}(\text{fod})_3$], Praseodymium [$\text{Pr}(\text{fod})_3$] and Ytterbium [$\text{Yb}(\text{fod})_3$] have been used here in order to change chemical shifts in NMR spectra. The requirements for an effective shift reagent include optimal shifting power with minimal line broadening effect and an ability to bind to the studied organic molecule. Some LSR were first tested on the unlabeled compound (12-fluorododecanal) with the intention of examining the ^{13}C -labeled one later.

2. THEORY

For quite some time now, organic chemists have been developing the use of lanthanide shift reagents (LSR) applied to chemical structure analysis using Nuclear Magnetic Resonance [5-8]. Generally known by their nature to alter the proton NMR spectra of the ligands that coordinate to them, paramagnetic transition metal ions as well as lanthanide shift reagents act like an additional magnetic field in the sample and notably change the chemical shifts of the signals. This effect occurs significantly on the nuclei in the neighborhood of the complexation site. Contact and dipolar (pseudocontact [5, 9]) interactions between the paramagnetic ion and the organic molecule cause the induced shifts. Consequently, proton and carbon NMR signals of complex organic and biological molecules, consisting of featureless clusters and very difficult to assign, could be separated. The change in chemical shift due to the addition of a shift reagent is the result of three component contributions and is given by the following equation [8]:

$$\Delta_{\text{tot}} = \Delta_{\text{dia}} + \Delta_{\text{con}} + \Delta_{\text{dip}} \quad (2.1)$$

where Δ_{dia} is the diamagnetic contribution caused by the complexation of the substrate, Δ_{con} is the contact contribution originating from the delocalization of electron spin density from the lanthanide ion to the substrate, and Δ_{dip} is the dipolar contribution depending on the distance r between the lanthanide ion and the observed nuclear spin. The latter term (Δ_{dip}) has the main contribution as compared to the first two components, whose contributions are smaller and usually negligible.

The McConnell-Robertson equation (2.2) [10] gives Δ_{dip} in terms of the distance r between the lanthanide ion and the observed spin, and the angle θ between the principal magnetic axis of the complex (in most of the cases: vector from the lanthanide ion to the nucleophilic center) and the distance vector (see Figure 2.1 (b) [8, 11]):

$$\Delta_{\text{dip}} = k(3\cos^2 \theta - 1)r^{-3} \quad (2.2)$$

where k is a constant characteristic of the lanthanide shift reagent and substrate complex.

The figure below illustrates a case where oxygen is the coordinating substrate atom and Europium(III) the metal. It should be noted that lanthanide shift experiments are only effective with substrates acting as a Lewis base to which complexation can occur [12].

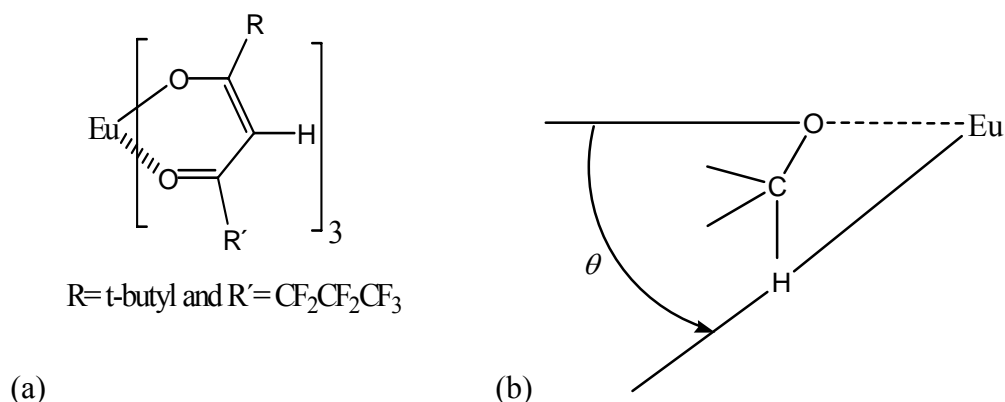


Figure 2.1: (a) Illustrative structure of the Europium complex. (b) Association of the Europium complex with the studied substrate (in this case the oxygen atom is the nucleophilic center).

The application of equation (2.2) in ¹³C NMR spectroscopy was impressively demonstrated through complete assignments as well as the identification of carbon resonances of some organic molecules such as borneol, isoborneol and steroids [13-16].

The study of the effects of Eu(fod)₃, Pr(fod)₃ and Yb(fod)₃ lanthanide shift reagents on the ¹³C NMR chemical shifts of our alkyl chain molecules is presented in the next section.

3. EXPERIMENTAL RESULTS AND DISCUSSION

Having no prior experience in the use of lanthanide shift reagents before, it was appropriate to make use of a test molecule to avoid unnecessary losses. Thus, molecules such as 2-methylundecanal and 1-octanol were chosen because of their similarity to the final studied products.

3.1 Experiment using a test molecule: 2-methylundecanal

2-methylundecanal, a molecule similar to 12-fluorododecanal and commercially available, has been used for the first tests with shift reagents. Samples were prepared by gradually adding small amounts (a few milligrams) of lanthanide shift reagents into a 2-methylundecanal solution (0.4 mmol in 0.6 mL CDCl₃).

¹H and ¹³C 1D NMR experiments of the substrate (0.4 mmol in 0.6 mL CDCl₃), without shift reagent, were acquired to serve as a reference. The resulting spectra are the following.

^1H NMR spectrum of 2-methylundecanal ($\text{C}_{12}\text{H}_{24}\text{O}$, $M=184.18\text{g/mol}$, 250 MHz in CDCl_3)

Only a few proton signals could be distinguished: δ (ppm) = 9.6 (H-C=O, H_1), 2.4 (CH_2 -C=O, H_2), 1.8 (CH_3 , H_3), 1.6 (CH_2 , H_4), 1.1 (CH_2 , H_{11}), 0.9 (CH_3 , H_{12}), methylene (CH_2) group protons H_5 - H_{10} broad signal $\sim 1.3\text{ppm}$.

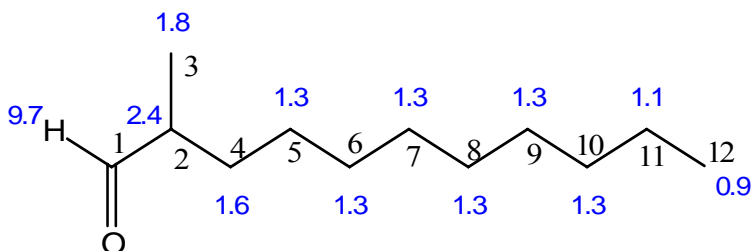


Figure 2.2: Tentative ^1H NMR assignment of 2-methylundecanal.

The assignment of ^1H NMR signals of 2-methylundecanal is based on our NMR data and also on the simulation using the ChemDraw program.

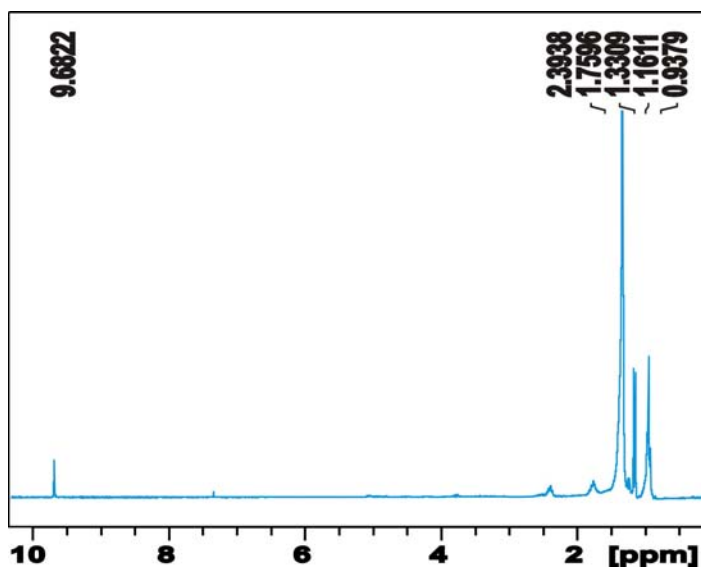


Figure 2.3: ^1H NMR spectrum of 2-methylundecanal (0.4 mmol) in CDCl_3 .

^{13}C NMR spectrum of 2-methylundecanal (62.5MHz in CDCl_3): δ (ppm) = 205.7 (-C=O, C_1), 13.3 (CH_3 , C_3), 14.1 (CH_3 , C_{12}), 46.4 (CH , C_2), 31.9 (CH_2 , C_{10}), 30.5 (CH_2 , C_4), 26.9 (CH_2 , C_5), 26.6 (CH_2 , C_6), 26.5 (CH_2 , C_7), 26.4 (CH_2 , C_8), 26.3 (CH_2 , C_9), 22.6 (CH_2 , C_{11}).

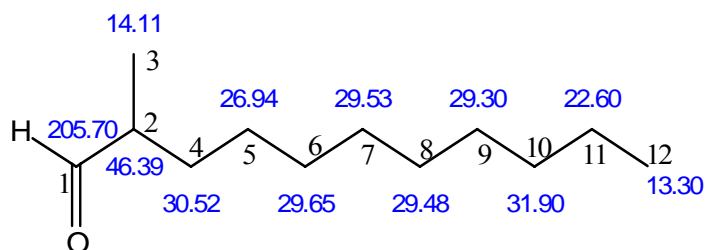


Figure 2.4: Tentative ^{13}C NMR assignment of 2-methylundecanal

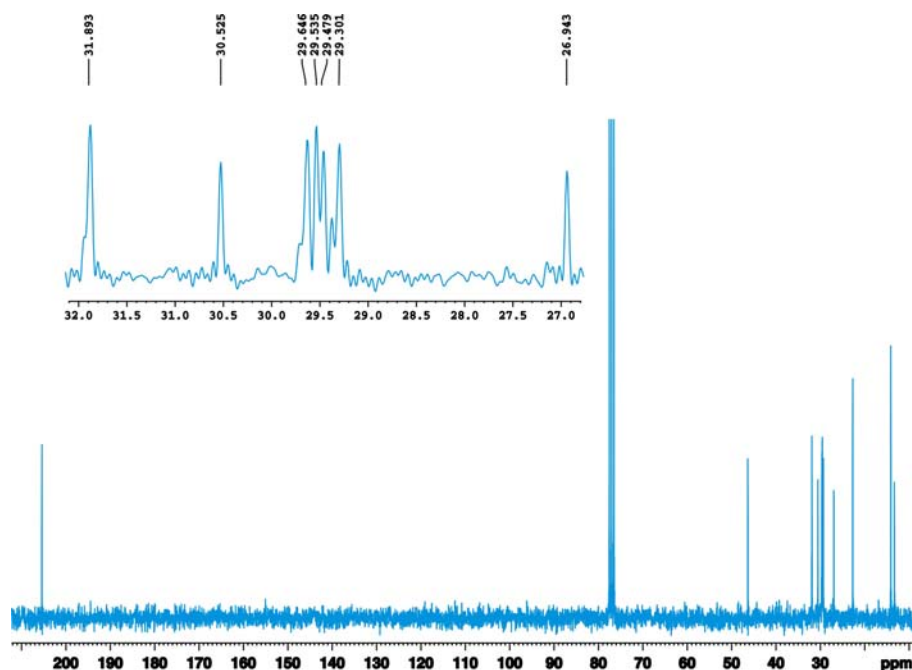


Figure 2.5: ^{13}C NMR spectrum of 2-methylundecanal (0.4 mmol) in CDCl_3

As mentioned above for protons, the ^{13}C NMR assignment of 2-methylundecanal is based on our NMR data and also on the simulation using the ChemDraw program. A complete assignment was not needed here since only the differences in the induced chemical shifts are of interest.

The ^{13}C NMR spectrum of 2-methylundecanal in CDCl_3 presents a crowded region involving about five carbon signals with a smallest difference in chemical shifts of $\Delta\delta \approx 0.18$ ppm. A lanthanide shift reagent suitable (convenient concentration) for the simplification of these spectra and for separating these ^{13}C NMR signals had to be found. Therefore, various lanthanide shift reagents (LSR) were added at different concentrations to the substrate and comparisons of the recorded ^1H and ^{13}C NMR spectra are shown below.

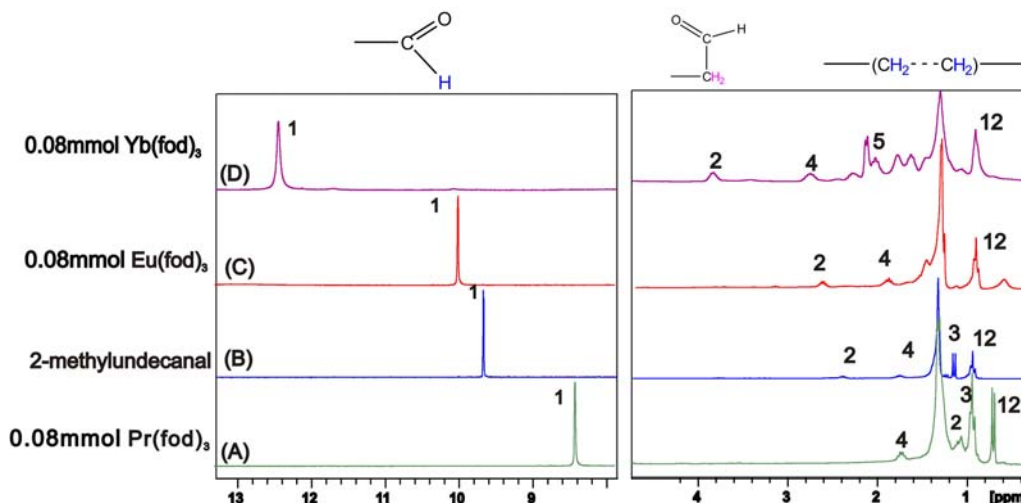


Figure 2.6: ^1H NMR spectra of 2-methylundecanal (0.4 mmol) with various LSR (0.2eq each).

In ^1H NMR spectra of 2-methylundecanal, for samples without shift reagent (B) or with 0.08 mmol (i.e. 0.2eq) each of $\text{Pr}(\text{fod})_3$ (A), $\text{Eu}(\text{fod})_3$ (C), and $\text{Yb}(\text{fod})_3$ (D), only proton signals for the aldehyde ($\text{H}-\text{C}=\text{O}$), the methyne (CH) and methyl (CH_3) protons are distinguishable whereas the remaining protons (methylene groups) appear as a broad signal around 1.3 ppm. But with 0.2eq $\text{Yb}(\text{fod})_3$ (D) signals are more shifted and severely broadened. The aldehyde proton signal is shifted to $\delta_{(\text{ppm})} = 12.3$ ($\Delta\delta = +2.6$ ppm).

The corresponding ^{13}C NMR spectra are presented below. The region 29-32 ppm, where carbon chemical shifts are very close, was of big interest.

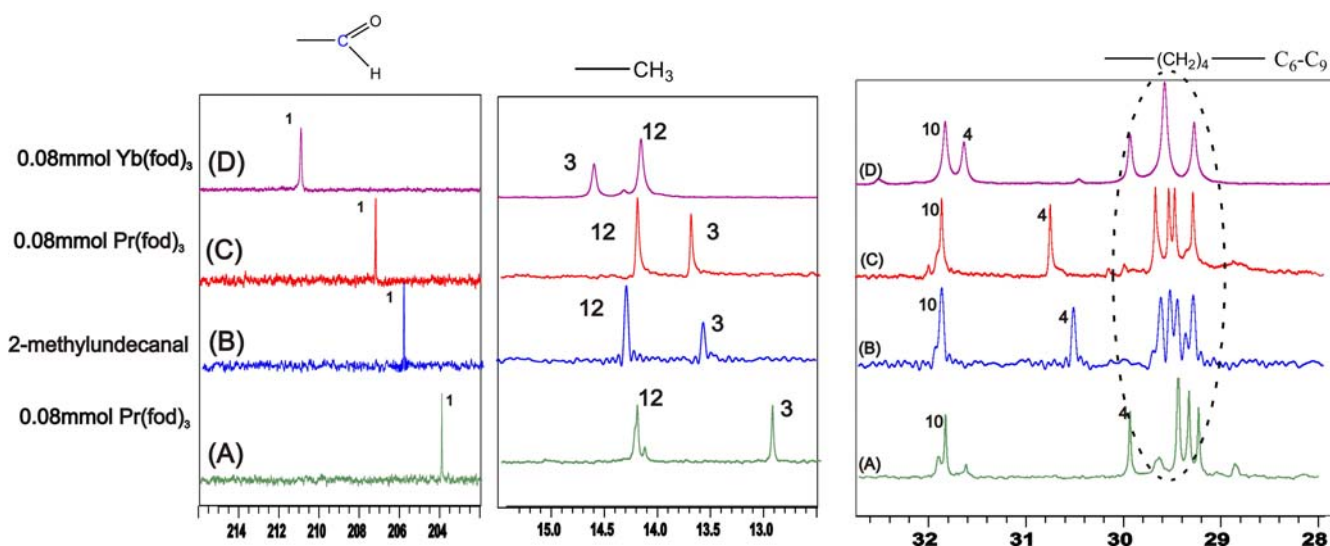


Figure 2.7: ^{13}C NMR spectra of 2-methylundecanal (0.4 mmol) with various LSR (0.2eq each).

In the above figure, the ^{13}C NMR spectrum of 2-methylundecanal without shift reagent (B) shows six signals in the region 29-32 ppm with the four closest signals (C_6 - C_9) at about 29.5 ppm. The smallest difference in chemical shifts between them is 0.05 ppm. In the spectra recorded for samples with shift reagents, the following observations were made:

(A) With 0.08 mmol $\text{Pr}(\text{fod})_3$, there are only three visible signals instead of four at ~29.5 ppm. The minimum difference in chemical shifts here is 0.1 ppm, and two signals are overlapped (C_6 , C_7).

(D) Although the smallest difference in carbon resonances is 0.36 ppm with the 0.08 mmol $\text{Yb}(\text{fod})_3$ sample, C_8 and C_9 overlap and signals are more broadened.

(C) With 0.08 mmol $\text{Eu}(\text{fod})_3$ sample all four signals are visible but still close, the smallest difference in chemical shifts in this case is about 0.06 ppm.

The observed lanthanide induced shifts of $\text{Eu}(\text{fod})_3$, $\text{Yb}(\text{fod})_3$, and $\text{Pr}(\text{fod})_3$ are summarized in the table below.

Table 2.1: Comparative shift effects of various¹ LSR used to alter the ^{13}C NMR spectrum of 2-methylundecanal (0.4 mmol) in CDCl_3 . δ and $\Delta\delta$ are given in ppm.

2-methylundecanal		$\text{Eu}(\text{fod})_3$		$\text{Yb}(\text{fod})_3$		$\text{Pr}(\text{fod})_3$	
Position ²	δ	δ	$\Delta\delta$	δ	$\Delta\delta$	δ	$\Delta\delta$
1	205.70	206.84	+1.14	210.94	+5.24	203.24	-2.45
2	46.39	46.90	+0.51	48.18	+1.79	46.05	-0.34
3	14.11	14.02	-0.09	14.44	+0.33	14.14	+0.03
4	30.52	31.86	+1.34	31.65	+1.13	29.95	-0.57
5	26.94	27.02	+0.08	27.59	+0.65	26.61	-0.33
6	29.65	29.98	+0.33	31.63	+1.02	29.46	-0.19
7	29.53	29.67	+0.14	29.94	+0.41	29.46	-0.07
8	29.48	29.52	+0.04	29.58	+0.10	29.35	-0.13
9	29.30	29.46	+0.16	29.58	+0.28	29.25	-0.05
10	31.90	31.99	+0.09	31.93	+0.03	31.85	-0.05
11	22.60	22.63	+0.03	22.59	-0.01	22.64	+0.04
12	13.30	13.47	+0.17	13.95	+0.65	12.66	-0.64

¹ 0.08 mmol (0.2eq) of each shift reagent was added to the substrate. ² Carbon positions mentioned in this table are based on the assignment from Chapter 1.

After experiments with LSR Eu(fod)₃ and Yb(fod)₃ for downfield shifts and Pr(fod)₃ for upfield shifts, the general observation was that the four ¹³C NMR signals (C₆-C₉) in the region 29-30 ppm are still close to each other. For the sample with Eu(fod)₃ all the carbon NMR signals were visible, and even the four closest signals were distinguishable. Spectrometers with frequencies of up to 900 MHz (¹H) are available to our group. Even at this highest frequency spectrometer the smallest difference in chemical shifts would correspond to 0.06 ppm (i.e. $\Delta \approx 13.5$ Hz at 900 MHz (¹H) or 225 MHz (¹³C)) which is not sufficient for our purpose. On the other hand, samples with Yb(fod)₃ and Pr(fod)₃ presented signals at quite considerable distance ($\Delta > 20$ Hz), but some of them were overlapped.

Knowing that the contact between the molecule and the shift reagent occurs at the carbonyl function, it was important to know if the signal is sharp enough for quantum computing experiments after the addition of different concentrations of the shift reagent to the substrate. Therefore in order to determine how much shift reagent could be added, the relaxation time T_2 of the carbonyl was measured. T_2 is a crucial parameter for quantum computing experiments; since the line width of an NMR signal depends on the relaxation time T_2 (line width at half-height $\approx 1/T_2$), this parameter also indicates the extend to which the lanthanide shift reagent affects the line width of the NMR signal. $T_2 \approx 1 / \pi \omega_{1/2}$.

Table 2.2: Relaxation time T_2 of -C=O of 2-methylundecanal (0.4 mmol) with different LSR (0.08 mmol, 0.2eq) in CDCl₃.

Sample	Carbonyl group -C=O (δ in ppm)	Line width (Hz)	T_2 (ms)
2-methylundecanal	205.4	n.m.	n.m.
0.08 mmol Eu(fod) ₃	206.7	2.5	1250
0.08 mmol Pr(fod) ₃	203.5	4.5	370
0.08 mmol Yb(fod) ₃	210.7	6	133

n.m.: not measured.

Based on these results it can be noted that Yb(fod)₃ has a stronger broadening effect (shorter T_2) than the other two reagents. The sample with 0.08 mmol Eu(fod)₃ may be better for quantum computing experiments compared to other samples, because of its longer relaxation time T_2 (1.25 s). With a relaxation time value of $T_2 = 370$ ms, the sample with 0.08 mmol Pr(fod)₃ can be also used for quantum computing but with some

limitations, whereas the concentration of Yb(fod)₃ has to be reduced. But, the ¹³C NMR spectrum of 0.08 mmol Eu(fod)₃ presented very close signals. Nevertheless, these results have provided starting reference points for the further experiments. The effects of the same lanthanide shift reagents added at different concentrations to the 12-fluorododecanal sample have also been studied.

3.2 Lanthanide shift reagents experiments with unlabeled 12-fluorododecanal

Based on experience with 2-methylundecanal and lanthanide shift reagents, experiments with unlabeled 12-fluorododecanal were done without too many preceding trials. Thus, the same LSR at the same concentration have been used as the starting point. ¹H and ¹³C 1D NMR spectra of unlabeled 12-fluorododecanal in CDCl₃ as well as the spectra recorded with samples containing LSR are presented and compared below.

¹H –NMR spectrum (600 MHz for ¹H, CDCl₃, δ in ppm): 9.76 (t, 1H, ³J_{HH} = 2 Hz, H-C=O), 4.43 (dt, 2H, ²J_{HF} = 47 Hz, ³J_{HH} = 6 Hz, CH₂-F), 2.41 (td, 2H, ³J_{HH} = 7 Hz, ³J_{HH} = 2 Hz (H_{ald}), CH₂-C=O), 1.62 (m, 4H, 2CH₂), 1.30 (m, 16H, 8CH₂).

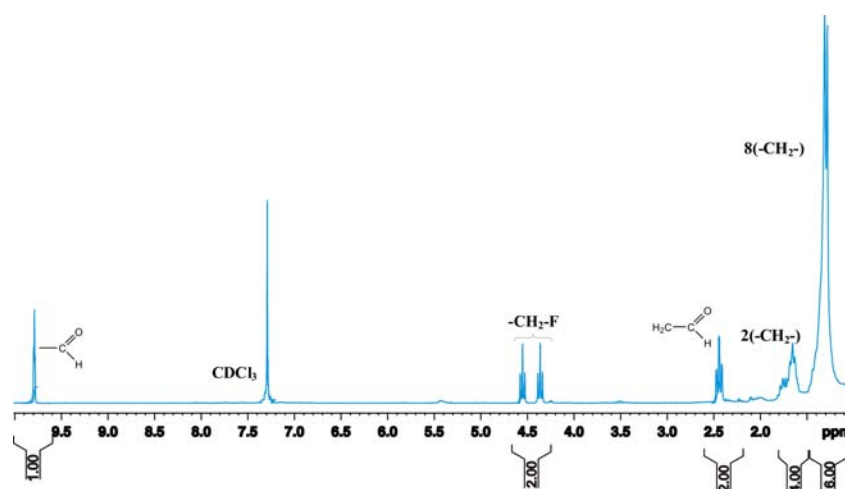


Figure 2.8: ¹H NMR spectrum of 12-fluorododecanal (0.07 mmol) in CDCl₃ (cf. Fig. 1.2, Chapter 1).

¹³C–NMR spectrum (150 MHz for ¹³C, in CDCl₃, δ in ppm): 202.76 (s, 1C, -C=O), 83.54 (d, 1C, ¹J_{CF} = 164 Hz, CH₂-F), 43.89 (s, 1C, CH₂-C=O), 30.41 (d, 1C, ²J_{CF} = 19 Hz, CH₂-CH₂-F), 29.71 (s, 1C, CH₂), 29.53 (d, 1C, ⁴J_{CF} = 3 Hz, CH₂-CH₂-CH₂-CH₂-F), 29.37

(s, 1C, CH₂), 29.33 (s, 1C, CH₂), 29.21 (s, 1C, CH₂), 29.14 (s, 1C, CH₂), 25.15 (d, 1C, $^3J_{CF}$ = 5 Hz, CH₂-CH₂-CH₂-F), 22.06 (s, 1C, CH₂).

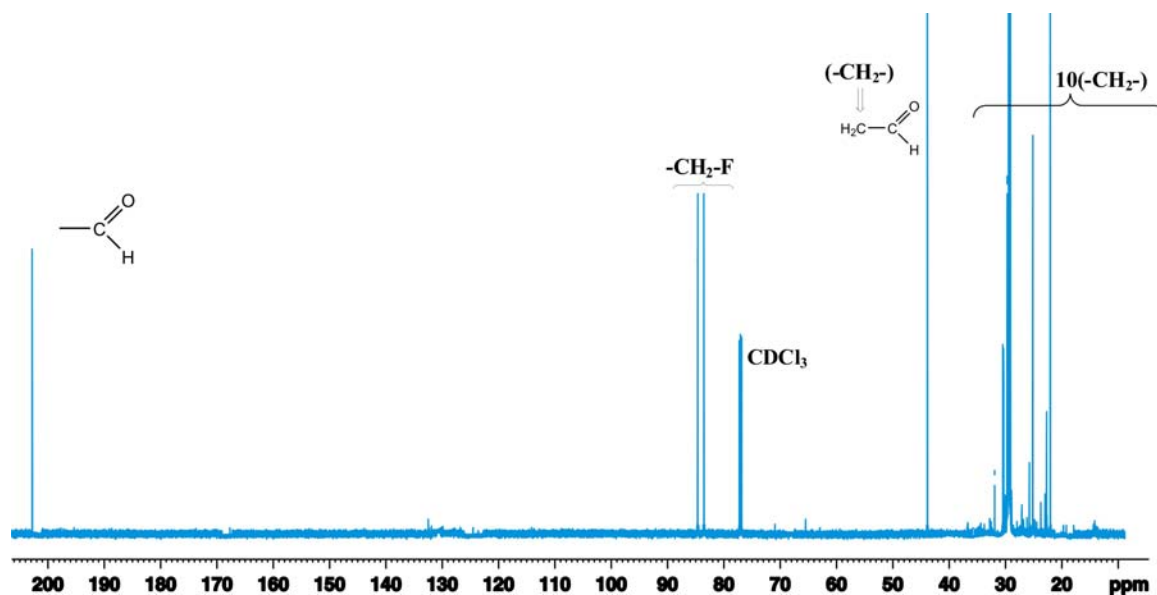


Figure 2.9: ^{13}C NMR spectrum of 12-fluorododecanal (0.07 mmol) in CDCl_3 (cf. Fig. 1.3, Chapter 1).

From the ^{13}C NMR spectrum of the unlabeled 12-fluorododecanal in CDCl_3 , it could be observed that the smallest difference in the carbon resonances is ~ 0.04 ppm, which corresponds to 9 Hz at 900 MHz spectrometer.

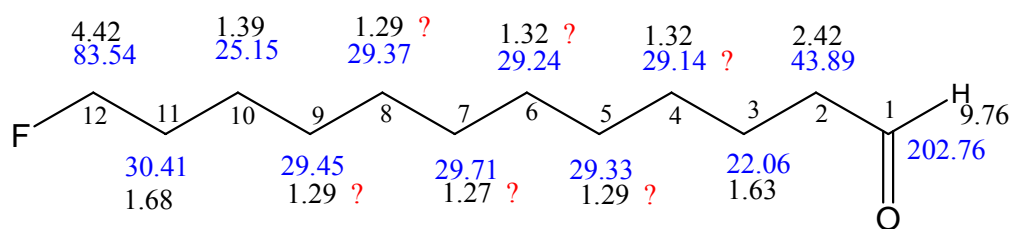


Figure 2.10: Possible assignment of the unlabeled 12-fluorododecanal molecule (cf. Fig. 1.10, Chap. 1). Variations in the chemical shifts of carbon atoms with a question mark (?) are of most interest.

The aim was to find a lanthanide shift reagent at a suitable concentration in order reasonably resolve the closest carbons (C₄-C₉). The desired shift reagent should fulfill some requirements including optimal shifting power with minimal line broadening to avoid loss of some signals.

^1H and ^{13}C 1D NMR spectra of the unlabeled 12-fluorododecanal samples with addition of shift reagents at different concentrations are presented below.

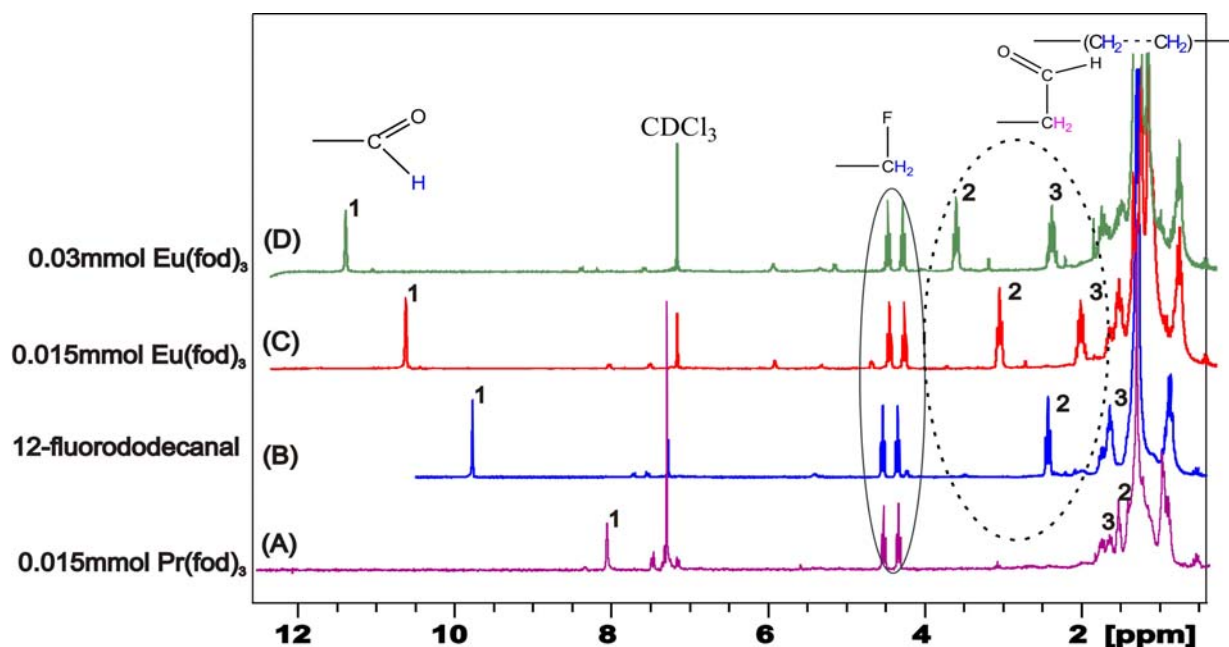


Figure 2.11: ^1H NMR spectra of 12-fluorododecanal (0.07 mmol) with LSR at different concentrations in CDCl_3 . 0.015 mmol (0.2eq) of each shift reagent was first added to the substrate, this amount was progressively increased according to the effects induced by each of the shift reagents.

The proton is one of the most widely employed nuclei in NMR because of its high sensitivity. It is known that lanthanide shift reagents have been almost exclusively used in ^1H NMR spectroscopy [16]. However, the effective separation of interfering NMR resonances of long alkyl chain protons is sometimes still very difficult. The addition of lanthanide shift reagents at different concentrations to the 12-fluorododecanal sample did not cause significant changes in the chemical shifts of the middle methylene protons. Changes in the chemical shifts of the aldehyde and its adjacent protons were the only noticeable effect.

However, considering the wider range of the carbon NMR signals, larger variations are expected for ^{13}C NMR signals.

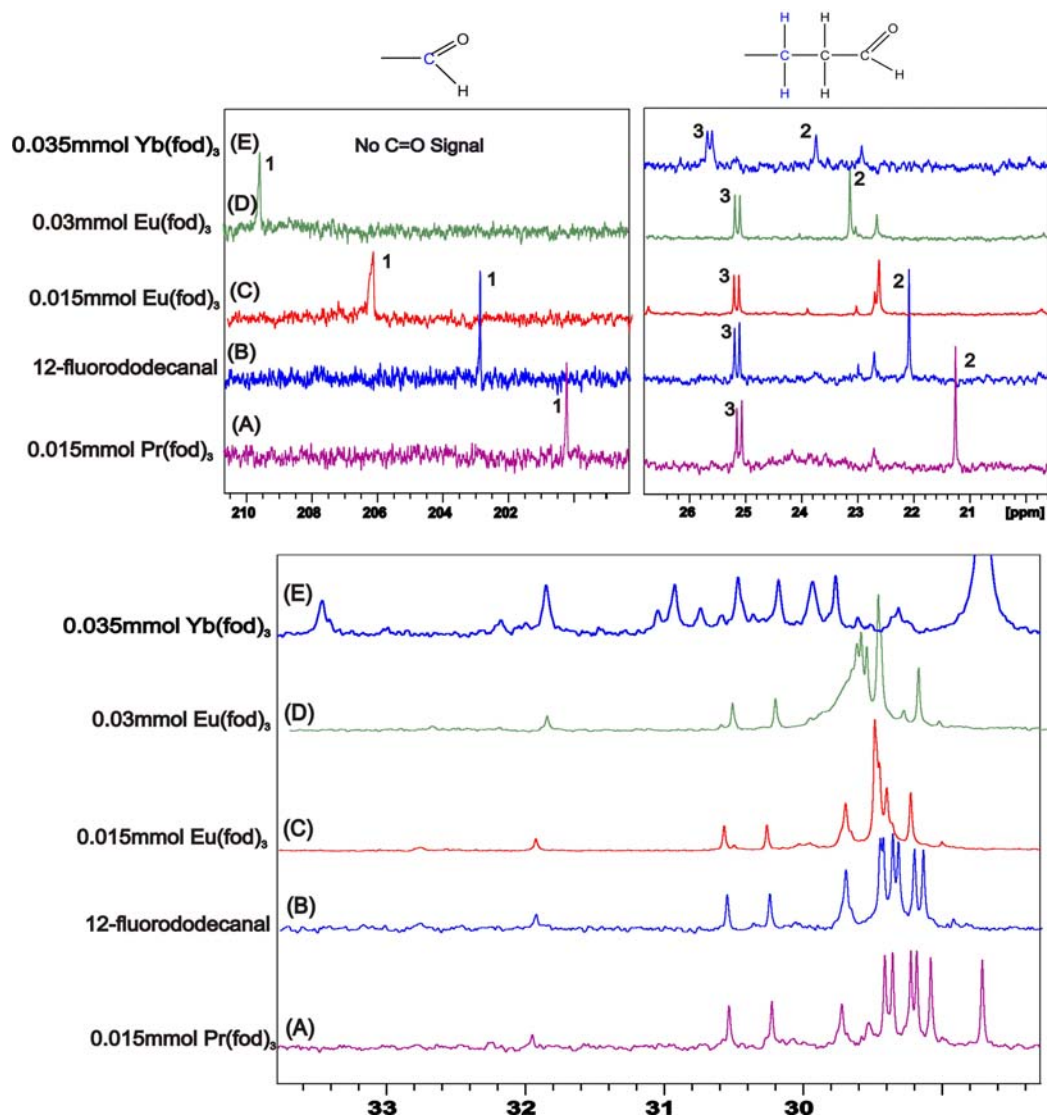


Figure 2.12: ^{13}C NMR spectra of 12-fluorododecanal (0.07 mmol) with LSR at different concentrations in CDCl_3 . 0.015 mmol (0.2eq) of each shift reagent was first added to the substrate, this amount was progressively increased, up to certain limit, and according to the effects induced by each of the shift reagents. These ^{13}C NMR spectra present the maximum amount reached for each shift reagent.

On the ^{13}C NMR spectrum of 12-fluorododecanal without shift reagent (B), the middle CH_2 signals are strongly coupled ($\text{C}_4\text{-C}_9$): the smallest difference in chemical shifts between them is 0.04 ppm (i.e. 9 Hz at 225 MHz for ^{13}C ; standard $^1J_{\text{CC}} = 35$ Hz).

(A) With 0.015 mmol $\text{Pr}(\text{fod})_3$ almost all signals are visible whereas the variation in chemical shifts here is still small and therefore the spins are still strongly coupled.

(C) and (D) with 0.015 mmol and 0.03 mmol Eu(fod)₃ respectively, no individual signal of the alkyl chain methylene groups between (29-30 ppm) is distinguishable. More broadened signals are observed in these two cases.

(E) With 0.035 mmol Yb(fod)₃ almost all signals are separated and shifted to the region 29-32 ppm, larger differences in chemical shifts have been measured here but signals are more broadened. The carbonyl signal (C=O) is no more perceptible. The smallest difference in chemical shifts between them is 0.12 ppm (i.e. 27 Hz at 225 MHz for ¹³C; standard ¹J_{CC}= 35 Hz).

The comparisons of lanthanide ¹³C NMR induced shift values are presented in the table below.

Table 2.3: Observed ¹³C NMR lanthanide induced shifts of substrate 12-fluorododecanal in CDCl₃ and the effect of added Eu(fod)₃, Yb(fod)₃ and Pr(fod)₃. δ and Δδ are given in ppm.

Substrate ^a		Eu(fod) ₃ ^b		Eu(fod) ₃ ^c		Yb(fod) ₃ ^d		Pr(fod) ₃ ^b	
Position [*]	δ	δ	Δδ	δ	Δδ	δ	Δδ	δ	Δδ
1	202.76	206.70	+3.94	209.55	+6.79	no –C=O signal		200.22	-2.54
2	43.89	44.90	+0.81	45.23	+1.34	48.94	+5.05	43.09	-0.80
3	22.06	22.69	+0.63	23.17	+1.11	23.48	+1.42	21.25	-0.81
4	29.14	29.45	+0.31	29.66	+0.52	33.19	+4.05	29.08	-0.06
5	29.33	29.50	/	29.70	/	31.57	+2.24	29.22	-0.11
6	29.21	29.24	+0.03	29.25	+0.04	30.19	+0.98	29.18	-0.03
7	29.71	29.71	0	29.70	/	29.91	+0.20	29.70	-0.01
8	29.37	29.50	/	29.70	/	29.49	+0.12	29.35	-0.13
9	29.53	29.53	0	29.70	/	29.66	+0.13	29.41	-0.12
10	25.15	25.15	0	25.18	+0.03	25.36	+0.21	25.11	-0.04
11	30.41	30.41	0	30.44	0	30.65	0	30.37	-0.04
12	83.53	83.53	0	83.53	0	83.53	0	83.53	0

^a Substrate: 12-fluorododecanal 0.07 mmol in 0.6 mL in CDCl₃.

^b 0.015 mmol (0.2eq) of shift reagent was used.

^c 0.03 mmol (0.4eq) of shift reagent was used.

^d 0.035 mmol (0.45eq) of shift reagent was used, but Carbons C₆-C₉ ambiguously assigned because more signals as expected in the corresponding region; –C=O signal is no more visible.

(/) Induced-shifts not determined because of signals overlap.

(*) Assignment is based on the results of chapter 1.

Based on the table above, it can be observed that:

- no sample could resolve our strong coupling problem
- the strongest shifting lanthanide ($\text{Yb}(\text{fod})_3$) leads to the loss of the carbonyl signal
- $\text{Eu}(\text{fod})_3$ did not at all resolve the overlap of $\text{C}_4\text{-C}_9$.

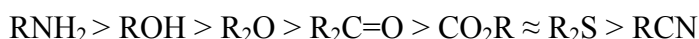
Therefore, the result obtained with 0.015 mmol (0.2eq) $\text{Pr}(\text{fod})_3$ seems to be the best compromise (even though it does not resolve our strong coupling problem). Hence, the relaxation time T_2 of the carbonyl and its adjacent carbon was measured.

Table 2.4: Relaxation T_2 time of 12-fluorododecanal with 0.015 mmol $\text{Pr}(\text{fod})_3$ in CDCl_3

^{13}C Nucleus	$\delta(\text{ppm})$	Line width in (Hz)	T_2 (ms)
C=O	200.22	4.2	256
CH_2 adjacent to C=O	43.09	1.5	769

It is reasonable to require that the shortest relaxation time T_2 of all nuclei (here the -C=O is the fastest relaxing nucleus) should not be smaller than eleven times $1/(2J)$ (considering the standard $^1J_{\text{CC}} = 35$ Hz) i.e. ~ 157 ms. This at least enables a transfer of magnetization through the complete spin chain (e.g. using TOCSY). The 12-fluorododecanal (^{13}C -labeled) sample with 0.015 mmol $\text{Pr}(\text{fod})_3$ in CDCl_3 satisfied the requirements for T_2 value (see Table 2.4). Moreover, all carbons of its alkyl chain, including the carbonyl, are discernible. However, the minimum interval between the nuclei (in the case of weak coupling, the difference in chemical shifts should be larger than $10J$ i.e. ~ 350 Hz, for $^1J_{\text{CC}} = 35$ Hz) required for successful quantum computing experiments was still not realized. In fact, only 51.75 Hz as the maximum difference was obtained. Hence, another way had to be found to resolve this issue.

Theoretical studies [4, 12, 17] state that besides the fact that the substrate must act as a Lewis basis, the lanthanide shift reagent effect usually depends on the type of the complex formed between the functional group of the substrate and the metal. The complexing strength varies with the nature of the substrate as follows:



The induced shift is about 40% more in the case of alcohols and amines than for ethers, esters and ketones [14]. Based on these statements the study of 12-(triphenylmethoxy)dodecan-1-ol in replacement of the unlabeled 12-fluorododecanal was initiated expecting better results with the complexation on the alcohol functional group.

4. EXPERIMENTAL STUDY: COMPLEXATION OF THE ALCOHOL FUNCTION WITH LANTHANIDE SHIFT REAGENTS

1-octanol which is similar to 12-(triphenylmethoxy)dodecan-1-ol, and commercially available, was used for pre-tests. Samples were prepared by adding small amounts (a few milligrams) of lanthanide shift reagents into a 1-octanol sample (0.2 mmol in 0.6 mL CDCl_3).

4.1. Experiments with 1-octanol and lanthanide shift reagents

^1H NMR spectrum of 1-octanol ($\text{C}_8\text{H}_{18}\text{O}$, $M = 180.14\text{g/mol}$, 250 MHz in CDCl_3 , δ in ppm): 3.64 (1H, CH_2OH), 1.64 (2H, CH_2), 1.57 (2H, CH_2), 1.30 (8H, 4 CH_2), 0.89 (2H, CH_3).

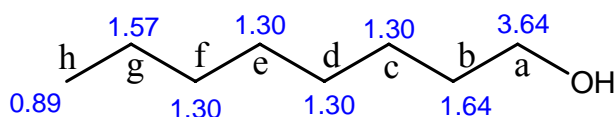


Figure 2.13: Tentative ^1H NMR assignment of 1-octanol.

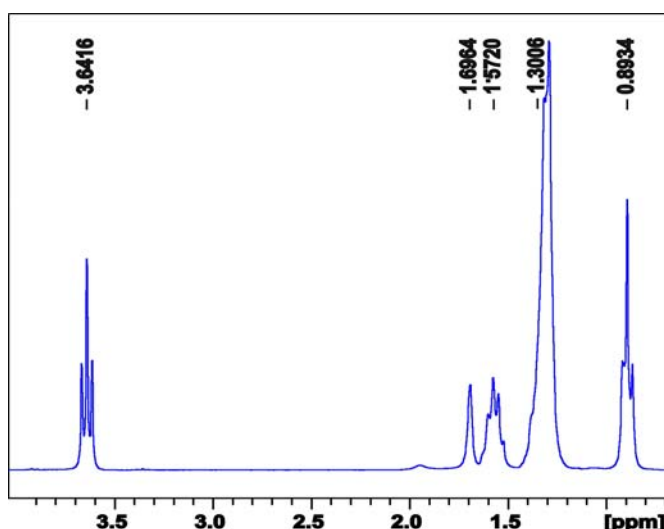


Figure 2.14: ^1H NMR spectrum of 1-octanol (0.2 mmol) in CDCl_3 .

^{13}C NMR spectrum of 1-octanol (62.5MHz in CDCl_3 , δ in ppm):

63.03 (a), 32.81(g), 31.88(c), 29.39 (e), 29.27 (d), 25.78 (f), 22.67 (b), 14.12 (h).

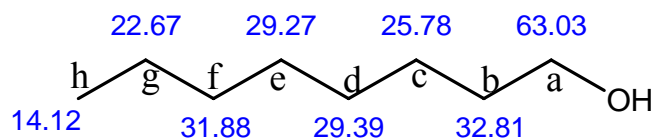


Figure 2.15: Tentative ^{13}C NMR assignment of 1-octanol.

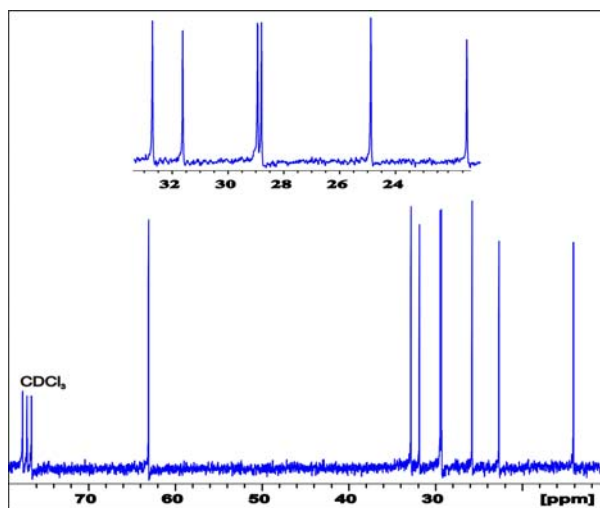


Figure 2.16: ^{13}C NMR spectrum (21-33 ppm) of 1-octanol (0.2 mmol) in CDCl_3 .

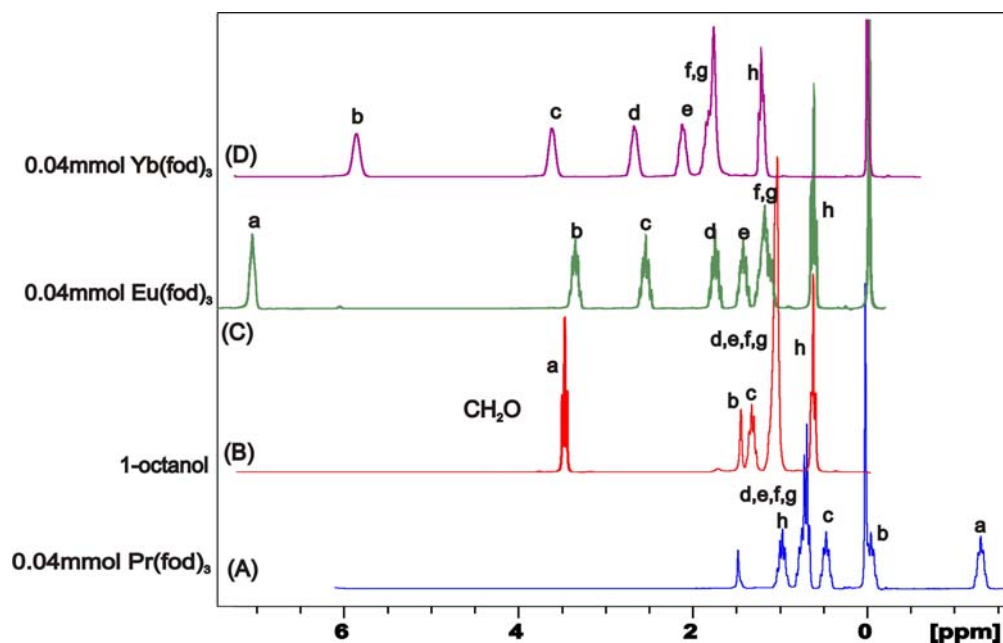


Figure 2.17: ^1H NMR spectra of 1-octanol (0.2 mmol) with different LSR in CDCl_3 .

(B) ^1H NMR spectra of 1-octanol without shift reagent only the protons of CH_2O (3.6 ppm) and CH_3 (0.89 ppm) groups and their direct neighbors are distinguishable. The remaining CH_2 appear as a broad signal around 1 ppm.

(A) With 0.04 mmol $\text{Pr}(\text{fod})_3$ the CH_2O protons have a chemical shift of $\delta_{(\text{ppm})} = -1.45$ and most of the remaining proton signals are overlapped.

(C) With 0.04 mmol $\text{Eu}(\text{fod})_3$ almost all the CH_2 of the octyl chain are separated and the CH_2O group now has a chemical shift of $\delta_{(\text{ppm})} = 6.9$.

(D) With 0.04 mmol $\text{Yb}(\text{fod})_3$ almost all the CH_2 are also separated but they are broadened, the CH_2O group here is too broadened and no longer visible. The amount of $\text{Eu}(\text{fod})_3$ should have been increased in order to separate all the seven CH_2 of the octyl chain but the experiment was more focused on the simplification of the ^{13}C NMR spin system (change the strong coupling to weak coupling).

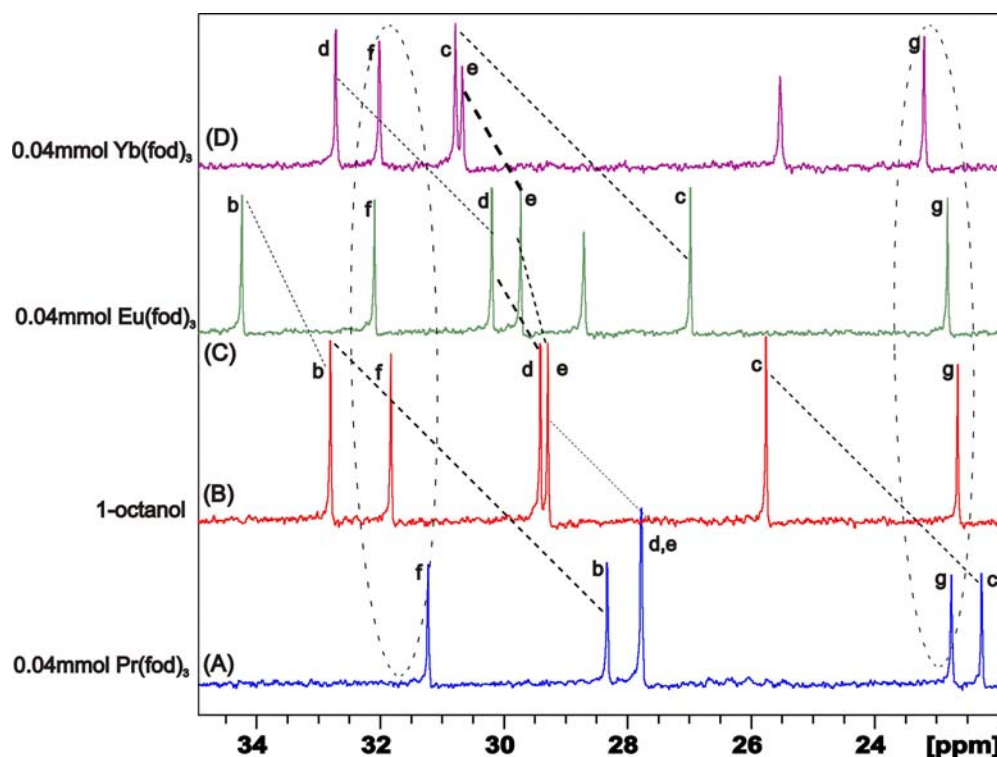


Figure 2.18: ^{13}C NMR spectrum of 1-octanol (0.2 mmol) with different LSR (0.2eq) in CDCl_3

(B) ^{13}C NMR spectrum of 1-octanol without shift reagent, all the seven CH_2 groups are discernible, but the smallest difference in chemical shifts is 0.12 ppm (i.e. 27 Hz at 225 MHz for ^{13}C).

(A) With 0.04 mmol Pr(fod)₃, the CH₂O group here has a chemical shift of $\delta_{\text{(ppm)}} = 50.39$ ($\Delta\delta_{\text{(ppm)}} = -12.64$) and some signals are still overlapped.

(C) With 0.04 mmol Eu(fod)₃, all the seven CH₂ of the octyl chain are separated with a difference of about 0.46 ppm (i.e. 103.5 Hz at 225 MHz for ¹³C) in chemical shifts of the two closest carbons; and the CH₂O group now has a chemical shift of $\delta_{\text{(ppm)}} = 71.38$ ($\Delta\delta_{\text{(ppm)}} = +8.35$).

(D) With 0.04 mmol Yb(fod)₃, almost all the CH₂ are also observable, but they are more broadened and the CH₂O group appears at $\delta_{\text{(ppm)}} = 82.46$ ($\Delta\delta_{\text{(ppm)}} = +19.43$) (smaller and broadened signal).

The induced shifts resulting from the addition of various lanthanide shift reagents to 1-octanol sample (in CDCl₃) are tabulated below.

Table 2.5: Summary of lanthanide ¹³C NMR induced shifts of 1-octanol in CDCl₃ and the effect of added¹ Eu(fod)₃, Yb(fod)₃ and Pr(fod)₃. δ and $\Delta\delta$ are given in ppm.

Position ²	1-octanol	Eu(fod) ₃		Yb(fod) ₃		Pr(fod) ₃	
	δ	δ	$\Delta\delta$	δ	$\Delta\delta$	δ	$\Delta\delta$
a	63.03	71.38	+8.35	82.46	+19.43	50.39	-12.64
b	32.81	34.23	+1.42	41.60	+8.79	28.34	-4.47
c	25.78	26.96	+1.18	32.02	+6.25	22.77	-3.01
d	29.39	30.19	+0.80	30.77	+1.38	27.78	-1.61
e	29.27	29.73	+0.46	30.65	+1.38	27.78	-1.49
f	31.88	32.08	+0.20	32.76	+0.89	31.22	-0.66
g	22.67	22.81	+0.14	23.19	+0.52	22.26	-0.41
h	14.12	14.12	0	14.39	+0.27	13.83	-0.29

¹ 0.04 mmol of each shift reagent were added to the substrate (1-octanol, 0.2 mmol).

² the assignment here is based on our NMR data and also on the simulation using ChewDraw program.

^{13}C -NMR spectrum (62.5MHz for ^{13}C , in CDCl_3 , δ in ppm): 144.67 (s, 3C, $\text{C}_{\text{quaternary}}$, C_{arom}), 127.20 (d, 12C, C_{arom}), 126.21 (s, 3C, C_{arom}), 86.33 (s, 1C, $-\text{O}-\text{CPh}_3$, $\text{C}_{\text{quaternary}}$), 63.75 (s, 1C, $\text{CH}_2-\text{OCPh}_3$), 63.06 (s, 1C, CH_2-OH), 32.83 (s, 1C, CH_2), 30.09 (s, 1C, CH_2), 29.67 (s, 5C, CH_2), 29.46 (s, 1C, CH_2), 26.31 (s, 1C, CH_2), 25.79 (s, 1C, CH_2).

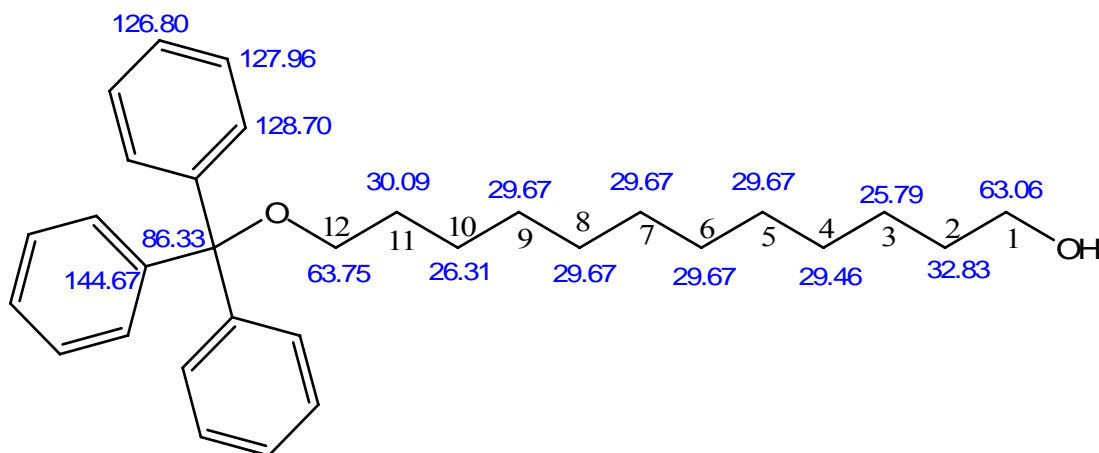


Figure 2.21: ^{13}C NMR assignment of 12-(triphenylmethoxy)dodecan-1-ol (based on our NMR data and also a simulation Chemdraw).

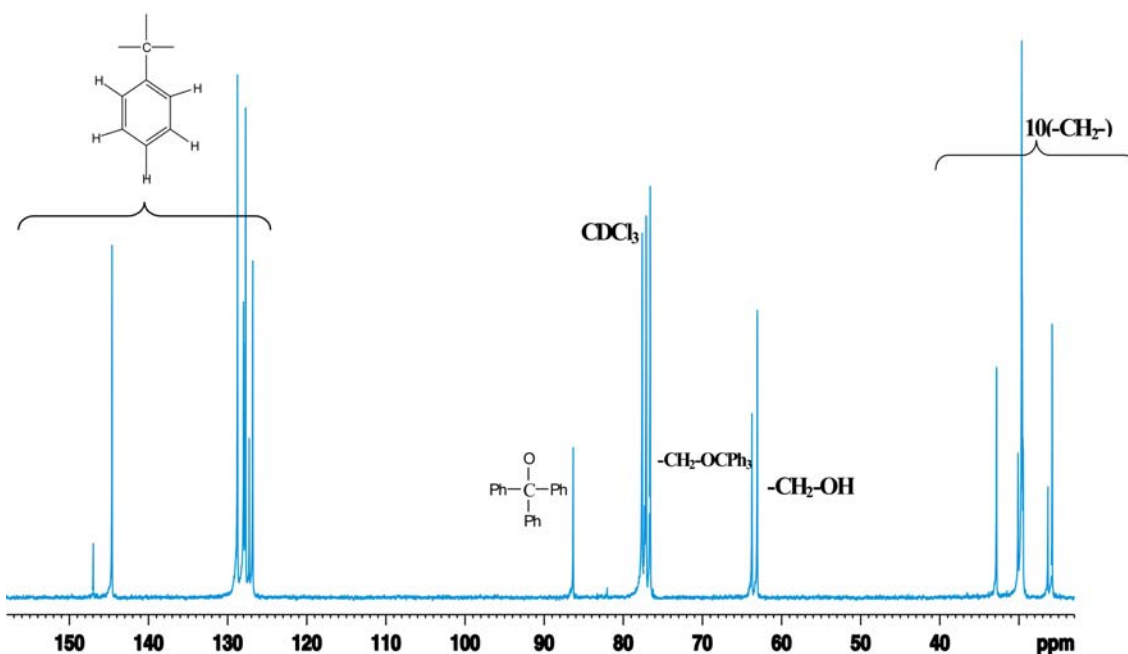


Figure 2.22: ^{13}C NMR spectrum of 12-(triphenylmethoxy)dodecan-1-ol in CDCl_3 (cf. Fig. 1.16).

4.2.2 Experimental results: 12-(triphenylmethoxy)dodecan-1-ol) with added Eu(fod)₃ LSR.

The addition of up to 10 mg (0.01 mmol) of Eu(fod)₃ shift reagent did not alter much the ¹³C NMR spectrum of 12-(triphenylmethoxy)dodecan-1-ol in CDCl₃ as it seen on the figure above. Therefore more interest has been focused on the use of Yb(fod)₃ which has proven to be the best shift reagent for the ¹³C NMR spectroscopy [11, 18].

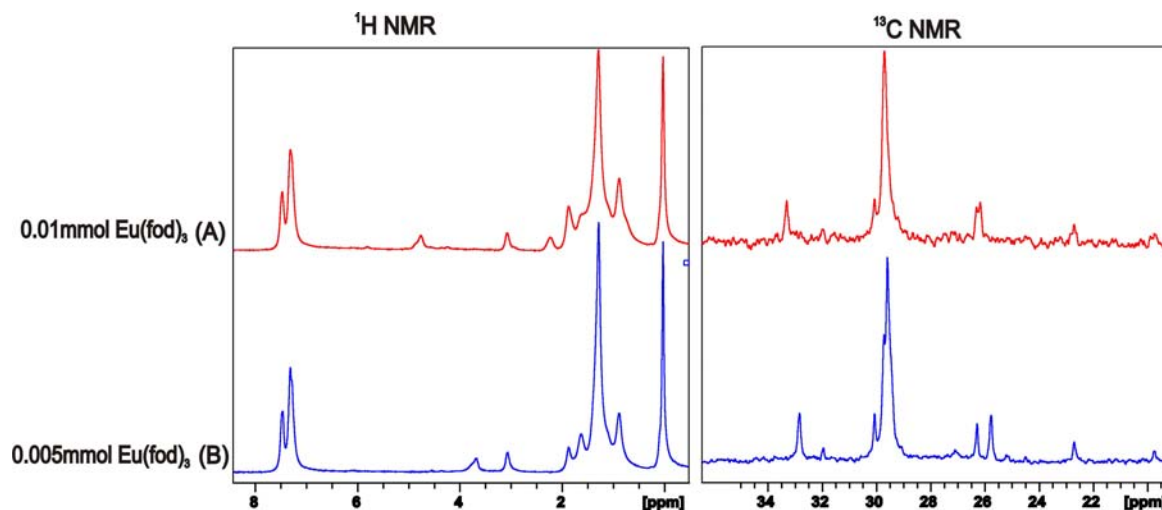


Figure 2.23: ¹H and ¹³C NMR spectra of 12-(triphenylmethoxy)dodecan-1-ol (0.07 mmol) with (A) 0.005 mmol and (B) 0.01 mmol Eu(fod)₃ in CDCl₃.

5. Comparative study: use of various concentrations of Yb(fod)₃ to alter the NMR spectra of 12-(triphenylmethoxy)dodecan-1-ol in CDCl₃.

The recorded ¹H NMR spectra of added Yb(fod)₃ at different concentrations are presented below.

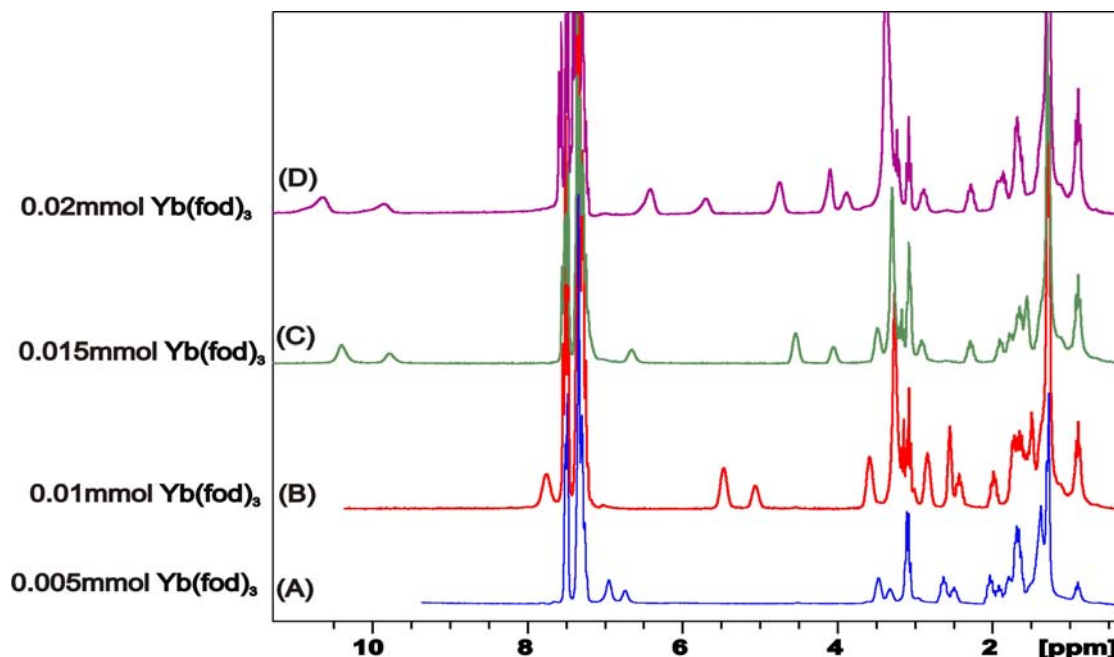


Figure 2.24: ^1H NMR spectra of 12-(triphenylmethoxy)dodecan-1-ol (0.07 mmol) with $\text{Yb}(\text{fod})_3$ at different concentrations in CDCl_3 .

By adding up to 0.02 mmol of $\text{Yb}(\text{fod})_3$ shift reagent to 12-(triphenylmethoxy)dodecan-1-ol sample (in CDCl_3), ^1H NMR spectra of samples with different concentrations of LSR were significantly and progressively altered. However, because of their similar chemical environment (about eight analogous methylene groups CH_2) it became very complex to assign unambiguously a chemical shift to each of the proton groups. The two highest chemical shifts can be assigned to the aldehyde and its adjacent protons, which are close to the complexation site and thus could be more shifted.

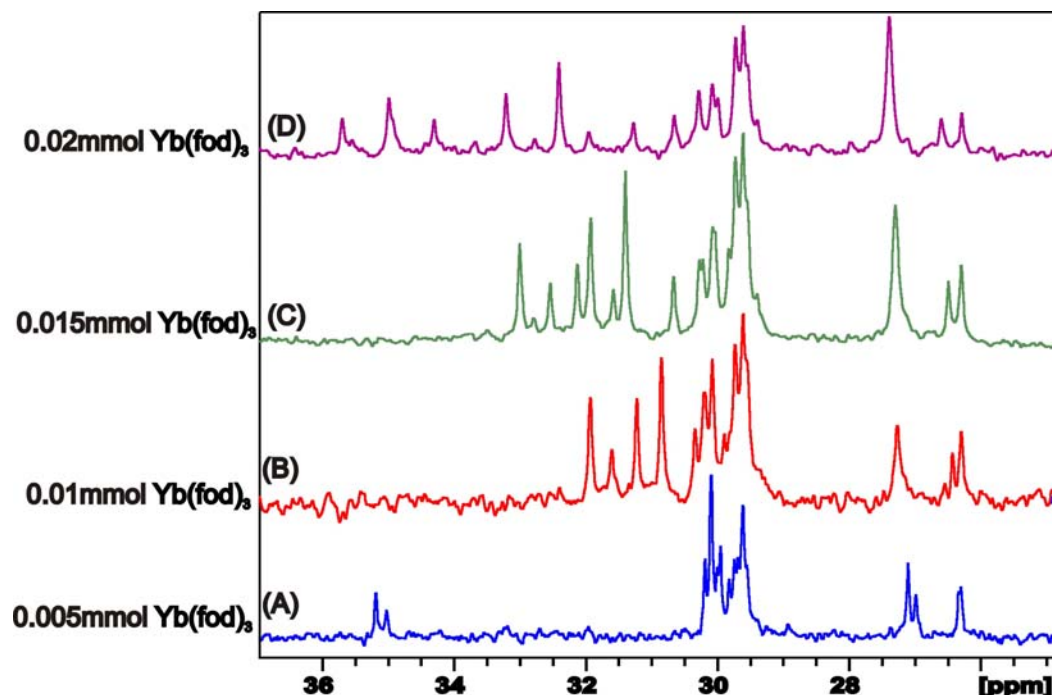


Figure 2.25: ^{13}C NMR spectra of 12-(triphenylmethoxy)dodecan-1-ol (0.07 mmol) with $\text{Yb}(\text{fod})_3$ at different concentrations in CDCl_3 .

The ^{13}C NMR spectrum of 12-(triphenylmethoxy)dodecan-1-ol with shift reagent 0.005 mmol (A) presents CH_2 ($\text{C}_4\text{-C}_9$) signals which are not discernible, the smallest difference in chemical shifts between them is 0.04 ppm (i.e. 9 Hz at 225 MHz for ^{13}C).

(B) With 0.01 mmol $\text{Yb}(\text{fod})_3$ some signals are detached from the broad peak, whereas the variation in chemical shifts here is still less.

(C) With 0.015 mmol $\text{Yb}(\text{fod})_3$ more signals came away from the block of closest signals; differences in chemical shifts between them are already considerable, but at least two pairs of signal are still very close.

(D) With 0.02 mmol $\text{Yb}(\text{fod})_3$ individual signals are much distant and visible in the region 29-36 ppm for the alkyl chain ($\text{C}_4\text{-C}_9$). Larger differences in chemical shifts have been measured, but signals are more broadened in this case.

The observed lanthanide induced ^{13}C NMR shifts are summarized in the following table.

Table 2.6: Comparison of the lanthanide induced ^{13}C NMR chemical shifts value of the substrate 12-(triphenylmethoxy)dodecan-1-ol (0.07 mmol) in CDCl_3 with varying amount of $\text{Yb}(\text{fod})_3$ added. δ and $\Delta\delta$ are given in ppm.

Position ^a	Substrate	0.005 mmol		0.01 mmol		0.015 mmol		0.02 mmol ^b	
	δ	δ	$\Delta\delta$	δ	$\Delta\delta$	δ	$\Delta\delta$	δ	$\Delta\delta$
1	63.06	no $-\text{C}=\text{O}$ signal		no $-\text{C}=\text{O}$ signal		no $-\text{C}=\text{O}$ signal		no $-\text{C}=\text{O}$ signal	
2	32.83	35.19	+2.36	40.70	+7.87	46.81	+13.98	50.45	+17.72
3	25.79	30.18	+4.39 ^c	31.94	+6.24	44.08	+18.29 ^b	47.04	+21.25 ^c
4	29.46	29.99	+0.53	31.23	+1.77	33.00	+3.54	34.99	+5.53
5	29.6	29.95	+0.35	30.86	+1.19	31.93	+2.33	33.21	+3.61
6	29.6	29.82	+0.22	30.21	+0.61	31.40	+1.8	32.41	+2.81
7	29.6	29.74	+0.14	29.75	+0.15	29.73	+0.13	30.29	+0.69
8	29.6	29.68	+0.08	29.68	+0.08	29.73	+0.13	29.71	+0.11
9	29.6	29.6	0	29.62	+0.02	29.62	+0.02	29.68	+0.08
10	26.31	26.31	0	26.31	0	26.31	0	26.31	0
11	30.09	30.09	0	30.09	0	30.09	0	30.09	0
12	63.75	63.75	0	63.75	0	63.75	0	63.75	0

^a the assignment here was based on our NMR data and also on a simulation using ChewDraw program.

^b 0.02 mmol of $\text{Yb}(\text{fod})_3$, but uncertain assignment because more signals than expected in the observed region.

^c The LSR seems to extend its effect more on the beta than the alpha carbon [13].

The addition of up to 0.02 mmol $\text{Yb}(\text{fod})_3$ to the 12-(triphenylmethoxy)dodecan-1-ol sample more or less resolves the ^{13}C NMR spectrum. Nevertheless, more signals than expected appeared in the considered region (29-30 ppm for sample without shift reagent, shifted to 30-36 ppm) and led to a more ambiguous assignment of interfering carbon resonances. As an attempt to solve this problem of attribution, 2D HSQC experiments were also performed with this sample.

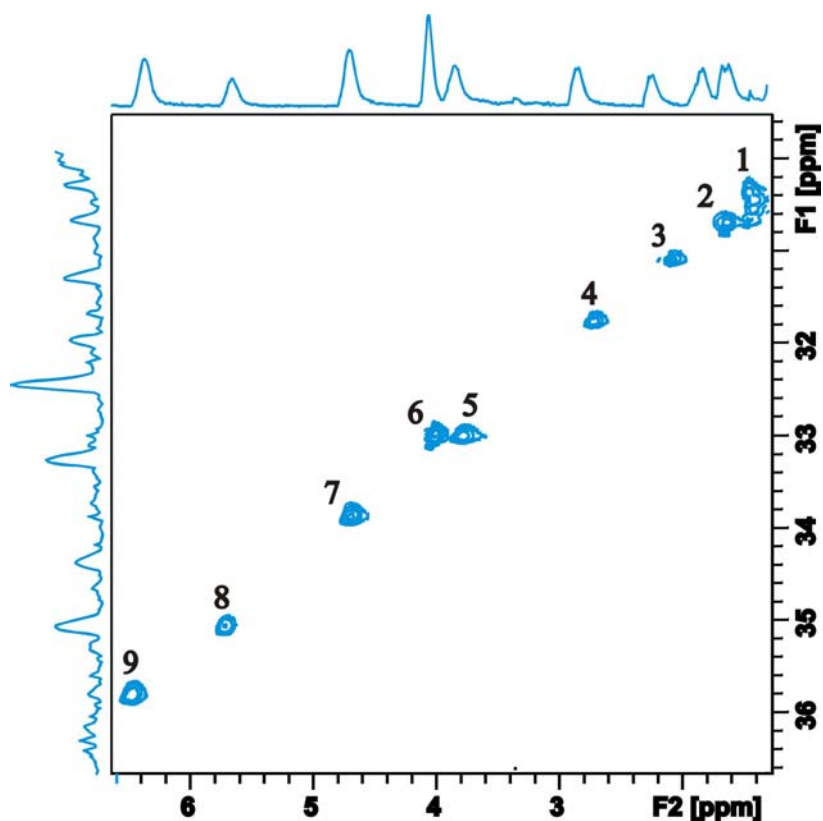


Figure 2.26: HSQC spectrum of 12-(triphenylmethoxy)dodecan-1-ol (0.07 mmol) with 0.02 mmol Yb(fod)₃ in CDCl₃ (expanded region 30-36 ppm).

The following HSQC cross peaks were observed.

Table 2.7: HSQC cross peaks of 12-(triphenylmethoxy)dodecan-1-ol (0.07 mmol) with 0.02 mmol Yb(fod)₃ in CDCl₃.

¹³ C δ(ppm)	¹ H δ(ppm)
30.05	1.64
30.28	1.85
30.67	2.24
31.28	2.85
32.44	3.83, 4.06
33.28	4.69
34.37	5.66
35.08	6.37, 9.79
35.84	10.59

But the appearance of nine, instead of six signals in the region of interest, has made the analysis of the spectrum more complex.

CONCLUSION AND OUTLOOK

Although LSR have been rarely employed for the simplification of ^{13}C NMR spectra (compared to ^1H NMR) that are otherwise uninterpretable in the first order, successful assignments of ^{13}C signals of some complex molecules have been reported [13, 19-22]. In the present work, this LSR feature has been exploited in order to change the strong couplings between the carbon nuclei to weak couplings and additionally differentiate the interfering ^{13}C NMR resonances of 12-fluorododecanal and 12-(triphenylmethoxy)dodecan-1-ol, the ^{13}C -labeled analogues of which could be used for quantum computing experiments. Some shift reagents including $\text{Eu}(\text{fod})_3$, $\text{Yb}(\text{fod})_3$ and $\text{Pr}(\text{fod})_3$ have been utilized at various concentrations leading to effective induced shifts. Although all shift reagents give observable values of $\Delta\delta_{(\text{ppm})}$ for the studied compounds, the average difference in the induced chemical shifts was unfortunately less than expected. Comparisons show that in the presence of 0.2eq of $\text{Pr}(\text{fod})_3$, overlapping ^{13}C NMR signals of 12-fluorododecanal were more or less resolved. On the other side, the result obtained with 0.2eq of $\text{Eu}(\text{fod})_3$ shows that signals were entirely indiscernible and when 0.2eq of $\text{Yb}(\text{fod})_3$ was added to the substrate, the carbonyl signal was lost. It is known that the magnitude of the change in chemical shift is not only related to the molar ratio of LSR to substrate, but also to the type of complex formed. Therefore, experiments were performed with 12-(triphenylmethoxy)dodecan-1-ol with the expectation to obtain better results by complexing the alcohol functional group instead of the aldehyde. Thus, when 0.3eq (0.2 mmol) of $\text{Yb}(\text{fod})_3$ was added to the substrate (12-(triphenylmethoxy)dodecan-1-ol, 0.07 mmol), carbons undergo larger changes in chemical shifts as compared to the variations observed for the aldehyde substrate. The smallest difference in chemical shifts observed was about 0.23 ppm i.e. 51.75 Hz if experiments are performed on a 900 MHz (^1H) or 225 MHz (^{13}C) spectrometer. This value is less than 350 Hz (equivalent to 10 times $^1J_{\text{CC}} \approx 35$ Hz, in case of weak coupling) which is the minimum interval required for successful quantum computing experiments using such a spin chain molecule. Nevertheless, only a provisional assignment has been done in this case because more than the expected number of signals has appeared in the crowded region of the ^{13}C spectra. The appearance of extra NMR signals could be due to slow exchange or to coexistence of different conformations. A possible solution to our strong coupling problem could be the following:

In our experiments, the lanthanide ion is attached to one end of the spin chain due to the nucleophilic center being at this point. Therefore, the strongest effects were performed on the atoms near the end of the chain which actually do not have any strong coupling problem. The atoms at the middle of the chain, where stronger variation in chemical shifts was needed, were much less affected by the lanthanide.

If we could bring a paramagnetic ion in close contact to the atoms in the middle of our spin chain, we would get the induced paramagnetic shift exactly where we need it. Also the magnitude of the induced shift would be much bigger than from an ion which is attached far away from the atoms of interest.

There are several possibilities to bring an ion near the middle of the spin chain: for example one could attach the ion via a flexible linker to the molecule; or one could design a molecule which can complex the spin chain and the ion at the same time and in close proximity.

REFERENCES

- [1] N. Khaneja and S. J. Glaser, *Phys. Rev. A*, **66**, 060301 (R) (2002).
- [2] J. Fitzsimons, and J. Twamley, *Phys. Rev. Lett.*, **97**:090502, (2006).
- [3] J. Fitzsimons, L. Xiao, S. C. Benjamin, and J. A. Jones, *Phys. Rev. Lett.*, **99**:030501, (2007).
- [4] B. D. Flockhart and Jonas J., (1976) "Lanthanide Shift Reagents in Nuclear Magnetic Resonance Spectroscopy", *Critical reviews in Analytical Chemistry*, **6**:1, 69-130.
- [5] J. A. Jackson, J. F. Lemons, and H. Taube, *J. Chem. Phys.*, **32**, 553 (1960).
- [6] C. C. Hinckley, *J. Am. Chem. Soc.* **91**, 5160 (1969).
- [7] R. E. Sievers, Ed., in NMR Shift Reagents. Academic Press, New York, N. Y., 1973.
- [8] Morill, T. C., Chiasson, J. B., Jankowski, K., Raber, D. J., Paasivirta, J., and Wenzel, T. J. in: Lanthanide Shift Reagents in Stereochemical Analysis. Ed.: Morill, T. C. VCH Publishers, Weinheim: 1986; Vol. 5, p. ix.
- [9] E. DeBoer and H. van Willigen, *Progr. NMR Spectroscopy*, 1967, **2**, 111.
- [10] H. M. McConnell and R. Robertson, *J. Chem. Phys.*, (1958), **29**, 6, 1361-1365.
- [11] Hesse, M., Meier, H, and Zeeh, B. in Spektroskopische Methoden in der organischen Chemie. 5. überarbeitete Auflage (5th Ed.). Stuttgart; New York: Thieme, 1995, pp. 128-129.
- [12] S. Braun, H.-O. Kalinowski, S. Berger in "150 and More Basic NMR Experiments" second expanded Ed.; WILEY-VCH, Weinheim: 1998, p. 253.
- [13] J. W. Apsimon, H. Beierbeck and J. K. Sanders. *Can. J. Chem.*, **51**, 3874.
- [14] J. Briggs, F. A. Hart, G. P. Moss, and E. W. Randall. *Chem. Commun.*, **364** (1971).
- [15] G. E. Hawkes, D. Leibfritz, D. W. Roberts, and J. D. Roberts. *J. Am. Chem. Soc.* **95**, 1659 (1973).
- [16] I. Armitage, J. R. Campbell, and L. D. Hall. *Can. J. Chem.* **50**, 1972. pp. 2139-2141
- [17] R. von Ammon and R.D. Fischer. *Angew. Chem. Internat. Edit.* / **11** (1972)/ No.8.
- [18] L. Pohl, Paramagnetische Verschiebungskomplexe in der Protonenkernspektroskopie, *Kontakte* 1, pp. 17-23.
- [19] H. Kessler and M. Motler. *Angew. Chem. Internat. Edit.* **13** (1974), No. 8.
- [20] D. J. Chadwick and D. H. Williams. *J. C. S. Chem. Comm.* 01 January 1974, p. 128.
- [21] H. J. Schneider and E. F. Weigand. *Tetrahedron* **31**, pp. 2125-2133, 1975.
- [22] H. J. Schneider, U. Buchheit and P. K. Agrawal. *Tetrahedron* **40**, 6, 1017 (1984).

CHAPTER 3: PROTON RELAXATION TIMES OF SMALL ORGANIC MOLECULES IN SUPERCRITICAL CARBON DIOXIDE (SC CO₂)

1. MOTIVATION AND MAIN OBJECTIVES

Over the past half century, Nuclear Magnetic Resonance (NMR) has become one of the preeminent techniques among spectroscopic methods for the analysis and structure elucidation of organic, bioorganic and organometallic compounds. Following the general goals of our research group, which are the development of novel theoretical and experimental techniques in NMR spectroscopy, with applications to structural studies of biopolymers as well as quantum computing, the latter issue has been further investigated.

All quantum computers are limited by their decoherence time as quantum algorithms must be completed before the coherence is lost. Therefore the question of how one can increase the relaxation time T_2 in order to apply much longer pulse sequences arises. The relaxation time of a solute is related to the viscosity of the milieu in which it is dissolved [1, 2]. Solvents properties (viscosity, density, polarity) play then a key role in liquid-state NMR spectroscopic experiments as well as in quantum computing. The solvent viscosity defines the molecular interactions and determines thus the rotational correlation time of the dissolved molecule. Wand et al. [3] proposed an approach to reduce the NMR relaxation times of large proteins. They claimed that the encapsulation of a protein in a reverse micelle dissolved in a low-viscosity fluid allows it to tumble as fast as a much smaller protein. Successful experiments have been performed using the following low viscosity solvents: alkanes [3], liquid carbon dioxide [4] and supercritical xenon [5].

Until now, quantum computers are made of molecules with up to 15 quantum qubits. Hence, the idea of measuring the relaxation times of small organic molecules (a few qubits) directly dissolved in supercritical carbon dioxide (SC CO₂), one of the least viscous solvents [6], and comparing them with values obtained with common low viscosity NMR solvents.

Table 3.1: Viscosity of some organic solvents (at 20°C unless otherwise indicated).

Compound	Viscosity (cP)
Pentane	0.23
Ethyl Ether	0.24
Methyl <i>t</i> -Butyl Ether	0.27
Hexane	0.31
Acetone	0.36
Triethylamine	0.36 (25°C)
Acetonitrile	0.38 (15°C)
Heptane	0.42
Methyl Ethyl Ketone	0.43
Cyclopentane	0.44
Dichloromethane	0.44
<i>n</i> -Butyl Chloride	0.45
Ethyl Acetate	0.45
Glyme	0.46 (25°C)
Iso-Octane	0.50
Methyl <i>n</i> -Propyl Ketone	0.51
Tetrahydrofuran	0.55
Chloroform	0.57
Methyl Isobutyl Ketone	0.58
Methanol	0.59
Toluene	0.59
1,1,2-Trichlorotrifluoroethane	0.71
<i>n</i> -Butyl Acetate	0.74
Ethylene Dichloride	0.79
<i>N,N</i> -Dimethylformamide	0.92
Trifluoroacetic Acid	0.93
Pyridine	0.95
Cyclohexane	1.0
Water	1.0
Ethyl Alcohol	1.1 (25°C)
<i>o</i> -Dichlorobenzene	1.32 (25°C)
1,4-Dioxane	1.37
<i>N</i> -Methylpyrrolidone	1.67 (25°C)
2-Methoxyethanol	1.72
Dimethyl Acetamide	2.14
Dimethyl Sulfoxide	2.24
<i>n</i> -Propyl Alcohol	2.3
Isopropyl Alcohol	2.4
<i>n</i> -Butyl Alcohol	2.98

Source: <http://macro.lsu.edu/HowTo/solvents7viscosity.htm> (available on 28.03.2011). cP is centipoise; 1 P (poise)= 1g.cm⁻¹.s⁻¹; 1Pa.s= 1kg.m⁻¹.s⁻¹= 10 P.

According to Table 3.1, pentane would be a good candidate for NMR experiments where long T_2 is needed. Unfortunately, only a few compounds are soluble in alkanes (for NMR of reverse micelles in alkanes [7]); also the price for deuterated pentane is considerably more expensive than typical deuterated NMR solvents. Ethers can dissolve slightly more compounds than alkanes, but they also suffer from very high cost for their deuterated versions and are not commonly used as NMR solvents.

Therefore, acetone- d_6 , acetonitrile- d_3 and dichloromethane- d_2 are commonly used when long T_2 is needed in the NMR experiments. Additionally, these solvents have to be degassed in order to remove paramagnetic oxygen which would decrease T_2 .

With a viscosity of about 0.075 cP at 180 bar and 35°C [6], the supercritical carbon dioxide (SC CO_2) is three times less viscous than pentane and more than four times less viscous than acetone- d_6 , acetonitrile- d_3 and dichloromethane- d_2 . Additionally, SC CO_2 is capable of dissolving a large variety of compounds. The chart below shows the dependence of the carbon dioxide viscosity against the pressure.

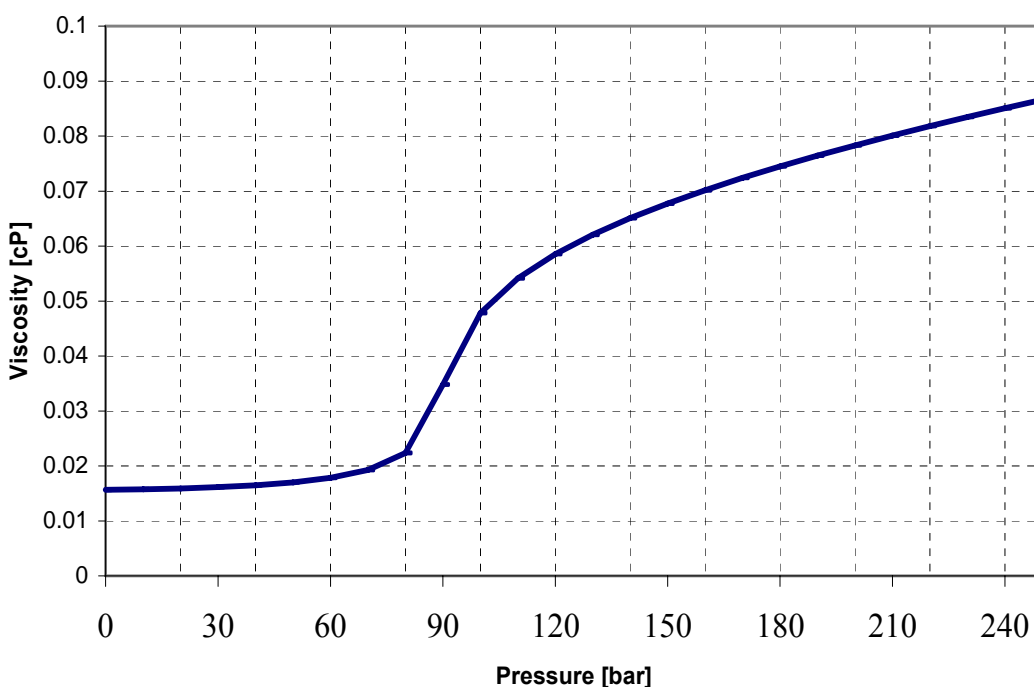


Figure 3.1 Plot of the viscosity of carbon dioxide versus the pressure [8, 9]. At 180 bar and 35°C, the viscosity of the SC CO_2 is about 0.075 cP, which is very low as compared to any common NMR solvent.

For reverse micelles which encapsulate proteins the dissolution in low viscosity solvents clearly reduces the relaxation time of the protein as compared to the dissolution of the same protein in water. But for small organic molecules, directly dissolved in low viscosity solvents, the dependence of T_2 on the viscosity of the solvent seems to be much more complicated.

Possible reasons could be:

- Clustering formation: in Wand et al. experiments the reverse micelles can be individually dissolved, whereas in the case of small organic molecules there may be small drops/clusters in supercritical CO_2 (not really dissolved).
- Interactions of molecules with CO_2 .
- Stokes-Einstein relation (see Equation 3.2) is not valid for small organic molecules.

Considering these two approaches, and willing to exploit the hypothesis that the relaxation time can be increased by dissolving the molecule in a medium that exhibits a very low viscosity (approach similar to [3]), supercritical carbon dioxide is a good candidate for such a solvent. Consequently, an extensive search using a large number of small organic molecules with different functional groups has been probed in order to find compounds where the increase of the relaxation time T_2 due to the solvent is very prominent. Relaxation time values obtained in supercritical CO_2 will be compared to those obtained in the most common NMR sample (low viscosity solvents such as CD_2Cl_2 and CD_3CN , and degassed sample (cf. Table 3.1)). If these molecules are found, they are candidates for the implementation of quantum computing experiments allowing longer pulse sequences than in the standard NMR sample. As the typical conditions for NMR spectroscopy in supercritical carbon dioxide are 180-200 bar and 40°C , a high pressure setup had to be established, at first.

2. CONCEPTION OF THE EQUIPMENT

The high pressure device was mounted step by step and optimized for an adequate use.

A high pressure NMR setup was established, consisting of a carbon dioxide cylinder with riser or ascending pipe (from Westfalen AG, Münster-Germany); a modified HPLC pump, and a high pressure NMR cell which was purchased. This sapphire NMR cell designed by Peterson et al. has several advantages including excellent NMR performance, high pressure tolerance, chemical inertness, and a relatively large active volume [10].

The High Pressure Liquid Chromatography (HPLC) pump (from Waters Associates, Inc. Model 6000A Solvent Deliver System) which normally receives solvents at a pressure of 1bar at the input side of the piston was modified in order to tolerate a pressure of ~80 bar. A pressure control (Electronic manometer ECO1 Mano 2000 from Keller GmbH, Jestetten-Germany) was also included near the NMR cell in order to check that the pressure inside the pump is correctly transmitted into the cell. Additional valves have been installed (from CS-chromatographie Service GmbH, Langerwehe-Germany) on the apparatus to permit not only the preparation of two samples at once, but also the monitoring of the liquid CO₂ flow (by means of an electronic manometer) and the cleaning of the pipes before and after use so as not to introduce some dirt into the high pressure NMR cell.

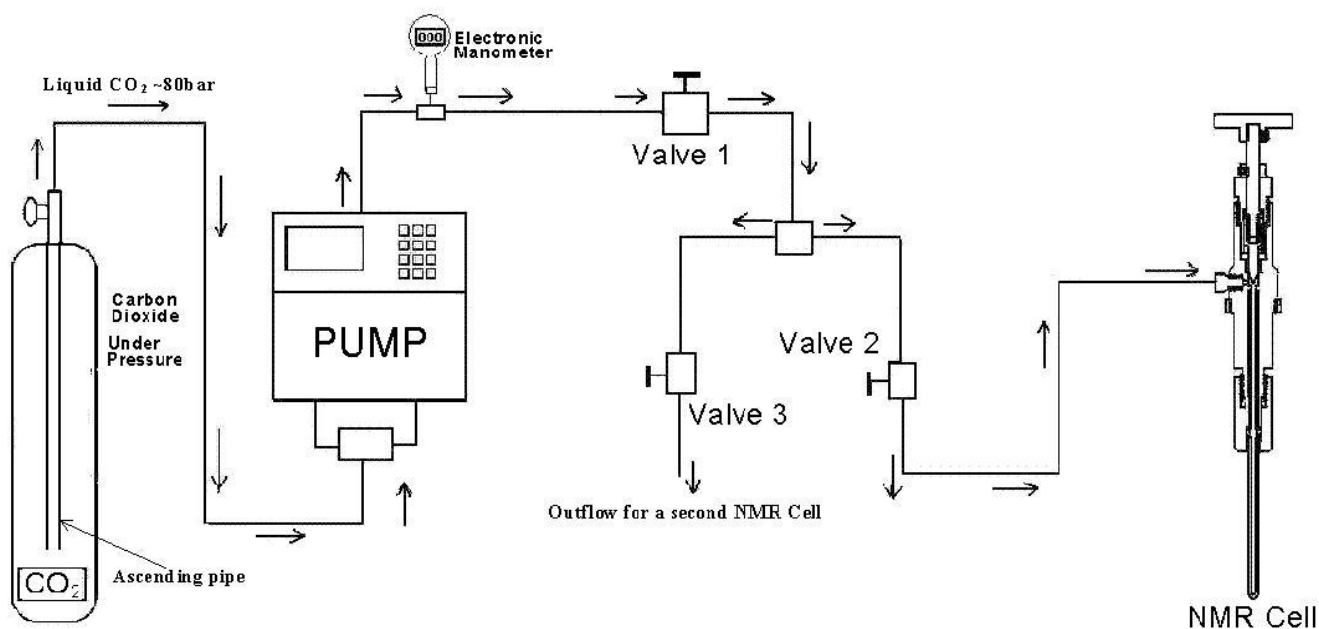


Figure 3.2: High pressure setup for the supercritical CO₂ sample preparation.

3. THEORY

3.1 Viscosity of fluids

The viscosity can be defined as the resistance to change exhibited by fluids. Practically the viscosity of a fluid or a solvent usually manifests itself as a resistance to flow, both in liquids and gases but at a much lower level in gases. Put simply, the less viscous the fluid is, the greater its ease of movement (fluidity) [11]. In mechanical and chemical engineering as well as in fluid dynamics the viscosity is usually symbolized by μ [12-14]. But the symbol η is mostly used by chemists and physicists. The viscosity is usually given in *poise* (P) or *centipoise* (cP).

3.2 Rotational Correlation Time τ_c and Relaxation Times T_1 and T_2

For a spherical particle dissolved in a solvent of viscosity η the rotational correlation time τ_c can be described by the Stokes-Einstein relation:

$$\tau_c = \frac{4\pi \cdot r^3 \eta}{3\kappa T} \quad (3.1)$$

where κ is the Boltzmann constant, r is the hydrodynamic radius of the considered particle, and T is the absolute temperature. The line width observed for the dissolved particles is determined by the transverse or spin-spin relaxation time T_2 . The dependence of relation times T_1 and T_2 to the rotational correlation time has been extensively studied [5, 15-17]. For a spherical molecule in motion in a solution, the relation between the spin-lattice, the spin-spin relaxation times and the rotational correlation time τ_c have been proved to be as follows [16, 17]:

$$\frac{1}{T_1} = M_2 \tau_c \left[\frac{2/3}{1 + (\omega_0 \tau_c)^2} + \frac{8/3}{1 + (2\omega_0 \tau_c)^2} \right] \quad (3.2)$$

$$\frac{1}{T_2} = M_2 \tau_c \left[1 + \frac{5/3}{1 + (\omega_0 \tau_c)^2} + \frac{2/3}{1 + (2\omega_0 \tau_c)^2} \right] \quad (3.3)$$

with $M_2 = \frac{9}{20} \left(\frac{\mu_0}{4\pi} \right)^2 \frac{\hbar^2 \gamma^4}{r^6}$ for a diatomic molecule.

3.3 Relaxation time measurements

3.3.1 Longitudinal or spin-lattice relaxation time T_1

The longitudinal or spin-lattice relaxation time T_1 represents the time constant necessary for the z-magnetization to return to the thermal equilibrium (Boltzmann equilibrium), after a radio frequency pulse [18]. The spin-lattice relaxation time T_1 highly depends on the type of nuclei and also on the other factors like the viscosity of the solution, the motion of the molecule and the chemical environment of the nucleus. The spin-lattice relaxation time T_1 can be measured using various techniques like the progressive saturation, the inversion recovery and the saturation recovery experiments [18, 19], but the most common used method is the Inversion Recovery experiment [20]: $d_1 - 180^\circ_x - \tau - 90^\circ_x - \text{detection (FID)}$.

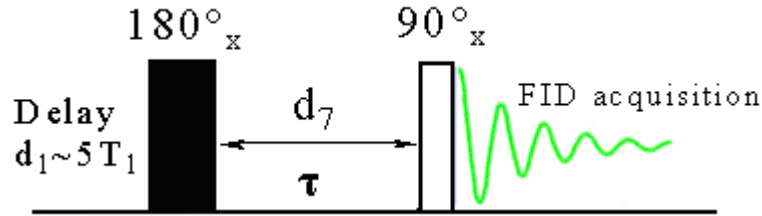


Figure 3.3: Inversion Recovery (IR) NMR pulse sequence.

After a radio frequency pulse, a nucleus relaxes toward its equilibrium value at an exponential rate. The value estimated as the spin-lattice relaxation time is actually the time constant of this exponential curve. The signal evolution versus T_1 is described as follows:

$$M_z = M_0(1 - 2e^{-\frac{\tau}{T_1}}) \quad (3.4)$$

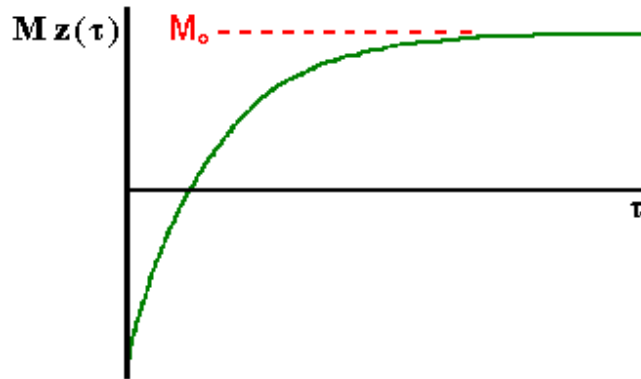


Figure 3.4: Plot of the longitudinal magnetization M_z versus the delay τ (adapted from J. P. Hornak, The Basics of NMR-<http://www.cis.rit.edu/htbooks/nmr/inside.htm>)

The relaxation time T_1 can also be roughly determined using τ_{null} (for $M_z = 0$) i.e.
 $T_1 = \tau_{null} / \ln 2$.

3.3.2 Transverse or spin-spin relaxation time T_2

The transverse or spin-spin relaxation time, known as T_2 , is a time constant which determines the decay of the $M_{x,y}$ magnetization in Nuclear Magnetic Resonance (NMR) and Magnetic Resonance Imaging (MRI). In other words, the relaxation time T_2 is related to the rate T_2^{-1} at which $M_{x,y}$, the transverse component of the magnetization vector, decays towards zero. The spin-spin relaxation time T_2 is a crucial parameter in NMR since knowledge of its value is essential for planning NMR experiments and usually for designing new pulse sequences, because their evolution periods must not considerably be longer than T_2 [16].

The standard method for measuring T_2 is the Carr-Purcell-Meiboom-Gill (CPMG) experiment [21] which uses a series of echoes that follows the 90° pulse. The pulse sequence is defined as follows: $d_1 - 90^\circ_x - (\tau - 180^\circ_y - \tau)_n - \text{detection (FID)}$

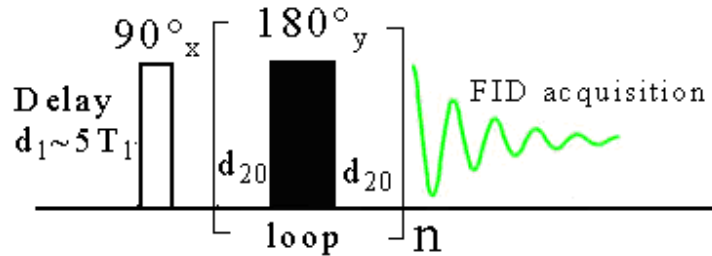


Figure 3.5: Carr-Purcell-Meiboom-Gill (CPMG) NMR pulse sequence.

The basic pulse sequence of the CPMG experiment is based on the spin-echo pulse sequence and consists of the following steps:

- A 90° pulse creates transverse magnetization
- A spin echo period (delay- 180° -delay block) determines the decay of the M_{xy} magnetization, this period is repeated n times.
- Acquisition.

The magnetization follows an exponential decay, hence the following relationship and plot:

$$M_{xy}(t) = M_{xy}(0)e^{\frac{-t}{T_2}} \quad (3.5)$$

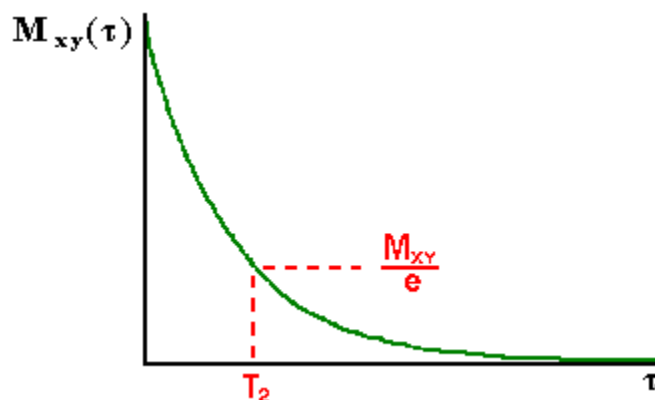


Figure 3.6: Plot of the transverse magnetization M_{xy} versus the delay τ (adapted from J. P. Hornak, The Basics of NMR-<http://www.cis.rit.edu/htbooks/nmr/inside.htm>).

4. EXPERIMENTAL RESULTS

Once the high pressure equipment was installed, samples were prepared and the relaxation times were measured without any problems. The results obtained for some small organic compounds are presented below.

EXPERIMENTAL SETUP

- For reference samples: 5 μ L (liquid) or 5 mg (solid) compound in 0.6 mL deuterated NMR solvent, room temperature and degassed (degassed sample).
- For supercritical carbon dioxide (SC CO₂) samples: 5 μ L (liquid) or 5 mg (solid) compound in SC CO₂ at 40°C and 180 bar.
- For reference/SC CO₂ samples including shift reagents: 5 μ L (liquid) or 5 mg (solid) compound in NMR solvent/SC CO₂ and addition of a few milligrams (0.005 to 0.01 mmol) of the lanthanide shift reagent.

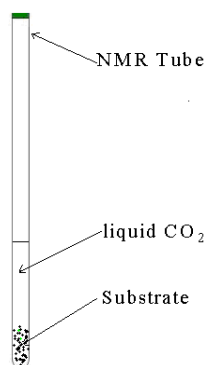
It is known that the addition of lanthanide shift reagents (LSR) to NMR samples affects the line widths of NMR signals (broadening), thus reduces the relaxation time T_2 of the nuclei. Moreover, from our experience with LSR (cf. Chapter 2), small amount of

lanthanide shift reagent was added to some samples prior to the relaxation time measurement and the behavior in both the NMR solvent and the SC CO₂ was studied.

- Experimentally, conventional pulse programs i.e. Inversion Recovery (IR) for T₁ and Carr-Purcell-Meiboom-Gill (CPMG) for T₂ were used to determine the relaxation times.

The use of small amounts of the desired compound has for advantages:

- If the compound is not soluble in SC CO₂, no NMR signal will be observed because the compound (substrate) will stay at the bottom of the NMR tube.
- The probability of clustering is reduced (less interactions between the compound and the SC CO₂).



The proton relaxation time values obtained for some small organic molecules are summarized in the tables below.

Table 3.2: Comparison of proton spin-lattice (T₁) and the spin-spin (T₂) relaxation times (in ms) of some organic molecules measured in common NMR solvents and in SC CO₂.

Compound ¹ H δ _[ppm]	Ref. solv.	T ₁ ref. solv.	T ₁ SC CO ₂	T ₂ ref. solv.	T ₂ SC CO ₂
Acetone 2.2	CDCl ₃	4829	1862	4520	1716
Chloroform 7.7	CD ₃ CN	9605	1310	4957	971
Ethyl Acetate 4.1	CD ₂ Cl ₂	6923	2912	5089	1478
2.0		6348	2583	6076	897
1.3		6583	3340	6503	1261
Ethyl Acetate 4.1	CDCl ₃	4572	2912	3089	1478
2.0		4148	2583	3347	897
1.3		3782	3340	3076	1261

Toluene	CD ₃ CN				
7.29		17247	1282	8398	1578
2.4		10243	2043	7384	1566
Acetonitrile	CD ₃ CN				
2.1		16306	680	6557	165
Acetic anhydride	CD ₃ CN				
2.6		11650	2537	10922	2210
Acetyl chloride	CD ₃ CN				
2.7		8413	1443	7331	1057
Acetic acid	CD ₃ CN				
2.06		8885	596	7574	57
Cyclohexane	CD ₃ CN				
1.5		7067	2141	1366	1231
DMF	CD ₃ CN				
2.9		5704	1780	2794	1032
7.9		7990	1661	-	1160
Diethylether	CD ₃ CN				
3.5		6371	1146	3478	338
1.2		6059	1241	3834	251
Methanol	CD ₃ CN				
3.3		7293	564	5362	355
2.4		8568	484	5300	93
Acetaldehyde	CD ₃ CN				
2.2		19302	2330	16104	1251
9.7		27326	2129	18288	990
tert-Butanol	CD ₃ CN				
1.2		9274	584	8238	519
2.5		10925	198	424	111
Acetone					
Dimethylacetal	CD ₃ CN				
1.3		4621	1593	4215	709
3.2		6309	1667	5667	1071

In all the above cases, dissolution of the compound in supercritical CO₂ did not yield longer T₂ relaxation times compared to optimal common samples (low viscosity NMR solvent; degassed sample). But in a few cases, we could find an increase of T₂ when the solvent was changed to supercritical CO₂. But in the individual case of the acetone sample with shift reagent, the relaxation times were almost the same in the SC CO₂ as well as in the common NMR solvent.

Table 3.3: Samples with added Yb(fod)₃ shift reagent of which an increase of relaxation times (in ms) in SC CO₂ were noted (in CDCl₃).

Compound ¹ H δ _[ppm]	Ref. solv.	T ₁ ref. solv.	T ₁ SC CO ₂	T ₂ ref. solv.	T ₂ SC CO ₂
Acetone + 0.01 mmol LSR	CDCl ₃				
3.6		364	255	97	88
Ethyl Acetate + 0.005 mmol LSR	CDCl ₃				
5.4		326	367	23	109
3.2		355	392	75	97
1.8		1155	837	244	263
Ethyl Acetate + 0.01mmol LSR	CDCl ₃				
6.5		185	208	54	83
4.1		202	219	45	72
2.2		739	355	121	163

The ethyl acetate sample was of bigger interest as a considerable increase in T₂ was observed in SC CO₂ compared to the values obtained in CDCl₃ (η= 0.57 cP). The relaxation times in SC CO₂ was again compared to those obtained with a lower viscosity solvent like CD₂Cl₂ (η= 0.44 cP).

Table 3.4: Samples with added Yb(fod)₃ shift reagent and increase of relaxation times (in ms) in SC CO₂ compared to CD₂Cl₂.

Compound ¹ H δ _[ppm]	Ref. solv.	T ₁ ref. solv.	T ₁ SC CO ₂	T ₂ ref. solv.	T ₂ SC CO ₂
Ethyl Acetate +0.005 mmol LSR	CD ₂ Cl ₂				
5.3		358	367	97	109
3.1		393	392	88	97
1.7		1302	837	294	263
Ethyl Acetate +0.01 mmol LSR	CD ₂ Cl ₂				
6.3		201	208	75	83
3.9		221	219	51	72
2.1		816	355	144	163

CONCLUSION AND PERSPECTIVES



The relaxation times were determined using the conventional methods (Inversion Recovery (IR) for T_1 and Carr-Purcell-Meiboom-Gill (CPMG) for T_2) and the values were obtained automatically by means of the analytical tool of the Topspin software. The measured proton spin-spin relaxation time T_2 varies between 23 ms and 16 s, these values are consistent with those reported in the literature [22, 23]. The accuracy of the measurements is estimated to an average of 0.5%. In general, the relaxation time values obtained in the “standard” supercritical CO_2 setup have been only in a few cases longer compared to those obtained in the best “classical” NMR setup. Relaxation times measured in supercritical CO_2 were found to be at least one tenth of those measured in the common NMR solvent. But, the addition of a small amount of the lanthanide shift reagent $\text{Yb}(\text{fod})_3$ into the sample led to a change of this ratio (1/10). Thus the relaxation times of the acetone sample with LSR in supercritical CO_2 were similar to those in the common NMR solvent (also with LSR). Nevertheless, a slight increase in the relaxation times T_1 and T_2 in supercritical CO_2 was noted in the case of ethyl acetate samples with little amount of lanthanide shift reagent (in CDCl_3 and in CD_2Cl_2).

Based on these results, the expectation of finding molecules with relaxation time T_2 , longer in supercritical CO_2 than in a standard NMR sample for quantum computing experiments, has not been fully satisfied. Nevertheless, supercritical CO_2 as solvent may help for shift reagent NMR samples where T_2 is crucial.

REFERENCES

- [1] S. Macura, Y. Huang, D. Suter and R. R. Ernst. *J. Magn. Reson.* **43**, 259-281 (1981).
- [2] Sudmeier, J. L.; Anderson, S. E.; Frye, J. S. *Concepts Mag. Reson.* 1990, **2**, 197.
- [3] A. J. Wand, M. R. Ehrhardt and P. F. Flynn, *Proc. Natl. Acad. Sci. USA*, **95**, 15299 (1998).
- [4] S. Gaemers, C. J. Elsevier, A. Bax. *Chem. Phys. Lett.* (1999), **301**, 138-144.
- [5] Mathias Meier, Alexander Fink and Eike Brunner, *J. Phys. Chem. B* 2005, **109**, 3494-3498.
- [6] A. Padua, W. A. Wakeham, and J. Wilhelm, *Int. J. of Thermodynamics*, **15**, 5. 1994.
- [7] R. W. Peterson, B. G. Lefebvre and J. A. Wand, *J. Am. Chem. Soc.*, **127**, 29 (2005), 10176.
- [8] E.W. Lemmon, M.O. McLinden and D.G. Friend, "Thermophysical Properties of Fluid Systems" in NIST Chemistry WebBook, NIST Standard Reference Database Number 69, Eds. P.J. Linstrom and W.G. Mallard, National Institute of Standards and Technology, Gaithersburg MD, 20899, <http://webbook.nist.gov>. Available on June 4, 2011).
- [9] A. Fenghour, W. A. Wakeham, and V. Vesovic. The Viscosity of Carbon Dioxide. *J. Phys. Chem. Ref. Data*, **27**, 1, 1998.
- [10] Ronald W. P. and A. J. Wand, *Review of Scientific Instruments* 76, 094101 (2005).
- [11] Symon, Keith (1971). *Mechanics* (Third ed.). Addison-Wesley.
- [12] V. L. Streeter, E. B. Wylie, and K. W. Bedford. *Fluid Mechanics*, McGraw-Hill, 1998 ISBN 0070625379.
- [13] J. P. Holman *Heat Transfer*, McGraw-Hill, 2002 ISBN 0071226214.
- [14] Frank P. Incropera, David P. DeWitt, *Fundamentals of Heat and Mass Transfer*, Wiley, 2007. ISBN 0471457280.
- [15] S. Chen, D. T. Miranda, and R. F. Evilia, *The Journal of Supercritical Fluids* (1995), **8**, 255.
- [16] G. Hirasaki, Sho-Wei Lo and Y. Zhang. *Magn. Reson. Imaging* (2003), **21**, 3-4, 269-277
- [17] Cowan B. Nuclear Magnetic Resonance and Relaxation. New York: 1997.
- [18] S. Braun, H.-O. Kalinowski, S. Berger in "150 and More Basic NMR Experiments", pp. 155-161.
- [19] <http://www.chem.queensu.ca/facilities/NMR7nmr/WEBCOURSE7T!.HTM>
- [20] R. L. Vold, J. S. Waugh, M. P. Klein, D. E. Phelps, *J. Chem. Phys.* 1968, **48**, 3831-3832.
- [21] S. Meiboom, D. Gill, *Rev. Sci. Instrum.* 1958, **29**, 688-691.
- [22] G. Bonera, L. Chiodi, G. Lanzi and A. Rigamonti. *IL NUOVO CIMENTO*. Vol. **XVII**, No. 2, 16, Luglio 1960.
- [23] R. Rowan III, J. A. McCammon, and B. D. Sykes. *J. Am. Chem. Soc.* / **96**:15/ July 24, 1974.

APPENDIX 1: MANUAL GUIDE OF THE HIGH PRESSURE DEVICE (English version)

<p>Date: March 2011</p> <p>Responsible persons: Arnaud Djintchui Ngongang, Raimund Marx</p> <p>Field: Organic Chemistry, AK Glaser Lehrstuhl Organische Chemie II</p>	<p>Technische Universität München</p>   <p>Department of Chemistry</p>
Application Domain	
<p>Operation of a High-pressure Pump with connected Carbon Dioxide Gas Cylinder (ca. 80 bar) and High-pressure NMR sample Tube</p> <p>Carbon dioxide under pressure; CO₂</p> <p>Physical and chemical properties</p> <p>Physical state at 20 °C: Gas</p> <p>Colour: Colourless.</p> <p>Odour: No odour warning properties.</p> <p>Molecular weight : 44.01</p> <p>Melting point [°C] : -56.6</p> <p>Boiling point [°C] : -78.5 (s)</p>	
Risks to Human and the Environment	
<p>Great risk of injury by falling</p> <ul style="list-style-type: none">• Releasing the stored pressure energy (gas cylinder rocket-like device in uncontrollable movements) due to mechanical damage or accidental opening of the valve.• The high pressure NMR tube (filled with CO₂) can explode if dropped. It should be transported in a foam-lined and labeled box. <p>Potential Hazards</p> <ul style="list-style-type: none">• Explosion of gas cylinder or NMR tube and hazards though overheating <p>Classification and hazard for man and environment</p> <p>Pressurized gas exposure may cause cold burns or frostbite.</p> <p>WGK-Class (Germany) : NWG – not hazardous identification Number-256</p> <ul style="list-style-type: none">• Physical Hazards: Gases under pressure <p>Classification according to EC 67/548 or EC: Annex VI CLP not mentioned. 1999/45. Not classified as a hazardous substance / preparation.</p>	



EC No warning necessary.

Toxicological information: Inhalation of high concentrations may cause rapid circulatory insufficiency. Symptoms include headache, nausea and vomiting, which can lead to unconsciousness. May also cause suffocation or asphyxiation.



Labeling according to EC Regulation 1272/2008 (CLP).

• **Precautionary statements**

• **Prevention:** P282: Wear gloves/face shield/eye protection.

• **Storage:** P403: Store in a well-ventilated place.



Labelling EC 67/548 or EC 1999/45

Danger and hazard pictograms code: Explosion

Signal word: Warning Explosion!

Symbol(s): Explosion

R Phrase(s): Explosion

S Phrase(s): Explosion

Other hazards: possible asphyxia if inhaled in high concentrations.



Protective Measures and Rules

Technical and organizational

- * well ventilated room with fume-hood
- * contingency plan (communication to the outside)
- * Emergency: 112 (fire Department)



In terms of Person

Operated only by trained personnel, always in pairs and in a fume hood.

- Protect eyes, head, face and skin: wear a face shield and gloves.
- Wear protective gloves (leather gloves)
- Wear closed shoes
- Do not move or roll the gas cylinder, but transport it with a cylinder carts
- Chain the bottle, to prevent against falling
- Do not throw the cylinder, to prevent high mechanical stress



- Open gas cylinder valves slowly to avoid pressure shock
- Close valves after work, screwing the cap when not in use
- Return gas cylinder up to a certain residual pressure (1.5 bar), empty with the valve closed
- Do not approach the gas cylinder with flame, do not put any oil or grease on it
- Protect the gas cylinder from fire hazards, for example do not store together with flammable liquids.

Prior to transport:

- Ensure the cylinder valve is closed and not leaking.
- Verify the valve outlet cap nut or plug (where provided) is correctly fitted.
- Ensure the valve protection (where provided) is correctly fitted.
- Be sure that there is adequate ventilation.
- Compliance with applicable regulations.

Behavior by Disorders

The occurrence of dangerous situations, securing accident site immediately and take immediate action, taking care to comply with its own safety! If necessary. Emergency call. Warn people at risk and possibly to leave the danger zone request. If leaking try to stop release. To sewers, basements and mines, or any place where its accumulation could be dangerous.

Accidental release measures

Personal precautions: Evacuate area.

Use protective clothing.

Wear self-contained breathing apparatus when entering area unless atmosphere is proved to be safe. Ensure adequate air ventilation.

Environmental precautions: Try to stop release.

Prevent from entering sewers, basements and work pits, or any place where its accumulation can be dangerous.

Clean up methods: Ventilate area.

First Aid Measures

Inhalation of CO₂:

In high concentrations may cause asphyxiation. Symptoms may include loss of mobility/consciousness. In this case, the person must be placed in a recovery position. Keep victim warm and quiet. Call a doctor. Apply artificial respiration if necessary.



Skin and eyes contact with pressurized CO₂:

Immediately flush eyes thoroughly with water for at least 15 minutes.

Ingestion of CO₂: Ingestion is not considered as a potential route of exposure.

Specific hazards: Exposure to fire may cause containers to rupture/explode.

Maintenance and Proper Disposal

General

At least short visual inspection of the pump and the gas connection before using the machine forever.

Electrical inspection once a year by specially trained person.

Not in the sewers, basements and pits, and similar places where the gas accumulation could be dangerous escape.

The discharge of large quantities of CO₂ gas into the atmosphere should be avoided.

Broken or not functional pump should be delivered to the garage

Empty bottle of gas returned to the material management.

Handling and storage under pressure CO₂ gas cylinder

Handling: Suck back of water into the container must be prevented.

Do not allow back feed into the container.

Use only properly specified equipment which is suitable for this product, its supply pressure and temperature. Contact your gas supplier if in doubt.

Refer to supplier's container handling instructions.

Storage: Keep container below 50°C in a well ventilated place.

User Guide

- 1. Operated only by trained personnel, always in pairs and in a fume hood.**
2. Use for each measurement a new top seal; and replace the bottom seal (seat of the sapphire tube) after 10 measurements
3. Inspect at visually the pump, the seals and the gas connection before each use
4. Attach the stand upright for the high-pressure NMR tube with clamp on the tripod
5. Introduce the substance to be measured in a clean Sapphire tube and close immediately to the headboard of the apparatus. Attention must adjust valve for volatile substances are already closed!
6. Carefully insert the High pressure NMR tube into the stand
7. Wear protective clothing: lab coat, face shield, gloves and safety glasses.
8. Open the gas cylinder
9. Turn on the pump
10. Turn on the manometer
11. Open valves 1 and 2
12. Wait until the pressure rises to the desired value (here ~ 180bar)
13. Open the valve of the high-pressure NMR tube (with the black cap) wait until the pressure rises to the set point, then close the valve.
14. Close the gas cylinder valve; turn off the pump and pressure gauge
15. Close valve 2
16. Unscrew the CO₂ supply line from the high-pressure NMR tube
17. Take the High-pressure NMR tube in the stand to the transport container, remove the tube from the rack and place it in the foam box.
18. Open valves 1 and 2 to release the pressure
19. Carefully transport the tube (in the box) to the spectrometer
20. Wear the leather gloves, the eye and face protections when inserting or removing the tube into/from the spectrometer; also when emptying the NMR tube.

APPENDIX 2: MANUAL GUIDE OF THE HIGH PRESSURE DEVICE (German version)

Erstellungsdatum: März 2011

Verantwortlicher:

Arnaud Djintchui Ngongang, Raimund Marx

Arbeitsbereich: Organische Chemie

AK Glaser, Lehrstuhl Organische Chemie II

Technische Universität München



Department of Chemistry

Anwendungsbereich

Betrieb von Hochdruckpumpe mit angeschlossener Kohlendioxid Gasflasche (ca. 80 bar) und angeschlossenen Hochdruck-NMR-Röhrchen

Kohlendioxid unter Druck; CO₂

Physikalischer Zustand bei 20 °C: Gas.

Farbe: Farblos.

Geruch: Keine Warnung durch Geruch.

Molekulargewicht: 44,01

Schmelzpunkt [°C]: -56,6

Siedepunkt [°C]: -78,5 (s)

Kritische Temperatur [°C]: 30

Dampfdruck [20°C]: 57,3 bar

Gefahren für menschen und Umwelt

Große Verletzungsgefahren beim Umfallen

- Freisetzen der gespeicherten Druckenergie (Gasflasche gerät in raketenartige unkontrollierbare Bewegungen) durch mechanische Beschädigung oder unbeabsichtigtes Öffnen des Ventils.
- Das Hochdruck NMR-Röhrchen (gefüllt mit CO₂) kann explodieren, wenn es herunterfällt. Es sollte mit schaumstoffausgekleideter und gekennzeichnete Kiste transportiert werden.

Mögliche Gefahren von unter Druck stehendem CO₂

* Explosion von Gasbehälter und NMR-Röhrchen Gefahren durch Überhitzung.

Einstufung und Gefahrenhinweise für Mensch und Umwelt

Unter Druck stehendes Gas Kontakt kann Kaltverbrennungen bzw. Erfrierungen verursachen.



WGK-Klasse (Deutschland) : NWG - nicht wassergefährdend
Kenn-Nr. 256.

Physikalische Gefahren : Unter Druck stehende Gase- Achtung (H281)



- **Einstufung nach EG 67/548 oder EG:** In Anhang VI CLP nicht genannt.

1999/45. Nicht als gefährlicher Stoff / Zubereitung eingestuft. Keine EG Kennzeichnung erforderlich.

- **Toxikologische Angaben:** Hohe Konzentrationen verursachen schnell Kreislaufschwäche. Symptome sind Kopfschmerz, Übelkeit und Erbrechen, wobei es zur Bewusstlosigkeit kommen kann. Kann auch erstickend wirken.



Kennzeichnung nach Verordnung EG 1272/2008 (CLP).

- **Gefahrenpiktogramm Code :** Explosion

- **Signalwort :** Achtung Explosionsgefahr!

- **Gefahrenhinweise:** Explosion

- **Sicherheitshinweise**



Prävention: P282: Schutzhandschuhe/Gesichtsschild/Augenschutz tragen.

Aufbewahrung: P403: An einem gut belüfteten Ort aufbewahren.

Kennzeichnung nach EG 67/548 oder EG 1999/45.



Schutzmaßnahmen und verhaltenregeln

- **Technisch und Organisatorisch**

gut belüftete Raum mit Abzug

Notfallplan (Kommunikation nach außen)

Notruf: 112 (Feuerwehr)



- **Personenbezogen**

Bedienung nur durch unterwiesene Personen, immer zu zweit sein und im Abzug arbeiten.

Augen, Kopf, Gesicht und Haut vor Flüssigkeitsspritzen schützen:

Gesichtsschutz und Schutzbrille tragen

Schutzhandschuhe tragen; Geschlossene Schuhe tragen



Beim Transport der Gasflasche, nicht schieben oder rollen, sondern mit Flaschenkarren transportieren; gegen Umfallen sichern (anketten)
Hohe mechanische Beanspruchung verhindern; nicht werfen
Gasflaschenventile langsam öffnen, um Druckstöße zu vermeiden
Ventile schließen bei Arbeitsende; Aufschrauben der Verschlußkappe bei Nichtbenutzung
Gasflasche nur bis zu einem gewissen Restdruck (ca. 1,5 bar) entleeren, mit geschlossenem Ventil zurückgeben
Gasflasche nicht mit der Flamme berühren, nicht ölen oder fetten
Schutz der Gasflaschen gegen Brandgefahr, z.B. nicht gemeinsam mit brennbaren Flüssigkeiten lagern.

Vor dem Transport :

- Gasflasche sichern; das Flaschenventil muss geschlossen und dicht sein.
 - Die Ventilverschlußmutter oder der Verschluss-Stopfen (soweit vorhanden) muss korrekt befestigt sein.
- Die Ventilschutzeinrichtung (soweit vorhanden) muss korrekt befestigt sein.
- Ausreichende Lüftung sicherstellen.
 - Geltende Vorschriften beachten.

Verhalten bei Störungen

Beim Auftreten gefährlicher Situationen Unfallstelle sofort sichern und umgehend Maßnahmen einleiten; dabei stets die eigene Sicherheit beachten! Ggf. Notruf absetzen.

Gefährdete Personen warnen und ggf. zum Verlassen des Gefahrenbereichs auffordern.

Bei Gasaustritt von unter Druck stehendem CO₂

Versuchen den Gasaustritt zu stoppen. Eindringen in Kanalisation, Keller, Arbeitsgruben oder andere Orte, an denen die Ansammlung gefährlich sein könnte, verhindern.

Reinigungsmethoden von CO₂

Den Raum belüften.

Erste Hilfe



Beim Einatmen von CO₂

Hohe Konzentrationen können Ersticken verursachen. Symptome können Verlust der Bewegungsfähigkeit und des Bewusstseins sein. In diesem Fall, ist die betreffende Person in stabiler Seitenlage zu lagern. Warm und ruhig halten. Arzt hinzuziehen. Bei Atemstillstand künstliche Beatmung.

Beim Augenkontakt mit unter Druck stehenden/komprimierten CO₂

Die Augen sofort mindestens 15 Minuten mit Wasserspülen.

Beim Verschlucken von CO₂

Verschlucken wird nicht als möglicher Weg der Exposition angesehen.

Instandhaltung und Sachgerechte Entsorgung

Allgemeines

- Sichtprüfung der Pumpe und der Dichtungen den Gasanschluss vor jeder Benutzung kontrollieren.
- Elektrische Prüfung der Pumpe einmal im Jahr durch Fachpersonal
- Nicht in die Kanalisation, Keller, Arbeitsgruben und ähnliche Plätze, an denen die Ansammlung des Gases gefährlich werden könnte, ausströmen lassen.
- Das Ablassen großer Mengen CO₂ in die Atmosphäre sollte vermieden werden.
- Kaputte Pumpe in die Werkstatt bringen und leere Gasflasche an die Materialverwaltung zurückgeben.

Handhabung und Lagerung von CO₂ Gasflasche

Handhabung: Eindringen von Wasser in den Gasbehälter verhindern.

Rückströmung in den Gasbehälter vermeiden

Nur Ausrüstungen verwenden, die für dieses Produkt und den vorgesehenen Druck und Temperatur geeignet sind. Im Zweifelsfall den Gaslieferanten konsultieren. Bedienungshinweise des Gaslieferanten beachten.

Lagerung von CO₂ Gasflasche: Behälter bei weniger als 50°C an einem gut gelüfteten Ort lagern.

Bedienungsanleitung

1. **Bedienung nur durch unterwiesene Personen, immer zu zweit sein und im Abzug arbeiten.**
2. Für jede Messung neue obere Dichtung verwenden, untere Dichtung (Sitz des Saphir-Röhrchens) nach 10 Messungen erneuern.
3. Vor jeder Benutzung Sichtprüfung der Pumpe, der Dichtungen und des Gasanschlusses.
4. Ständer für das Hochdruck NMR-Röhrchen mit Klammer auf der Stativ stehend befestigen.
5. Die zu messende Substanz in das saubere Saphir-Röhrchen geben und sofort mit dem Kopfteil der Apparatur verschrauben. Achtung! Ventil muss dazu bei flüchtigen Substanzen schon geschlossen sein!
6. Hochdruck NMR-Röhrchen vorsichtig in dem Ständer stecken.
7. Schutzkleidung anziehen: Laborkittel, Schutzbrille, Gesichtschutz und Handschuhe.
8. Gasflasche öffnen
9. Pumpe anschalten
10. Manometer anschalten
11. Ventile 1 und 2 öffnen
12. Warten bis der Druck auf den gewünschten Wert steigt (hier ~180bar)
13. Das Ventil des Hochdruck NMR-Röhrchen (mit der schwarzen Kappe) öffnen, warten bis der Druck auf den Sollwert steigt, anschließend Ventil schließen.
14. Gasflaschenventil schließen, Pumpe und der Manometer abschalten.
15. Ventil 2 schließen.
16. CO₂-Zuleitung an das Hochdruck NMR-Röhrchen abschrauben.
17. Hochdruck NMR-Röhrchen in Ständer zum Transportbehälter bringen, Röhrchen aus dem Ständer entfernen und in die mit Schaumstoff ausgekleidete Kiste legen
18. An der Apparatur den Druck durch Öffnen der Ventile 1 und 2 ablassen und Anlage stromlos machen.
19. Vorsichtiger Transport des Röhrchens in der Kiste zum Spektrometer.
20. Beim Einbringen/Entnehmen des Röhrs in/aus das Spektrometer, muss die Schutzbrille und Gesichtschutz weiterhin getragen werden; auch beim Ausleeren.

CHAPTER 4: DEVELOPMENT OF A 3-QUBIT THERMAL STATE NMR QUANTUM COMPUTER FOR THE EXPERIMENTAL IMPLEMENTATION OF THE AHARONOV/JONES/LANDAU (AJL) QUANTUM ALGORITHM

INTRODUCTION

A knot can be described as a closed, non-self-intersecting curve that is embedded in three-dimensional space [1]. Because of its many applications including chemistry, molecular biology, quantum mechanics and particles physics, knot theory is a very exciting field of study in mathematics.

One of the “big problems” in knot theory is to decide, whether two given knots are equivalent (see Section 1.1) or not. There is still no algorithm available that solves this problem in a reasonable amount of time. A famous historic example is the “Perko Pair” [2]: two knots which were listed as different knots in a commonly used knot table. It took several decades before Kenneth Perko found that these knots are equivalent.

Knot invariants help in answering the question, if two given knots are equivalent or not: a knot invariant always assigns the same value or function to equivalent knots. But unfortunately, different knots may have the same knot invariant. The Jones Polynomial [3] is such a knot invariant: If the Jones Polynomials of two given knots are different, one knows for sure, that the two knots are different. But, if the Jones Polynomials of two given knots are the same, one does not know if the knots are equivalent or different.

In the last decade, two important connections between knot theory and quantum computing have been developed:

- Topological quantum computer [4-8].
- Approximative evaluation of the Jones Polynomial using a quantum computer [9].

The latter is ideally suited for an implementation on a thermal state NMR quantum computer [10-16].

1. KNOT THEORY: KNOTS AND BRAIDS

1.1 Equivalent knots

According to knot theory, two knots (or links) are equivalent if they can be transformed to each other by using only so-called Reidemeister moves and trivial moves (moves that do not change the number of crossing at any time of the move) [17].

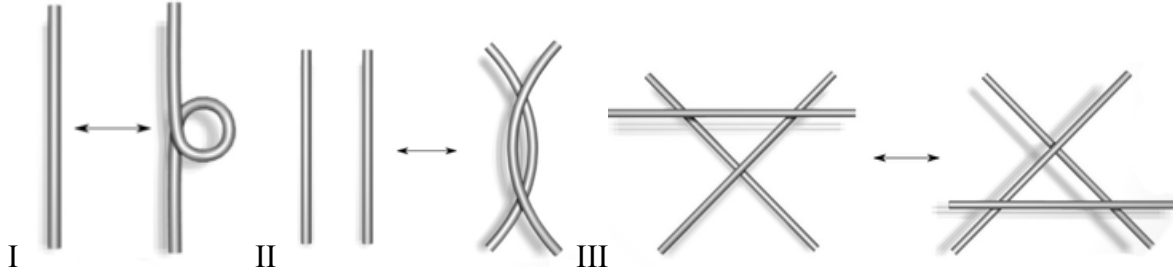


Figure 4.1: The three Reidemeister moves

1.2 Knot functions: Bracket Polynomial and Jones Polynomial

The Bracket Polynomial [9] is an important function from the set of all knots to a set of polynomials $\langle L \rangle(A, B, d)$; but the Bracket Polynomial is not a knot invariant. Nevertheless, there is a close connection between the Bracket Polynomial and the Jones Polynomial:

a) If one sets $B = A^{-1}$ and $d = (-A^2 - A^{-2})$, the resulting polynomial $\langle L' \rangle(A)$ is invariant under Reidemeister moves II and III.

b) If $\langle L' \rangle(A)$ is multiplied with a factor, which depends on the writhe [1] of the knot, the resulting polynomial also becomes invariant under Reidemeister move I and is then called the Jones Polynomial.

1.3 Determination of the Bracket Polynomial and the Jones Polynomial

The determination of the Bracket Polynomial is exponentially complex. As the Jones Polynomial can easily be derived from the Bracket Polynomial (see above), the demanding part of the determination of the Jones Polynomial is to determine $\langle L' \rangle(A)$.

The following sections will describe, how $\langle L' \rangle(A)$ can be derived in a way, that can easily be transferred into a quantum computing algorithm:

Step #1:

It is known that by using a classical theorem of J. W. Alexander [18], every knot and link can be obtained as the closure of a braid. An example of the Figure-Eight knot and its corresponding trace-closed 3-strand braid is illustrated below.

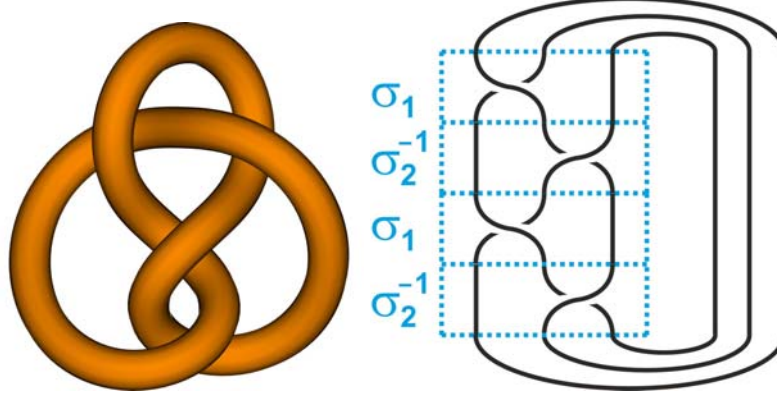


Figure 4.2: The Figure-Eight knot represented as a 3-strand braid

Therefore, the Figure-Eight knot corresponds to the following sequence of braid group elements: $\sigma_1 - \sigma_2^{-1} - \sigma_1 - \sigma_2^{-1}$

Step #2:

L. H. Kauffman showed [9] how to obtain matrix representations U for the generators of a given braid group σ . For the 3-strand braid group the following matrix representations can be derived:

$$\sigma_1 \rightarrow U_1 = \begin{pmatrix} e^{-i\theta} & 0 \\ 0 & -e^{i\theta} \frac{\sin(4\theta)}{\sin(2\theta)} + e^{-i\theta} \end{pmatrix}$$

$$\sigma_2 \rightarrow U_2 = \begin{pmatrix} -e^{i\theta} \frac{\sin(6\theta)}{\sin(4\theta)} + e^{-i\theta} & -e^{i\theta} \frac{\sqrt{\sin(6\theta)\sin(2\theta)}}{\sin(4\theta)} \\ -e^{i\theta} \frac{\sqrt{\sin(6\theta)\sin(2\theta)}}{\sin(4\theta)} & -e^{i\theta} \frac{\sin(2\theta)}{\sin(4\theta)} + e^{-i\theta} \end{pmatrix}$$

The inverses of the braid group elements correspond to the inverses of the matrices:

$$\sigma_1^{-1} \rightarrow U_1^{-1} \quad \text{and} \quad \sigma_2^{-1} \rightarrow U_2^{-1}$$

Therefore, the Figure-Eight knot corresponds to the following sequence of matrices:

$$U_1 - U_2^{-1} - U_1 - U_2^{-1}$$

Step #3:

The matrix product is calculated from the derived sequence of matrices. Finally, the trace of that matrix product leads to the desired Bracket Polynomial:

$$tr\{U_{\text{Figure-Eight}}\} = tr\{U_1 \cdot U_2^{-1} \cdot U_1 \cdot U_2^{-1}\}$$

The evaluation of the matrix trace of $U_{\text{Figure-Eight}}$ for different values of θ corresponds to the evaluation of $\langle L'_{\text{Figure Eight}} \rangle(A)$ for different values of A .

1.4 Evaluation of the Bracket Polynomial using NMR quantum computing

The trace of a unitary matrix can be evaluated by NMR quantum computing concepts:

- i) From a unitary U , a controlled unitary matrix cU is created:

$$cU = \begin{pmatrix} \mathbb{1} & 0 \\ 0 & U \end{pmatrix}, \text{ where } \mathbb{1} \text{ is the identity matrix.}$$

In our example for the Figure-Eight knot, the unitaries U are 2 by 2 matrices, and the controlled unitaries cU are 4 by 4 matrices.

Therefore, the Figure-Eight knot corresponds to the following matrix product:

$$cU_{\text{Figure-Eight}} = cU_1 \cdot cU_2^{-1} \cdot cU_1 \cdot cU_2^{-1}$$

- ii) The cU -s which correspond to braid group elements ($cU_1, cU_1^{-1}, cU_2, cU_2^{-1}$) are now translated into 2-qubit NMR pulse sequence blocks:

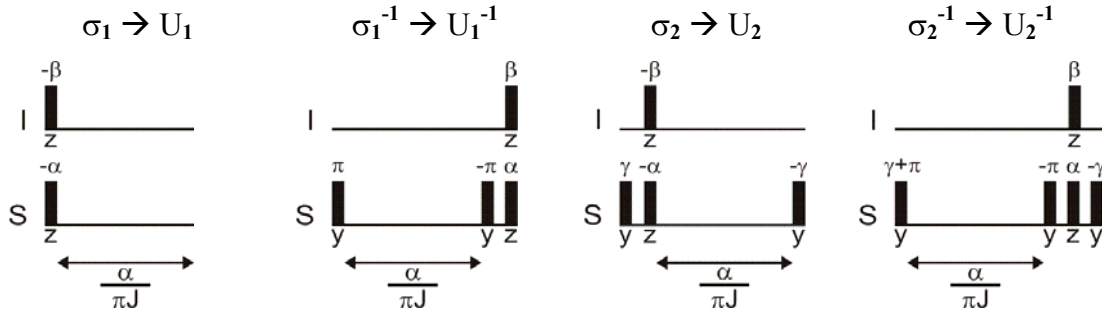


Figure 4.3: Pulse sequence elements translation of different operators of the Figure-Eight knot.

- iii) The controlled unitary matrix cU is applied on the NMR product operator I_x , where the I-spin is the “*control spin*” which was virtually added to the NMR sample when the mapping from the unitaries U to the controlled unitaries cU was performed.

$$cU \cdot I_{1X} \cdot cU^+ = \frac{1}{2} \begin{pmatrix} 0 & U^\dagger \\ U & 0 \end{pmatrix} \quad (4.2)$$

iv) Finally, the expectation values of I_x and I_y will be measured. They are proportional to the desired trace of the matrix U :

$$\langle I_{1X} \rangle = \text{tr} \left\{ I_{1X} \cdot \frac{1}{2} \begin{pmatrix} 0 & U^\dagger \\ U & 0 \end{pmatrix} \right\} = \frac{1}{2} \cdot \text{Re}[\text{tr}\{U\}] \quad (4.3)$$

$$\langle I_{1Y} \rangle = \text{tr} \left\{ I_{1Y} \cdot \frac{1}{2} \begin{pmatrix} 0 & U^\dagger \\ U & 0 \end{pmatrix} \right\} = \frac{1}{2} \cdot \text{Im}[\text{tr}\{U\}] \quad (4.4)$$

In our example of the Figure-Eight knot, we therefore have to apply the following pulse sequence:

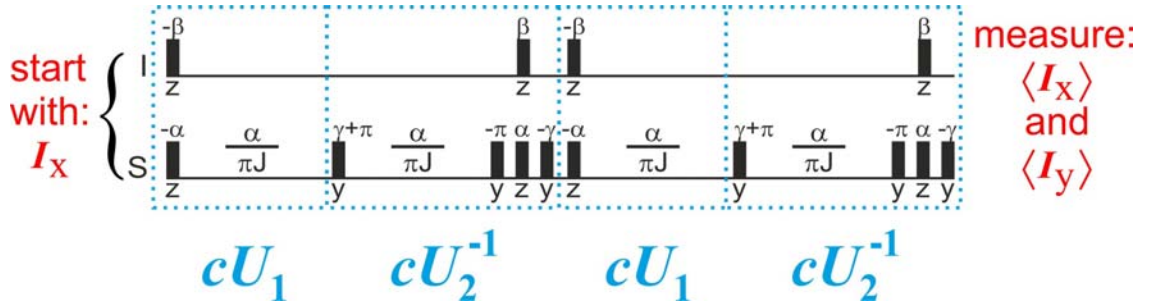


Figure 4.4: Pulse sequence blocks translation of different operators of the Figure-Eight knot.

If this is done for different values of θ (which translates into different values of α , β , and γ in the pulse sequence), the Bracket Polynomial of the Figure-Eight knot $\langle L'_{\text{Figure Eight}} \rangle(A)$ is evaluated for different values of A .

2. PREVIOUS EXPERIMENTAL RESULTS

2.1 Use of a 2-qubit NMR quantum computer for the Jones Polynomial approximation of the Trefoil knot

The natural abundance chloroform (CHCl_3), a molecule containing two spin $\frac{1}{2}$ nuclei, has recently been used for approximating the Jones Polynomial of the Figure-Eight knot as well as other knots (Trefoil knot and Borromean rings) [16, 19].

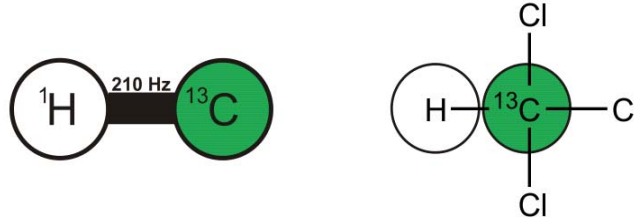


Figure 4.5: Coupling topology of chloroform (use as a 2-qubit NMR quantum computer).

The experimental procedure described in Section 1.a) was used for the approximation of the quantum algorithm of the Figure-Eight knot. The experimental measurements were achieved in two single-scan experiments. The following experimental results were obtained.

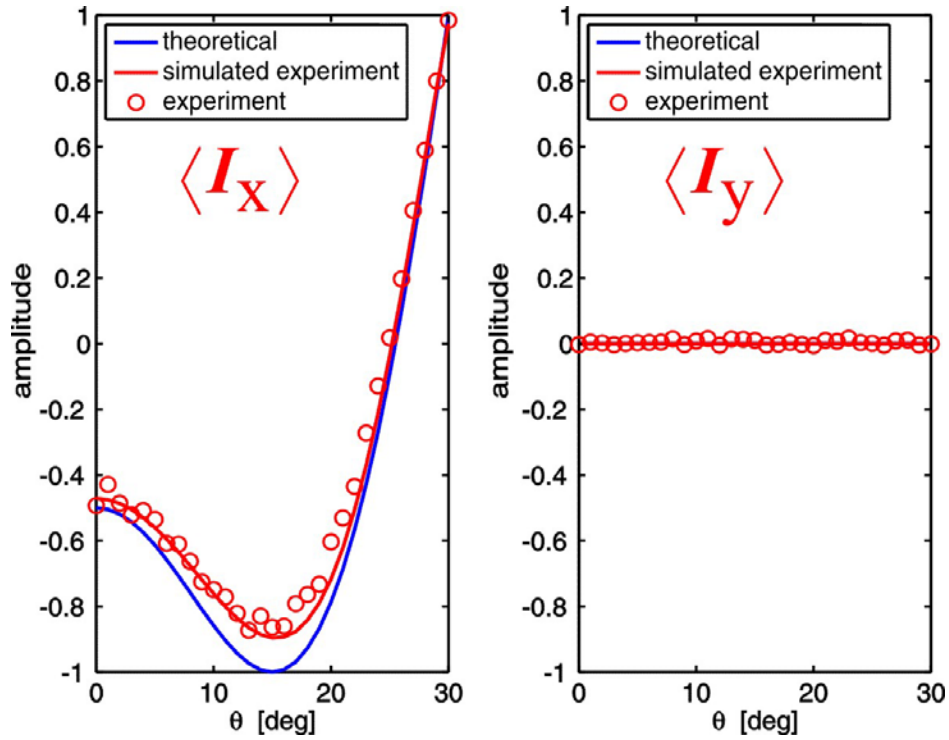


Figure 4.6: Real (I_x) and Imaginary (I_y) parts for the implementation of the 2x2 block U (4x4 block cU) operator of the Figure-Eight knot. The variable θ is related to the variable of the Bracket Polynomial A as follows: $A = e^{-i\theta}$ [19].

The theoretical values were in excellent agreement with the experimental results.

2.2 Approximation of the Jones Polynomial of the non-trivial link 6.2.3 by NMR using a 3-qubit quantum computer

A link, as compared to a knot, is defined as one or more disjointly embedded closed, non-self-intersecting curves that are embedded in three dimensions [1]. Recently, the approximation of the Jones Polynomial of the non-trivial link 6.2.3 by means of NMR and using a 3 qubit quantum computer has been implemented [15]. As mentioned in the Section 1, knots and links can be represented by closed-strand braids. The example of the non-trivial link 6.2.3 is illustrated below.

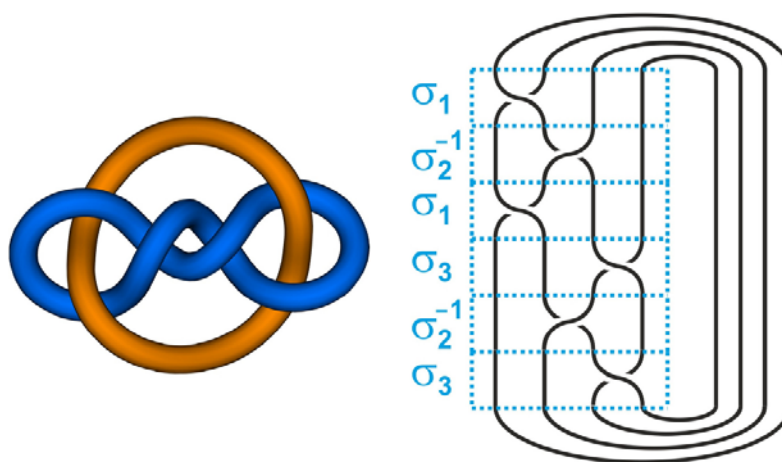


Figure 4.7: The link 6.2.3 represented as a 4-strand braid.

Two molecules, a 3-qubit system (^1H , ^{19}F , ^{31}P) and a 5-qubit system (^1H , ^{19}F , ^{31}P , ^{15}N and ^{13}C), were also used for approximating the Jones Polynomial of the link 6.2.3 but the experimental results were not entirely satisfactory [20].

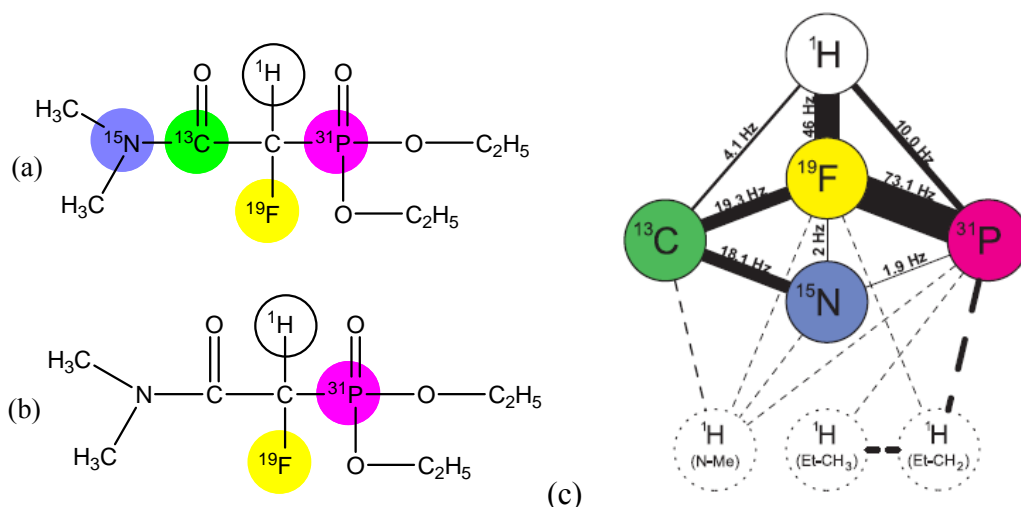


Figure 4.8: (a) 5-qubit molecule; (b) 3-qubit molecule; (c) Topology of the 5-qubit thermal state NMR quantum computer used for the approximation of the Jones Polynomial of the link 6.2.3.

It should be noted that the experiments were performed on a Bruker DMX-600-spectrometer with a prototype 6-channel NMR probe head (^2D , ^1H , ^{19}F , ^{31}P , ^{15}N and ^{13}C). The experimental results using the 3-qubit (^1H , ^{19}F , ^{31}P) system for the implementation of the representative matrix 4x4 block of U (8x8 block of cU) is shown below.

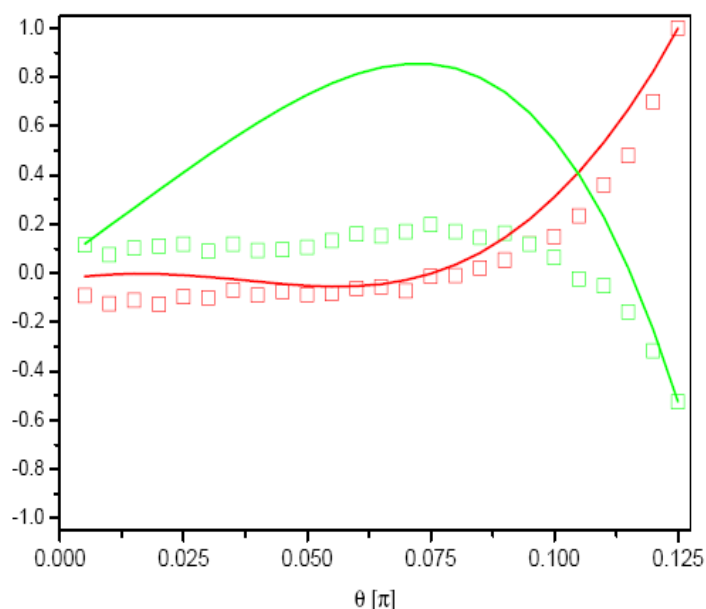


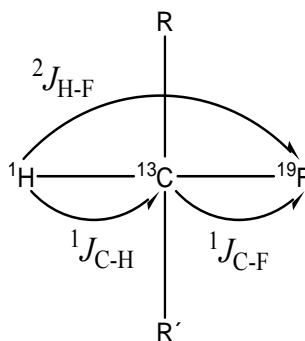
Figure 4.9: Experimental results for the implementation of the 4x4 block of U (8x8 block of cU) obtained with the 3-qubit (H-F-P) molecule. Real (red) and Imaginary (green) components; Simulation (lines) and experimental results (squares) [20].

As can be seen on the previous figure, there were some deviations between the simulation and the experimental results due to several reasons. The 3-qubit system has presented only medium ($^1J_{\text{FP}} = 73.1$ Hz) and small coupling constants ($^1J_{\text{HF}} = 46$ Hz, $^1J_{\text{HP}} = 10$ Hz) between the different nuclei (see Fig. 4.7). Furthermore, the ^{31}P nucleus relaxed fast (short T_2) and its NMR signal was not visible at the end of the pulse sequence. The presence of not needed couplings (J_{NF} and J_{NP}) required extra pulses for decoupling. Therefore the pulse sequence blocks became too long and complex. Hence a new molecule had to be found in order to successfully complete the experiments.

3. DESIGN AND SYNTHESIS OF A 3-QUBIT THERMAL STATE QUANTUM COMPUTER

For the reasons mentioned above, a new qubit system (new molecule) had to be found in order to realize the results predicted by the simulations. The candidate molecule should fulfill the following requirements regarding the 3-qubit system:

- Nuclei should be all heteronuclear
- The coupling constants between these three nuclei, used as qubits, should be as large as possible. So most of them should be 1J couplings.
- Nuclei should have long relaxation times T_2



(^1H , ^{13}C , ^{19}F) 3 qubit-system
with two 1J and one 2J coupling constants

Based on these constraints, it turns out that a system like (^1H , ^{13}C , ^{19}F) could be realizable knowing that organic synthesis involving the Silicium element (^{29}Si) requires

special equipments and is somehow not easy to be handled and ^{15}N usually has a small coupling constants whereas ^{31}P often has a short relaxation time T_2 .

A molecule which fulfills all the requirements listed above was not commercially available, therefore 2- ^{13}C -labeled Diethyl malonate was chosen as the starting material for an appropriate synthesis.

4. EXPERIMENTAL SECTION

4.1 Synthesis of the desired product

The target molecule was obtained after a one step synthesis. To the substrate (a solution of 2- ^{13}C -labeled Diethyl malonate (100 mg, 0.62 mmol) in dry tetrahydrofuran (THF) (10 mL), was added an oil-free suspension of NaH (30 mg, 0.69 mmol) under Argon at room temperature and stirred until no more hydrogen was evolved (ca. 15 min) i.e. the reaction mixture has ceased bubbling. The fluorinating reagent F-TEDA- BF_4 (221 mg, 0.62 mmol) was then added under Argon and the mixture was stirred for about 24 hours at room temperature [21, 22].

The mixture was quenched (ca. 15 min) with a solution (20 mL) of NaHCO_3 neutralized with H_2SO_4 and extracted twice with 30 mL CHCl_3 . The organic layer was then dried with Na_2SO_4 and evaporated on open air for 48 hours to obtain 52 mg of a residue made of 75% of the desired product 2- ^{13}C -labeled Diethyl 2-fluoromalonate (percentage deduced from the ^1H NMR signal integrals) and 25% of the reactant (2- ^{13}C -labeled Diethyl malonate). A signal at 106 ppm was not perceptible on the ^{13}C NMR spectrum, which would mean that no difluorinated product was formed (see Figure 4.11).

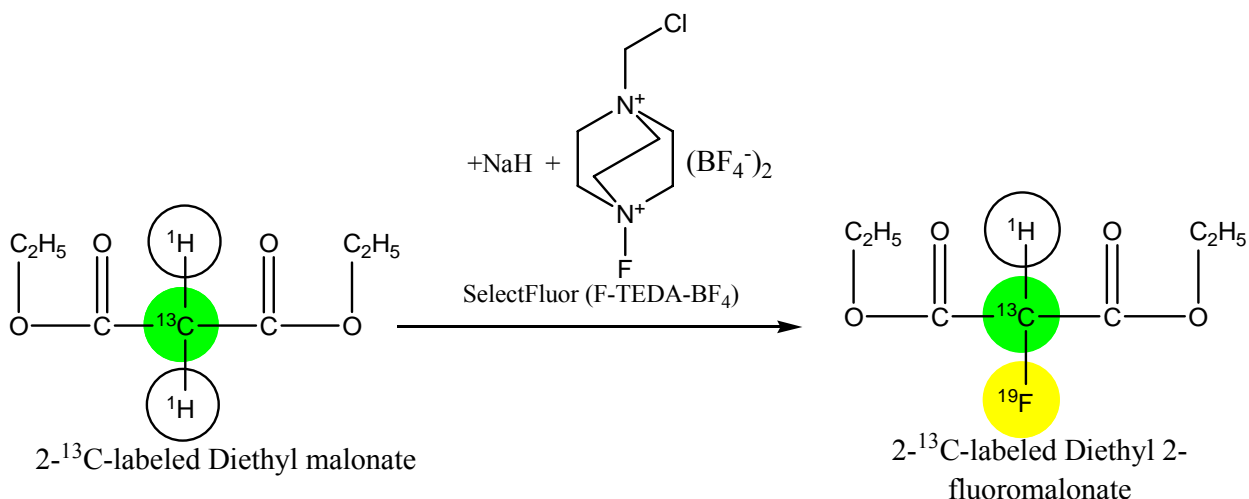


Figure 4.10: Synthesis route of the 2- ^{13}C -labeled Diethyl 2-fluoromalonate molecule.

The NMR samples (CDCl_3 and CD_3CN) have been prepared with the above mentioned mixture of compounds without further purification. In fact, the flash chromatography technique which has been used in order to separate the product from the reactant was not successful because both compounds have almost the same polarity. But a sample made of a mixture of all these two compounds is not a problem for our quantum computing experiments since the ^{13}C NMR signals of the ^{13}C -labeled carbon atom of the product is quite different and distant from the one of the reactant. In fact, the first appears at 85.3 ppm as a doublet of doublets (dd), while the latter appears at 40.2 ppm as a triplet (t) (see Figure 4.11, non ^1H -decoupled ^{13}C NMR spectrum). The 1D and 2D NMR spectra recorded with the prepared sample are shown below.

4.2 NMR spectroscopy

4.2.1 One Dimensional (^1H and ^{13}C) NMR spectra of the product

The 1D (^1H and ^{13}C) NMR spectra recorded with the product are presented below.

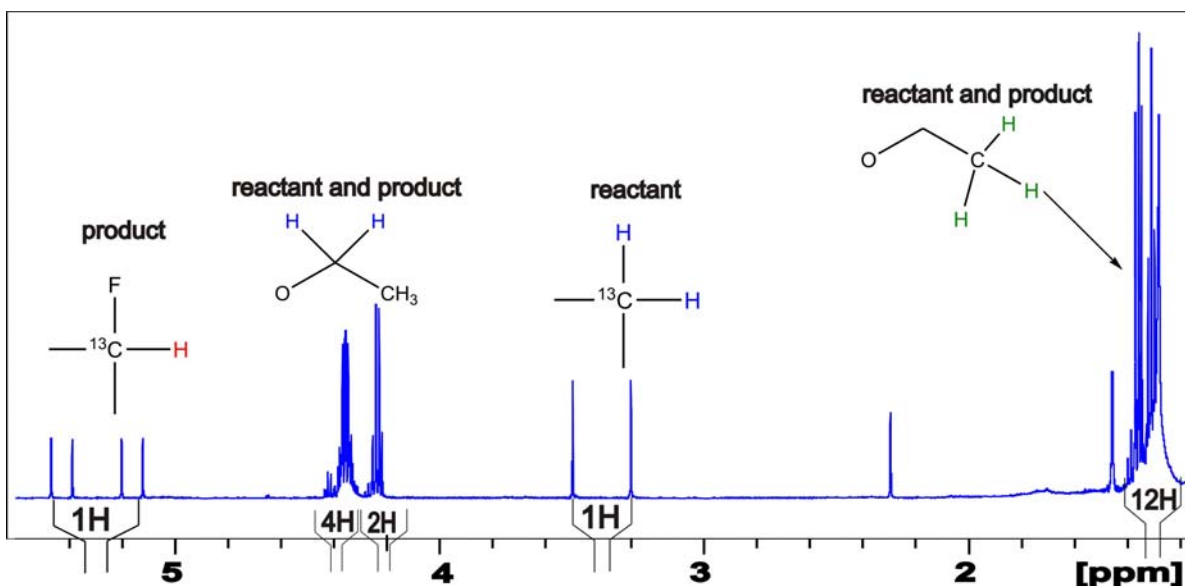


Figure 4.11: ^1H NMR spectrum of 2- ^{13}C -labeled Diethyl 2-fluoromalonate. The protons bond to the ^{13}C -labeled carbon atom of the reactant appear at 3.4 ppm (d) whereas the single proton bonds to the ^{13}C -labeled carbon atom of the product appears at 5.3 ppm (dd).

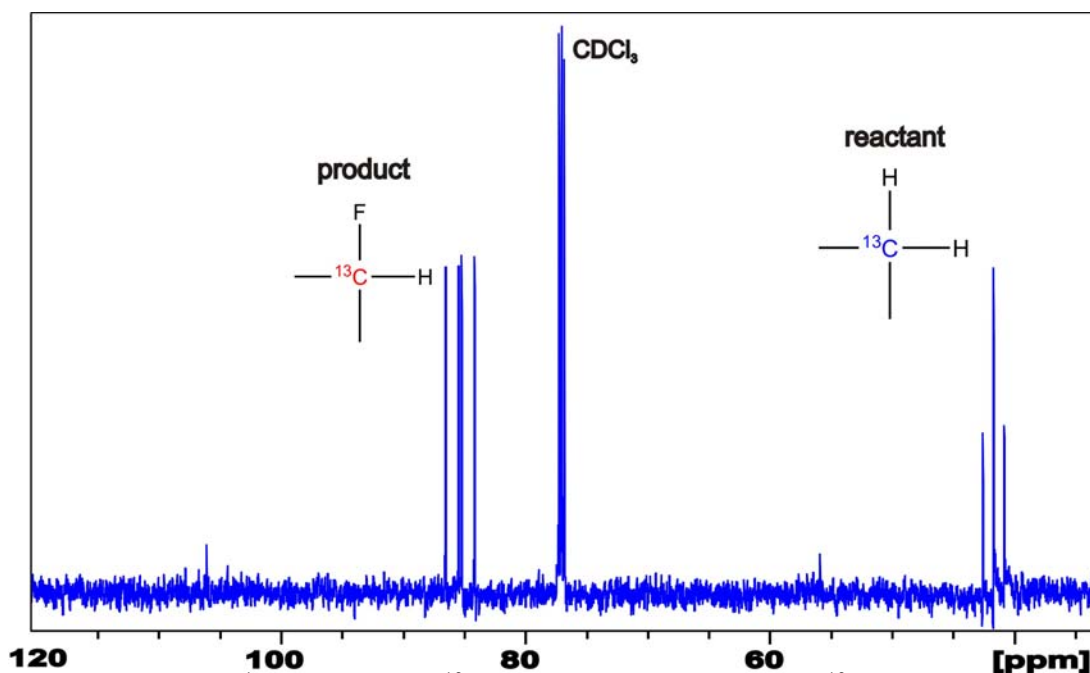


Figure 4.12: Non ^1H -decoupled ^{13}C NMR spectrum of 2- ^{13}C -labeled Diethyl 2-fluoromalonate. The ^{13}C -labeled carbon atom of the reactant appears at 40.2 ppm (t) whereas the ^{13}C -labeled carbon atom of the product appears at 85.3 ppm (dd).

The coupling constants between the different nuclei were measured. Their values as well as the topology of the 3-qubit system are given below.

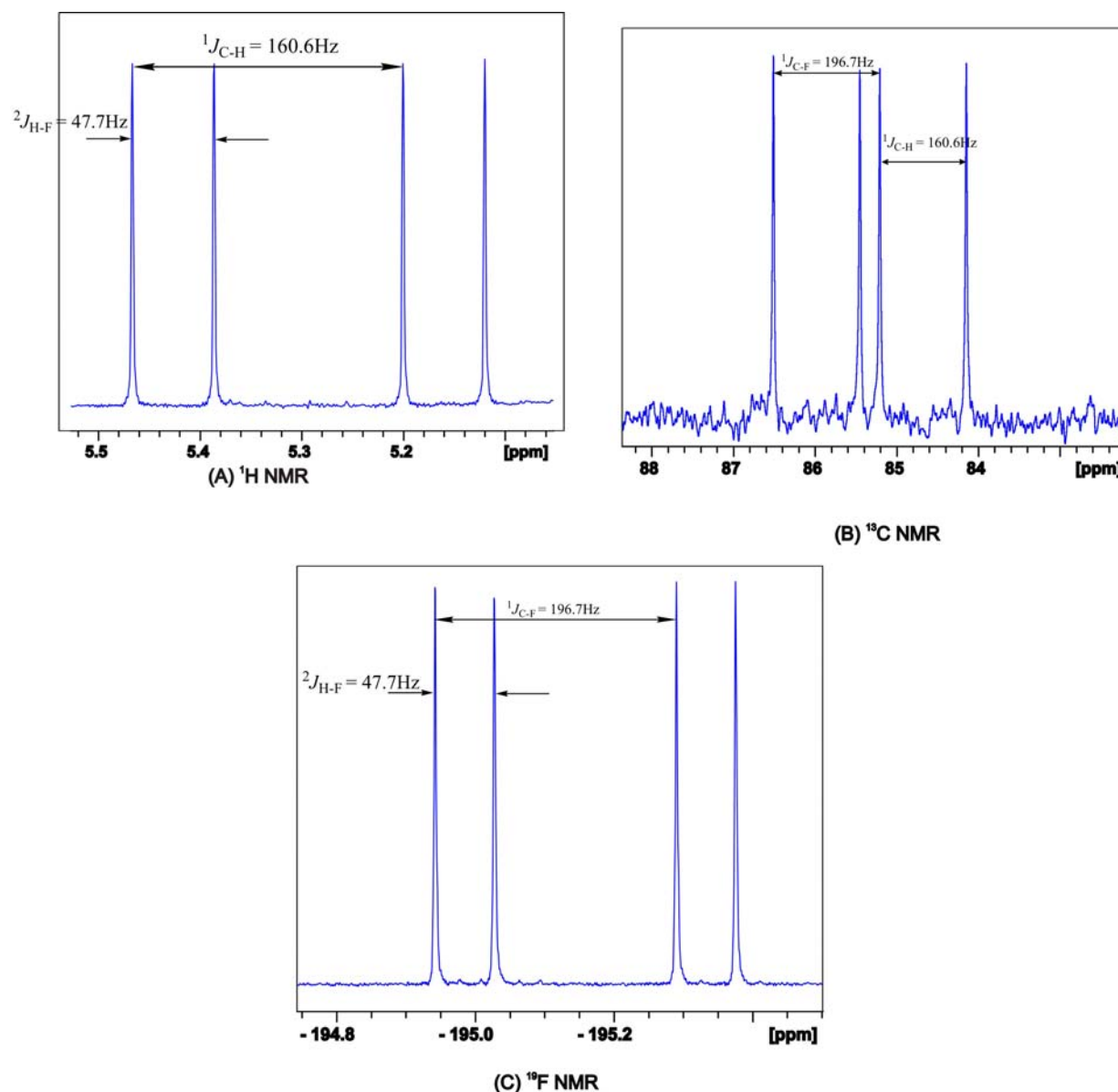


Figure 4.13: Non-decoupled 1D NMR spectra of 2- ^{13}C -labeled Diethyl 2-fluoromalonate showing the different coupling constants between the nuclei. (A) ^1H NMR; (B) ^{13}C NMR; (C) ^{19}F NMR.

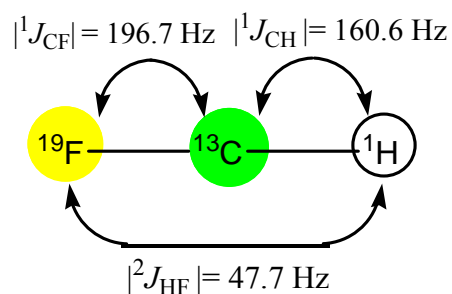


Figure 4.14: Coupling topology of the 3-qubit thermal state NMR quantum computer (2- ^{13}C -labeled Diethyl 2-fluoromalonate molecule).

4.2.2 Two Dimensional HSQC NMR spectra of the product

In order to determine the sign of the different coupling constants between the nuclei, two dimensional HSQC NMR experiments [23] were acquired. In fact the outcome, after the application of a pulse sequence (function of the delay $1/(2J)$) on a nucleus, depends on the signs of the coupling between a nucleus and its neighboring nuclei. Because only the cross peaks between the nuclei were of interest, highly resolved spectra were not necessary. Therefore HSQC experiments were performed with a few scans and the recorded spectra are presented below.

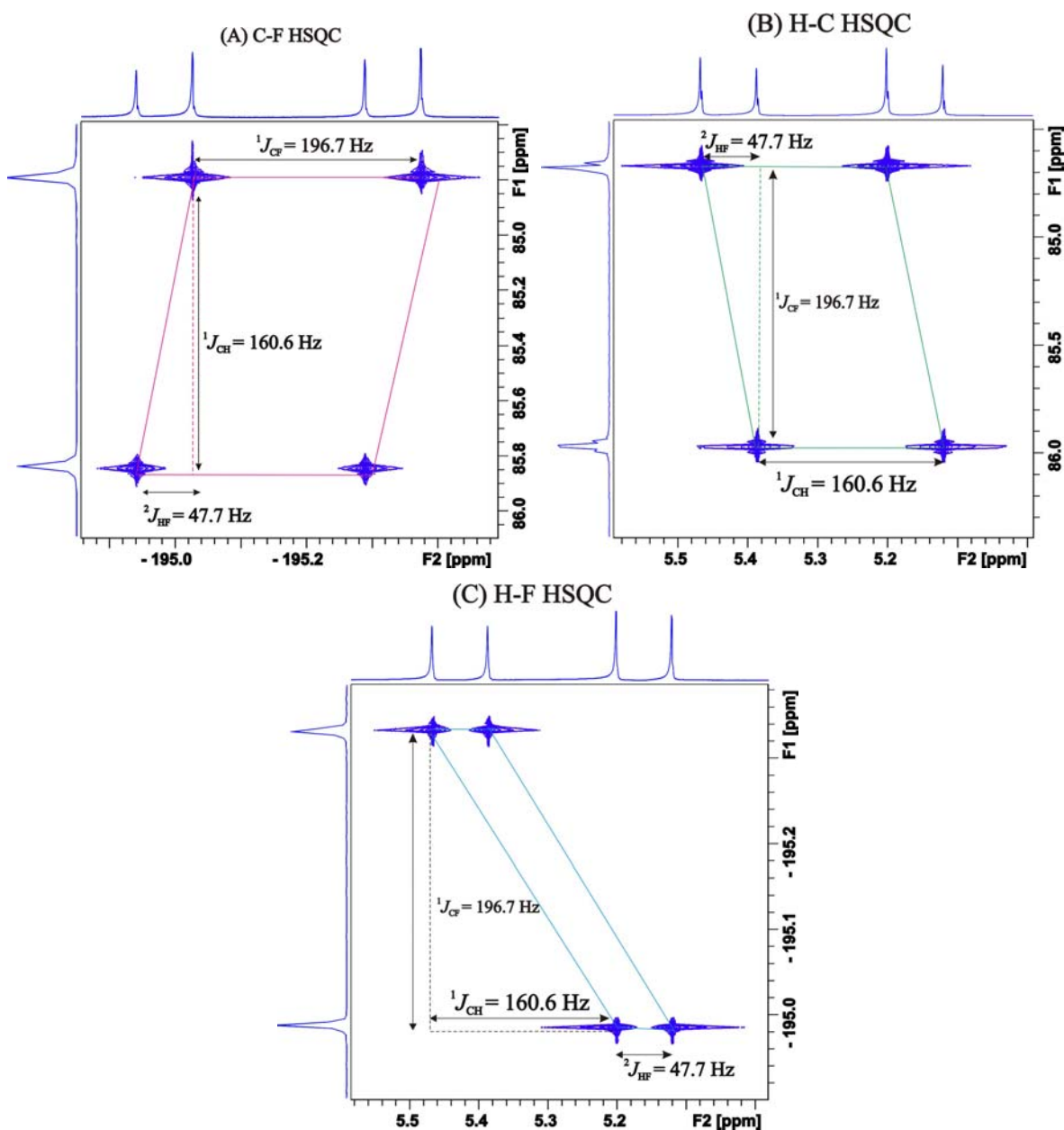


Figure 4.15: 2D HSQC NMR spectra of 2-¹³C-labeled Diethyl 2-fluoromalonate.

It is known that coupling constants can be positive or negative, but the sign can not be extracted from simple 1D NMR spectra.

However, the relative signs of coupling constants can be determined using the E.COSY (Exclusive Correlation Spectroscopy) [24-26] technique. Considering the above HSQC cross peaks as E.COSY like cross peaks patterns, the following procedure [27] can be applied to determine the sign of the coupling constants between the three nuclei (^1H , ^{13}C , and ^{19}F).

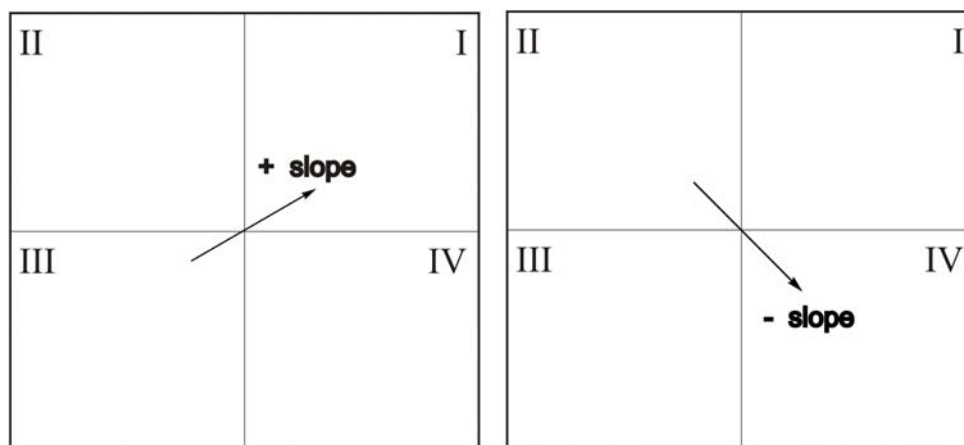


Figure 4.16: Mapping of a four quadrant system representing E.COSY like HSQC patterns.

- Observing the cross peaks of the two spin system ^{13}C and ^{19}F (I), a drawn line connecting the quadrants I and III (Fig. 4.15) has a positive slope (case A, see Fig. 4.14), therefore the passive couplings (i.e. $^1J_{\text{CH}}$ in the F_1 and $^2J_{\text{HF}}$ in the F_2 dimensions) have the same sign (so, $^1J_{\text{CH}} \times ^2J_{\text{HF}} > 0$).
- In the case of a negative tilt, that is if the slope of the line connecting the quadrants II and IV (Fig. 4.15) is negative, this indicates that the passive couplings i.e. $^1J_{\text{CF}}$ in the F_1 and $^2J_{\text{HF}}$ in the F_2 dimensions for the case (B) and $^1J_{\text{CF}}$ in the F_1 and $^1J_{\text{C-H}}$ in the F_2 dimensions for the case (C) are of opposite sign (thus, $^1J_{\text{CF}} \times ^2J_{\text{HF}} < 0$ and $^1J_{\text{CF}} \times ^1J_{\text{CH}} < 0$).

Furthermore, knowing that $^1J_{\text{CF}}$ is always negative, whereas $^1J_{\text{CH}}$ is always positive [28], it can be easily deduced that the coupling constant $^2J_{\text{HF}}$ is positive.

It should be noted that the E.COSY patterns have emerged here since only the active spins are involved during the 2D HSQC NMR sequence while the passive spin is unperturbed (there is no pulse applied on a third spin).

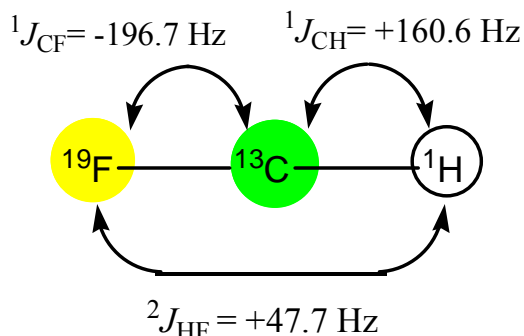


Figure 4.17: Coupling topology of the 3-qubit thermal state NMR quantum computer ($2\text{-}^{13}\text{C}$ -labeled Diethyl 2-fluoromalonate molecule) with the sign of the couplings.

5. USE OF A 3-QUBIT THERMAL STATE QUANTUM COMPUTER FOR APPROXIMATING THE QUANTUM ALGORITHM OF THE NON-TRIVIAL LINK 6.2.3.

The $2\text{-}^{13}\text{C}$ -labeled Diethyl 2-fluoromalonate molecule which is a 3-qubit (H-C-F) thermal state NMR quantum computer presents large coupling constants and thus allows the use of the standard probe head instead of the 6-channel probe head. In fact, the 90 degree pulse is always longer when it is measured with the 6-channel probe head. Therefore, the use of the standard probe head instead of the 6-channel probe head was a great advantage for experimental processes since the length of the pulse sequence blocks were considerably shorter. The experimental results obtained are presented below.

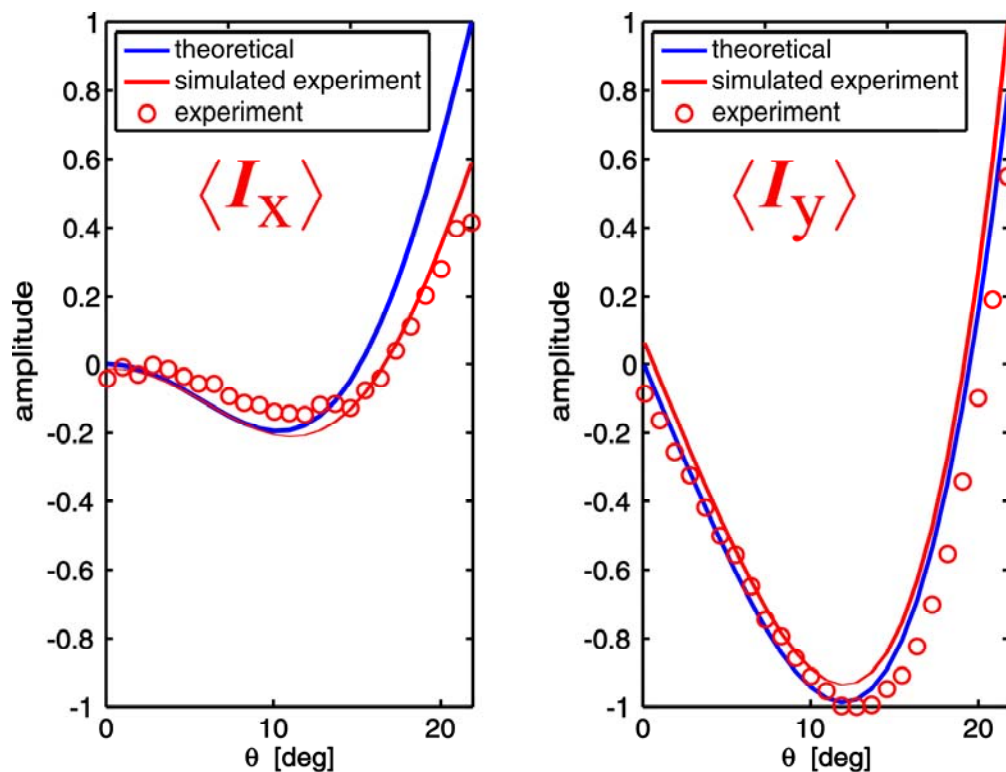


Figure 4.18: Experimental results for the implementation of the 4x4 block of U (8x8 block of cU) operator of the non-trivial link 6.2.3. The experiments were performed with the CD_3CN sample which presented better lock signal and shimming.

CONCLUSION

The development of 2- ^{13}C -labeled Diethyl 2-fluoromalonate, a molecule made of 3 qubits (1H , ^{13}C , and ^{19}F), all heteronuclear, was successful. This molecule has been of considerable advantages for the desired experiments. The large coupling constants between the different nuclei of the system and the use of the standard QXI NMR probe head instead of the 6-channel NMR probe head have let to very good results. In fact, the full quantum algorithm for the approximation of the Jones Polynomial was implemented on our 3-qubit system. The Jones Polynomial of the non-trivial link 6.2.3. was evaluated on several values of the domain of definition. The experimental results obtained with this 3-qubit thermal state NMR quantum computer (2- ^{13}C -labeled Diethyl 2-fluoromalonate) were entirely satisfactory. These results (see figure 4.15) are in very good agreement with the theoretical expectations (simulations) and lead to the confirmation that the developed 3-qubit molecule was very well suited for our quantum computing experiments.

EXPERIMENTAL SETUP

For NMR experiments, two samples were prepared with 50 mg of the compounds dissolved in CD₃CN and in CDCl₃.

All 1D and 2D NMR experiments were performed at 600 MHz Bruker AV spectrometer equipped with a QXI standard probe head at room temperature.

Table 4.1 One Dimensional NMR experimental setup (CDCl₃ sample).

1D NMR experiments	¹ H	¹³ C	¹⁹ F
Pulse program (pulseprog)	zg	zg	zg
TD (Size of FID)	2k	2k	4k
Number of scans (NS)	1	1	1
Acquisition time AQ(s)	0.68	0.68	0.73
FID Resolution (Hz)	0.73	0.73	0.69
Spectral Width (SW) ppm (Hz)	10 (6002.4)	10 (1510)	4.5 (2824)
Transmitter frequency	5.3 (3178)	85.3 (12882)	-195.2 (-110251)
Offset in (Ox) ppm (Hz)			

Table 4.2 Two Dimensional HSQC experimental setup (CDCl₃ sample).

2D HSQC NMR experiments	F2 (¹ H)	F1 (¹³ C)	F2 (¹ H)	F1 (¹⁹ F)	F2 (¹⁹ F)	F1 (¹³ C)
pulseprog	hsqcetgp		hsqcetgp		hsqcetgp	
NS	8		2		2	
D ₁ (s)	8		2		2	
TD	2k	256	2k	256	2k	256
AQ(s)	1.71	0.13	1.71	0.26	1.7	0.73
FIDRES (Hz)	0.29	3.91	0.29	1.95	0.29	3.91
SW ppm (Hz)	1	6.6	1	0.9	1.06	1
	(600)	(3738.9)	(600)	(497.1)	(600.5)	(150)
Ox ppm (Hz)	5.3	85.3	5.3	-195.2	-195.2	85.3
	(3178)	(12882)	(3178)	(-110251)	(-110251)	(12882)

APPENDIX

Table 4.3: Some NMR data of the 2-¹³C-labeled Diethyl 2-fluoromalonate dissolved in CD₃CN and CDCl₃.

CD ₃ CN sample Better for lock and shimming. This sample was used for quantum computing experiments.	CDCl ₃ sample
Offsets and 90 degree hard pulses	Offsets and 90 degree hard pulses
¹ H: O1: 3260 Hz	¹ H: O1: 3178 Hz
90 degree pulse: 10.38@18W	90 degree pulse: 10.5@ 18W
¹⁹ F: O1: -110898 Hz	¹⁹ F: O1: -110251 Hz
90 degree pulse: 24.0@39W	90 degree pulse: 25.25@ 39W
¹³ C: O1: 12916 Hz	¹³ C: O1: 12882 Hz
90 degree pulse: 21.0@94W	90 degree pulse: 22.5@ 94W
Coupling constants	Coupling constants
² J _{HF} : 47.6 Hz	² J _{HF} : 47.7 Hz
¹ J _{CH} : 162 Hz	¹ J _{CH} : 160.3 Hz
¹ J _{CF} : -191.8 Hz	¹ J _{CF} : -196.7 Hz
Relaxation times of the nuclei	Relaxation times of the nuclei
¹ H ¹⁹ F ¹³ C	¹ H ¹⁹ F ¹³ C
T ₁ : 2.2s 3.2s 1.3s	T ₁ : 2.0s 3.0s 1.6s
T ₂ : 1.8s 2.2s 2.0s	T ₂ : 1.1s 2.0s 1.6s

REFERENCES

- [1] Louis Kauffman: *Knoten, Diagramme, Zustandsmodelle, Polynom invarianten*, Spektrum, Heidelberg/Berlin/oxford 1995, ISBN 3-86025-232-1
- [2] Kenneth A. Perko Jr., On the classification of knots. *Proc. Amer. Math. Soc.* **45** (1974), 262-266.
- [3] V. F. R. Jones, *Bull. Am. Math. Soc.* **12**, 103 (1985).
- [4] Collins, Graham (2006), "Computing with Quantum knots". *Scientific American*.
- [5] M. Freedman, A. Kitaev and Z. Wang. Topological quantum Computation. *Bull. Amer. Math. Soc.*, 40(1):31-38, 2003.
- [6] Chetan Nayak et al. Non-Abelian Anyons and Topological Quantum Computation. *Rev Mod. Phys.* **80**, 3, pp. 1083-1159 (2008).
- [7] S. Das Sarma, M. Freedman and C. Nayak. Topologically Protected Qubits from a Possible Non-Abelian Fractional Quantum Hall State. *Phys Rev. Lett.* **94**, 166802 (2005).
- [8] R. Raussendorf, J. Harrington and K. Goyal. Topological fault-tolerance in cluster state Quantum computation. *New J. Phys.* **9** (2007) 199.
- [9] L. Kauffman, AMS Contemp. Math. Series, 305, edited by S. J. Lomonaco, (2002), 101-137.
- [10] E. Knill and R. Laflamme, *Phys. Rev. Lett.* **81**:5672-5675, 1988.
- [11] S. Parker and M. B. Plenio, *Phys. Rev. Lett.* **85**, N° 14, 2 October 2000.
- [12] J. M. Myers, A. F. Fahmy, S. J. Glaser and R. Marx, *Phys Rev. A* **63**, 032302 (2001).
- [13] D. Poulin, R. Laflamme, G. J. Milburn, and J. P. Paz, *Phys Rev. A* **68**, 20302 (2003).
- [14] A. F. Fahmy, R. Marx, W. Bermel, and S. J. Glaser, *Phys Rev. A* **78**, 022317 (2008).
- [15] G. Passante, O. Moussa, C. A. Ryan, and R. Laflamme, *Phys. Rev. Lett.* **103**.250501 (2009)
- [16] R. Marx, A. F. Fahmy, L. Kauffman et al., Nuclear-Magnetic-Resonance Quantum Calculations of Jones Polynomial. *Phys. Rev. A* **81**, 032319 (2010).
- [17] K. Reidemeister. *Knotentheorie*. Chelsea, New York (1948), Julius Springer (1932).
- [18] J. W. Alexander, "A lemma on systems of knotted curves". *Proc. Nat. Acad. Sci. USA*, **9**, 93-95 (1923).
- [19] Spoerl, A. *Numerische und Analytische Lösungen für Quanteninformatisch-relevante Probleme*. TU Muenchen 2008, Ph.D Thesis.
- [20] Pomplun, N. *Polarisationstransfermechanismen und Kontrolle von Elektronen-Kern-Spinsystemen sowie die Implementierung von NMR-Quantenalgorithmen*. TU

Muenchen 2010, Ph.D Thesis.

- [21] G. Sankar Lal. S *J. Org. Chem.* 1993, **58**, 2791-2796.
- [22] R. Eric Banks, Nicholas J. Lawrence and Allan L. Popplewell. *J. Chem. Soc., Chem. Commun.* 1994, pp. 343-344.
- [23] G. Bodenhausen, D. J. Ruben, *Chem. Phys. Lett.* 1980, **69**, 185-188.
- [24] C. Griesinger, O. W. Sorensen, and R. R. Ernst, *J. Am. Chem. Soc.* **107**, 6394 (1985).
- [25] C. Griesinger, O. W. Sorensen, and R. R. Ernst, *J. Chem. Phys.* 1986, **85**, 6837-6852
- [26] C. Griesinger, O. W. Sorensen, and R. R. Ernst, *J. Magn. Reson.* 1987, **75**, 474-492.
- [27] G. Otting, B. A. Messerle, and L. P. Soler, *J. Am. Chem. Soc.* **118**, 5096 (1996).
- [28] Hesse, M, Meier, H, and Zeeh, B. in *Spektroskopische Methoden in der organischen Chemie*. 5. überarbeitete Auflage (5th Edition). Stuttgart; New York: Thieme, 1995, pp. 152.